Biofilm formation and extracellular polymeric substances of acidophilic metal/sulfur-oxidizing archaea

Dissertation

zur Erlangung des akademischen Grades eines

Doktors der Naturwissenschaften

– Dr. rer. nat. –

vorgelegt von

Ruiyong Zhang

geboren in Kaifeng, China

Biofilm Centre, Fakultät für Chemie

der

Universität Duisburg-Essen

2015

Die vorliegende Arbeit wurde im Zeitraum von Januar 2011 bis Januar 2015 im Arbeitskreis von Prof. Dr. W. Sand in der Fakultät für Chemie, Biofilm Center der Universität Duisburg-Essen durchgeführt.

Tag der Disputation: 22.12.2015

Gutachter: Prof. Dr. Wolfgang Sand

                Prof. Dr. Thomas R. Neu

Vorsitzender: Prof. Dr. Jochen S. Gutmann

Thought is impossible without an image

Aristotle (384 – 322 BC)

The results obtained during the promotion are partly in the following original publications published or in press:

Zhang R, Vera M, Bellenberg S, Sand W (2013) Attachment to minerals and biofilm development of extremely acidophilic archaea. Adv Mat Res 825:103-106

Zhang R, Bellenberg S, Castro L, Neu TR, Sand W, Vera M (2014) Colonization and biofilm formation of the extremely acidophilic archaeon *Ferroplasma acidiphilum*. Hydrometallurgy 150:245-252

Zhang R, Neu T, Bellenberg S, Kuhlicke U, Sand W, Vera M (2015) Use of lectins to in situ visualize glycoconjugates of extracellular polymeric substances in acidophilic archaeal biofilms. Microb Biotechnol 8:448-461

Zhang R, Neu T, Zhang Y, Bellenberg S, Kuhlicke U, Li Q, Sand W, Vera M (2015) Visualization and analysis of EPS glycoconjugates of the thermo-acidophilic archaeon *Sulfolobus metallicus*. Appl Microbiol Biotechnol 99:7343-7356

Zhang R, Zhang Y, Neu TR, Li Q, Bellenberg S, Sand W, Vera M (2015) Initial attachment and biofilm formation of a novel crenarchaeote on mineral sulfides. Adv Mat Res 1130:127-130

Zhang R, Liu J, Neu TR, Li Q, Bellenberg S, Sand W, Vera M (2015). Interspecies interactions of metal-oxidizing thermo-acidophilic archaea *Acidianus* and *Sulfolobus*. Adv Mat Res 1130:105-108

Zhang R, Bellenberg S, Neu TR, Sand W, Vera M (2016) The biofilm lifestyle of acidophilic metal/sulfur-oxidizing microorganisms. In: Rampelotto PH (ed) Biotechnology of Extremophiles: Advances and Challenges. Springer, Switzerland

Contents

Contents

List of Abbreviations

AFM	Atomic force microscopy
AHLs	N-acyl homoserine lactones
AMD	acid mine drainage
ARD	acid rock drainage
ATR-FTIR	Attenuated Total Reflection-Fourier Transmission Infra-Red spectroscopy
BRGM	Bureau de Recherches Géologiques et Minières
BSA	bovine serum albumin
CLSM	Confocal laser scanning microscopy
Con A	Concanavalin A
DAPI	4',6-diamidino-2-phenylindole
DDAO	7-hydroxy-9H-1,3-dichloro-9,9-dimethylacridin-2-one
DSMZ	Deutsche Stammsammlung von Mikroorganismen und Zellkulturen
eDNA	extracellular DNA
EFM	Epifluorescence microscopy
EPS	Extracellular polymeric substances
FITC	Fluorescein isothiocyanate
FLBA	Fluorescence lectin-binding analysis
G6PDH	Glucose-6-phosphate-dehydrogenase

GalNAc	N-acetylgalactosamine
GlcNAc	N-acetylglucosamine
HPLC	High-performance liquid chromatography
KDO	3‑deoxy-α-D-manno-octulosonic acid
LPA	*Limulus polyphemus* agglutinin
MAC	Mackintosh basal salt medium
MIC	Minimum inhibitory concentration
MIP	Maximum intensity projection
MS	Metal sulfides
NA	Numerical aperture
QS	Quorum sensing
RISCs	Reduced inorganic sulfur compounds
ROS	Reactive oxygen species
SEM	Scanning electron microscopy
STXM	Scanning transmission X-ray microscopy
TRITC	Tetramethylrhodamine isothiocyanate
S-layer	Surface-layer
SOR	Sulfur oxygenase reductase
SQR	Sulfide:quinone oxidoreductase
μ-XRF	Micro X-ray fluorescence

Abstract

In this study, biofilm formation and extracellular polymeric substances (EPS) of acidophilic archaea were investigated. Three representative archaeal species extremely acidophilic archaeon *Ferroplasma acidiphilum*, thermoacidophilic archaea *Acidianus* sp. DSM 29099 and *Sulfolobus metallicus* were chosen as test organisms. Several cultivation and advanced microscopical techniques e.g. CLSM, AFM & EFM and SEM were used to visualize and characterize biofilm development and EPS of acidophilic archaea. In addition, FLBA, ATR-FTIR and conventional spectroscopic methods were applied for qualification and quantification of EPS components.

F. acidiphilum biofilms were heterogeneously distributed on polycarbonate filters over time, and varied within the different growth conditions such as supplementation with glucose. Cells formed a monolayer biofilm and were preferably attached to the defect sites of pyrite surfaces. Biofilm and planktonic cells exhibited significant morphological differences as revealed by AFM. Low coverage of pyrite surface by cells seems to correlate with their low leaching ability.

Screening of a lectin library resulted in the detection of 21 lectins able to bind archaeal biofilms on pyrite and to *Acidianus* sp. DSM 29099 biofilms on elemental sulfur (S^0). These lectins can be used in studies for assessment of interactions between various members of microbial bioleaching communities, especially in order to elucidate the role of archaea in detail. The major binding patterns, e.g. tightly bound EPS and loosely bound EPS, were detected on both substrates pyrite and S^0. The three archaeal species produced various EPS glycoconjugates containing sugar moieties like glucose, galactose, mannose, GlcNAc, GalNAc, sialic acid, and fucose. Additionally, the substratum induced

different EPS glycoconjugates and biofilm structures for cells of *Acidianus* sp. DSM 29099.

EPS analysis of *S. metallicus*[T] on S^0 showed that capsular EPS from planktonic cells were mainly composed of carbohydrates and proteins. In contrast, colloidal EPS from planktonic cells were dominated by carbohydrates. Proteins were found to be major components in EPS from biofilms on S^0. In addition, extracellular proteins and nucleic acids were present in the EPS matrix. The existence of these compounds suggest their potential roles in biofilm formation and stabilization. *S. metallicus*[T] cells were shown to be embedded in a gel-like and flexible EPS matrix, where cells were often found to be motile (back and forth) either self-propelled by cellular appendages or by 'Brownian motion'.

1. Introduction

1.1 State of art of bioleaching/biomining

Around 166 A. D., the medical doctor Galenus reported that blue copper sulfate containing water was extracted from copper mines on Cyprus (Rossi 1990). Since then the capacity of microbes to dissolve sulfide minerals has been explored for the last millennia. The process that metal sulfides (MS) are dissolved into bulk solutions under the effects of microorganisms is called bioleaching (Vera et al. 2013b; Schippers et al. 2014). On the one hand, bioleaching can be used for valuable metal recovery from ore deposits and concentrates. On the other hand, bioleaching may cause acidification of water resources, leading to serious environment pollution like acid mine/rock drainage (AMD/ARD) (Sand et al. 2007; Hallberg 2010; Nordstrom et al. 2015).

Biomining is the term to describe the technology that uses microbes to achieve metal extraction from minerals or waste materials. Biomining of gold or other precious metals normally involves a pre-treatment process using metal/sulfur-oxidizing bacteria or archaea prior to cyanide extraction (Syed 2012). This process is known as biooxidation. Compared to the traditional mineral processing technology like ore smelting/toasting, biomining is more attractive regarding to its lower energy costs and also is more environmentally friendly. In addition, due to the autotrophic lifestyle of most bioleaching microbes, CO_2 is fixed by during their bio-processing of MS. This means that bioleaching involves less carbon footprints (CO_2 fixation by autotrophs) compared to smelting operations (CO_2 emission) (Johnson 2014).

Normally, MS dissolution is a metal oxidation process due to the presence of reduced metal ions in MS. Some oxide ores can be leached by a bioreductive leaching, a process called "Ferredox" (du Plessis et al. 2011).

It is assumed that 15 % of copper, 5 % of gold and smaller amounts of other metals (such as nickel and zinc) are currently produced globally using

biomining technologies. Apart from base metals like copper and nickel, precious metals like gold, uranium, and rare-earth elements have also been exploited from underground ore bodies *in situ* (Johnson 2015).

Biomining is also applied to recover valuable metals from electrical-electronic wastes (Pant et al. 2012; Hong and Valix 2014), spent petroleum and fly ash (Akcil et al. 2015), oxide ores (i.e. lateritic ores) (Johnson et al. 2013; Nancucheo et al. 2014), process waters and water streams (Johnson 2013). In addition, biomining has been actively studied over the last several years as a bioremediation tool for treating heavy metals contained in sewage sludge, sediment, and contaminated soil and mine tailings (Liu et al. 2007; Lim et al. 2009; Pathak et al. 2009; Deng et al. 2013; Lee et al. 2015).

Modern "Omics" techniques such as genomics, proteomics, transcriptomics and metabolomics have been used to elucidate diversity and some ecological aspects of acidophilic communities, bioleaching mechanisms, and will be helpful in future attempts to optimize the design, control, and optimization of bioleaching applications (Vera et al. 2013a; Goltsman et al. 2015; Martinez et al. 2015). Increased standards for environmental protection and the demand of base and precious metals as well as rare-earth elements will definitely intensify the use of bio-processing of ore minerals.

1.2 Bioleaching mechanisms

The mechanisms involved in mineral dissolution conducted by microorganisms have been debated for decades (Evangelou and Zhang 1995; Bosecker 1997; Tributsch 2001; Crundwell 2003). Microbial dissolution of minerals has been postulated to be a result of direct and indirect leaching mechanisms. However, it is now well accepted that the originally discussed "direct leaching mechanism" (assuming that the cells are able to enzymatically oxidize the sulfur moiety at the MS surface) does not exist (Sand et al. 2001). The indirect mechanism consists two sub-mechanisms: contact and non-contact mechanisms. In case of

the contact mechanism, cells attach to and form biofilms on MS via extracellular polymeric substances (EPS) and consequently enhance mineral degradation. In the non-contact mechanism, microorganisms in the planktonic phase are responsible for regeneration of iron(III) ions which attack the MS and lead to its dissolution (Sand et al. 2001; Rawlings 2002). As a result, a combined mechanism in which both cell subpopulations (i.e. biofilm forming cells on the MS and planktonic cells contribute to MS dissolution by providing iron(III) ions and/or protons thanks to their iron/sulfur oxidation activities (Vera et al. 2013b).

1.3 Pathways of metal sulfide dissolution

Based on the acid solubility of MS, there are two different pathways of mineral dissolution (Fig. 1). The thiosulfate pathway is involved in the dissolution of acid-insoluble MS, such as pyrite, molybdenite (MoS_2), and tungstenite (WS_2). The polysulfide pathway is relevant for dissolution of acid-soluble MS, such as sphalerite (ZnS), galena (PbS) or chalcopyrite (Schippers et al. 1996; Schippers and Sand 1999; Sand et al. 2001).

These two pathways are indirect mechanisms, since in acidic solution the acid-insoluble MS are solely oxidized chemically by iron(III) ions, which are supplied by the microbial oxidation of iron(II) ions (Schippers et al. 1996; Rodriguez et al. 2003; Gleisner et al. 2006). The electrochemical processes that result in the dissolution of sulfide minerals take place at the interface between the bacterial cell and the mineral sulfide surface.

Thiosulfate mechanism   **Polysulfide mechanism**
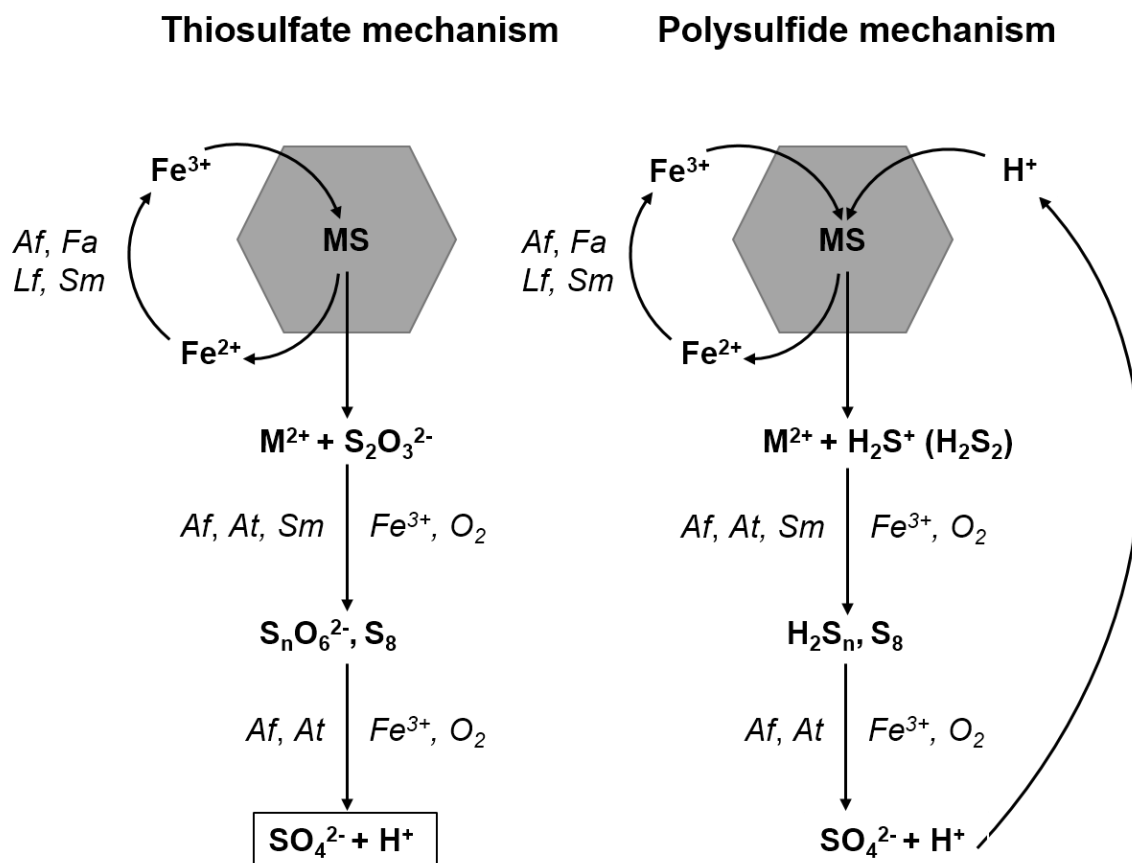
Figure 1. Scheme of the thiosulfate and polysulfide mechanisms in the bioleaching of MS (modified from Schippers and Sand 1999). Iron(III) ions attack MS by electron extraction and are thereby reduced to the iron(II) ion form. As a result, the metal sulfide crystal releases metal cations (M^{2+}) and water-soluble intermediary sulfur compounds. Iron(II)-oxidizing bacteria and archaea such as *Acidithiobacillus ferrooxidans* (*Af*), *Ferroplasma acidiphilum* (*Fa*), *Leptospirillum ferrooxidans* (*Lf*), and *Sulfolobus metallicus* (*Sm*) catalyze the recycling of iron(III) ions in acidic solutions.

For the case of pyrite the anodic and cathodic reactions have been reviewed. In the first step, a cathodic reaction transfers electrons from the surface of the pyrite (cathode) to the aqueous oxidant species, usually O_2 or iron(III) ions. The second step transports charge (electrons) from the site of an anodic reaction to replace the electron lost from the cathodic site. In the third step, at an anodic site, the oxygen atom of a water molecule interacts with a sulfur atom to create

a sulfoxy species. This releases an electron into the pyrite and one or two hydrogen ions to the bulk solution. These three steps occur more or less simultaneously in the actual oxidation process (Rimstidt 2003). These anodes and cathodes may be resulting from imperfections in the crystal lattice where the iron to sulfur ratio is imbalanced due to inclusion of other metal atoms during the process of crystallization and/or from variations of temperature during crystallization (causing amorphous up to highly crystalline structures).

1.4 Biodiversity of acidophilic microorganisms

Bioleaching of MS is performed by a diverse group of microorganisms (Schippers 2007; Schippers et al. 2010). Several species have been identified in bioleaching operations and AMD environments (Johnson 1998; Schippers 2007; Méndez-García et al. 2015). Leaching bacteria are distributed among the *Proteobacteria* (*Acidithiobacillus*, *Acidiphilium*, *Acidiferrobacter*, *Ferrovum*), *Nitrospirae* (*Leptospirillum*), *Firmicutes* (*Alicyclobacillus*, *Sulfobacillus*) and *Actinobacteria* (*Ferrimicrobium*, *Acidimicrobium*, *Ferrithrix*). Few fungal species like *Phanerochaete chrysosporium*, *Aspergillus niger* and *Penicillium citrinum* have been reported in bio-oxidation of gold-bearing ores or metal recovery (Acharya et al. 2002; Ofori-Sarpong et al. 2013; Yang et al. 2013). The most studied acidophilic archaea generally include the order *Thermoplasmatales* and *Sulfolobales*. To date, the only known extreme thermoacidophiles belong to the crenarchaeotal class of *Thermoprotei*, represented by the orders *Desulfurococcales*, *Thermoproteales*, *Fervidococcales*, *Acidilobales*, and *Sulfolobales*. The order *Sulfolobales* is comprised of the genera *Sulfolobus*, *Acidianus*, *Metallosphaera*, *Sulfurococcus*, *Stygioglobus*, and *Sulfurisphaera*. Only several species from the order *Sulfolobales* like *Acidianus*, *Sulfolobus* and *Metallosphaera* have been reported to be relevant for bioleaching applications (Norris 2007; Auernik et al. 2008; Pradhan et al. 2008; Wheaton et al. 2015).

The Euryarchaeota order *Thermoplasmatales*, which grow at mesophilic or moderately thermophilic conditions, are also often found in bioleaching and AMD systems (Golyshina and Timmis 2005; Golyshina 2011). The general physiology of members of *Sulfolobales* and *Thermoplasmatales* is presented in Table 1. Among those, the phylogenetic relationships of the main bacterial and archaeal species involved in bioleaching are illustrated in Fig. 2.

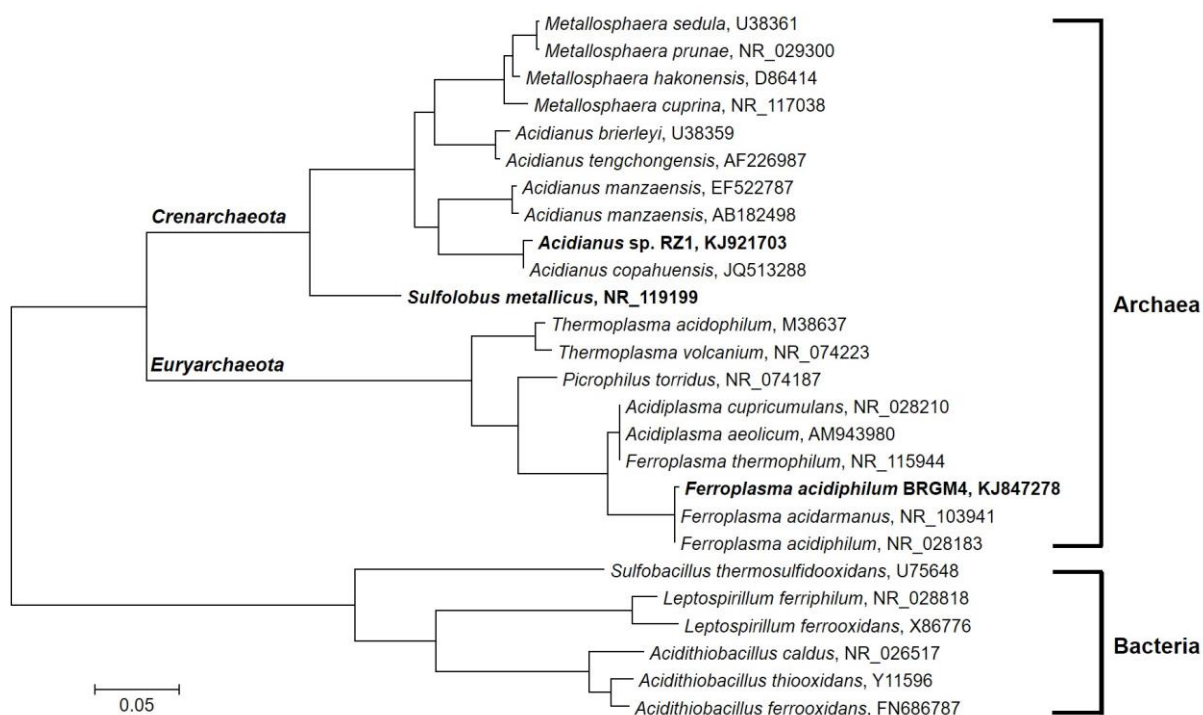**Figure 2.** Phylogenetic tree showing affiliations of acidophilic archaea and bacteria based on their 16S rRNA sequences. The GenBank accession number downloaded from NCBI database is shown after each species. The three archaeal species used in the current study are shown in bold. The scale bar represents of 5 % sequence divergence. MEGA 6 was used to construct the maximum-likelihood (ML) phylogenetic tree (Tamura et al. 2013).

Table 1. Characteristics of the acidophilic archaea *Thermoplasmales* and *Sulfolobales*. CW: cell wall. A: Aerobic. FA: Facultative anaerobic. COC: complex organic compounds. Opt.: Optimum. T°: Temperature (°C).

Species	Origin	Cell shape	CW	Relation to O_2	Energy substrates	Growth T°		Growth pH		Growth modes	References
						Opt.	Range	Opt.	Range		
Thermoplasma acidophilum (DSM1728[T])	Coal refuse pile, Indiana	Cocci	-	FA	COC, sugars	59	45-63	1-2	0.5-4	Heterotrophic	(Darland et al. 1970; Segerer et al. 1988)
Thermoplasma volcanium (DSM 4299[T])	Acid solfatara Vulcano, Italy	Irregular cocci	-	FA	COC, sugars	60	33-67	2	1-4	Heterotrophic	(Segerer et al. 1988)
Picrophilus oshimae (DSM 9789[T])	Solfatara, Hokkaido, Japan	Irregular cocci	+	Aerobic	COC, sugars	60	47-65	0.7	0-3.5	Heterotrophic	(Schleper et al. 1995)
Picrophilus torridus (DSM 9790[T])	Solfataric field Hokkaido, Japan	Irregular cocci	+	Aerobic	COC, sugars	60	47-65	0.7	0-3.5	Heterotrophic	(Schleper et al. 1995)
Ferroplasma acidiphilum (DSM 12658[T])	Bioreactor for arsenopyrite Kazakhstan	Pleomorphic	-	FA	Fe^{2+}, sulfide ores, COC, sugars	37	15-45	1.7	1.3-2.2	Mixtrophic	(Golyshina et al. 2000)
Ferroplasma acidarmanus (Fer 1)	Iron Mountain, California	Pleomorphic Irregular cocci	-	FA	Fe^{2+}, sulfide ores, COC, sugars	42	23-46	1.2	<0.2-2.5	Mixtrophic	(Edwards et al. 2000b; Dopson et al. 2004)
Ferroplasma thermophilum (L1)	Daye Copper mine, China	Cocci	-	FA	Fe^{2+}, sulfide ores, COC, sugars	45	30-60	1	0.2-2.5	Mixtrophic	(Zhou et al. 2008)

Thermogymnomonas acidicola (DSM 18835^T)	Solfataric field Hakone, Japan	Pleomorphic	-	Aerobic	COC, sugars	60	38-68	3	1.8-4	Heterotrophic	(Itoh et al. 2007)
Acidiplamsa cupricumulans (DSM 16551^T)	Chalcocite heaps, Myanmar	Irregular cocci	-	FA	Fe^{2+}, sulfide ores, COC, sugars	53.6	22-63	1-1.2	0.4-1.8	Mixtrophic	(Hawkes et al. 2006; Golyshina et al. 2009)
Acidiplasma aeolicum (DSM 18409^T)	Hydrothermal pool, Vulcano	Pleomorphic Irregular cocci	-	FA	Fe^{2+}, sulfide ores, COC, sugars	45	15-65	1.4-1.6	0-4	Mixtrophic	(Golyshina et al. 2009)
Sulfolobus acidocaldarius (DSM 639^T)	Hot spring, Yellowstone National Park	Irregular lobed	+	Aerobic	COC, sugars	70-75	55-85	2-3	1-5.9	Heterotrophic	(Brock et al. 1972)
Sulfolobus solfataricus (DSM 1616^T)	Hot spring, Pisciarelli Solfatara, Italy	Spherical irregular polyhedrons	+	Aerobic	COC, sugars	80	65-87	3	2-4	Heterotrophic	(Zillig et al. 1980)
Sulfolobus shibatae (DSM 5389^T)	Geothermal pool, Kiushu Island, Japan	Irregular cocci	+	Aerobic	COC, sugars, S^0	81	ND-86	3	ND	Heterotrophic	(Grogan et al. 1990)
Sulfolobus metallicus (DSM 6482^T)	Solfataric fields, Iceland	Irregular lobed cocci	+	Aerobic	Fe^{2+}, sulfide ores, S^0, $K_2S_4O_6$	65	50-75	ND	1-4.5	Autotrophic	(Huber and Stetter 1991)
Sulfolobus rivotincti	Rio Tinto Huelva, Spain	ND	ND	Aerobic	Fe^{2+}, sulfide ores	68.5	ND	ND	ND	Autotrophic	(Gómez et al. 1999)
Sulfolobus yangmingensis (YM1^T)	Yang-Ming National Park, Taiwan	Lobed	ND	Aerobic	COC, sulfide ores, sugars, S^0, $K_2S_4O_6$	80	65-95	4	2-6	Autotrophic or mixtrophic	(Jan et al. 1999)
Sulfolobus tokodaii (DSM 16993^T)	Hot Springs, Kyushu Island, Japan	Irregular cocci	+	Aerobic	COC, sugars, S^0	80	70-85	2.5-3	2-5	Mixtrophic	(Suzuki et al. 2002)

Sulfolobus tengchongensis (RT8-4[T])	Hot spring, Tengchong, China	Irregular cocci	ND	Aerobic	COC, sugars, S^0	85	65-95	3.5	1.7-6.5	Mixtrophic	(Xiang et al. 2003)
Acidianus brierleyi (DSM 1651[T])	Hot spring, Yellowstone National Park	Spherical, irregular polyhedrons	+	FA	Fe^{2+}, sulfide ores, COC, sugars, S^0	70	45-75	1.5-2	1-6	Autotrophic or heterotrophic	(Zillig et al. 1980; Segerer et al. 1986)
Acidianus infernus (DSM 3191[T])	Solfatara Crater, Naples, Italy	Irregular cocci	+	FA	H_2S, S^0	90	65-96	2	1-5.5	Autotrophic	(Segerer et al. 1986)
Acidianus ambivalens (DSM 3772[T])	Solfatara, Iceland	Irregular lobed cocci	+	FA	H_2S, S^0	80	70-87	2.5	1-3.5	Autotrophic	(Zillig et al. 1986; Fuchs et al. 1996)
Acidianus tengchongensis (AS 1.3347[T])	Hot spring, Tengchong, China	Irregular cocci	ND	FA	S^0, $S_2O_3^{2-}$	70	60-75	1.5-2	1-5.5	Autotrophic	(He et al. 2004)
Acidianus manzaensis (NBRC 100595[T])	Fumarole in Manza, Japan	Cocci	+	FA	S^0, COC, sugars	80	60-90	1.0-5.0	1.2-1.5	Autotrophic or Mixtrophic	(Yoshida et al. 2006)
Acidianus sulfidivorans (DSM 18786[T])	Solfatara, Papua New Guinea	Irregular cocci	+	FA	S^0, Fe^{2+}, sulfide ores	74	45-83	0.8-1.4	0.35-3	Autotrophic or Mixtrophic	(Plumb et al. 2007)
Acidianus copahuensis (DSM 29038)	Copahue geothermals, Argentina	Irregular cocci	+	FA	S^0, Fe^{2+}, sulfide ores, sugars	75	55-80	2.5-3	1-5	Autotrophic or Mixtrophic	(Giaveno et al. 2013)
Metallosphaera sedula (DSM 5348[T])	Thermal pond in Pisciarelli Solfatara, Italy	Slightly irregular cocci	+	Aerobic	Fe^{2+}, S^0, $K_2S_4O_6$, sulfide ores, COC, sugars	75	50-80	2	1-4.5	Autotrophic or Mixtrophic	(Huber et al. 1989)
Metallosphaera prunae (DSM 10039[T])	Smoldering slag heap, Thüringen	Lobed cocci	+	FA	S^0, sulfide ores, COC, sugars	75	55-80	2	1-4.5	Autotrophic or Mixtrophic	(Fuchs et al. 1995)

Metallosphaera hakonensis (DSM 7519^T)	Geothermals, Hakone National Park	Lobed	+	Aerobic	H$_2$S, Fe^{2+}, S^0, K$_2$S$_4$O$_6$, S$_2$O$_3$$^{2-}$, sulfide ores, COC, sugars	70	50-80	3	1-4	Autotrophic or Mixtrophic	(Takayanagi et al. 1996; Kurosawa et al. 2003)
Metallosphaera yellowstonensis (MK1^T)	Acidic iron mat, Yellowstone National Park	Lobed cocci	+	Aerobic	Fe^{2+}, S^0, sulfide ores, COC	65-75	45-85	2-3	1-4.5	Autotrophic or Mixtrophic	(Kozubal et al. 2008)
Metallosphaera cuprina (Ar-4^T)	Hot spring, Tengchong	Irregular cocci	ND	Aerobic	Fe^{2+}, S^0, K$_2$S$_4$O$_6$, S$_2$O$_3$$^{2-}$, sulfide ores, COC, sugars	65	55-75	3.5	2.5-5.5	Autotrophic or Mixtrophic	(Liu et al. 2011)
Stygiolobus azoricus (DSM 6296^T)	Geothermals São Miguel Island	Highly irregular cocci	+	Anaerobic	H$_2$	80	57-89	2.5-3	1-5.5	Autotrophic or Mixtrophic	(Segerer et al. 1991)
Sulfurisphaera ohwakuensis (DSM 12421^T)	Hot spring Ohwaku Valley, Japan	Slightly irregular cocci	+	FA	S^0, COC	84	63-92	2	1-5	Mixtrophic	(Kurosawa et al. 1998)
Sulfurococcus yellowstonensis (Str6kar^T)	Thermal spring, Yellow Stone National Park	Spherical	+	Aerobic	Fe^{2+}, S^0, sulfide ores, COC, Sugars	60	40-80	2-2.6	1.0-5.5	Autotrophic or Mixtrophic	(Karavaiko and Lobyreva 1994; Karavaiko et al. 1994)
Sulfurococcus mirabilis (INMI AT-49^T)	Uzon volcano, Kamchatka, Russia	Spherical	+	Aerobic	S^0, sulfide ores, COC, sugars	70-75	50-86	2-2.6	1-5.8	Autotrophic or Mixtrophic	(Golovacheva et al. 1987; Karavaiko and Lobyreva 1994)

Note:

+: with CW. -: without CW. ND: not determined

Table modified from Wheaton et al. 2015

1.4.1 The genus *Ferroplasma*

The first *Ferroplasma* species *Ferroplasma acidiphilum* was isolated from a semi-industrial bioleaching pilot plant processing gold-containing arsenopyrite from Kazakhstan (Golyshina et al. 2000). Since then, two other recognized species *Ferroplasma acidarmanus* and *Ferroplasma thermophilum* and several isolates have been reported (Okibe et al. 2003; Dopson et al. 2004; Zhou et al. 2008; Bryan et al. 2009). *Ferroplasma* spp. can oxidize iron(II) ions, MS or organic compounds to sustain growth. Although genomic data showed that *Ferroplasma* spp. possess some genes encoding enzymes probably involved in hydrogen sulfide oxidation such as sulfide:quinone oxidoreductase (SQR) and elemental sulfur (S°) oxidation such as sulfur oxygenase reductase (SOR) (Jones et al. 2014; Janosch et al. 2015), sulfur oxidation by cells of *Ferroplasma* spp. has not been reported yet. All the isolated strains are capable of growing mixotrophically and aerobically, and most of them can also grow anaerobically (Dopson et al. 2004). Anaerobic growth of *Ferroplasma* spp. occurs by coupling oxidation of organic compounds with the reduction of iron(III). Sulfate, nitrate, sulfite, thiosulfate, and arsenate are not utilized as electron acceptors. Rates of iron(III) reduction by *Ferroplasma acidarmanus* fer1 are comparable with other acidophilic heterotrophs such as *Acidiphilium acidophilum* (Dopson et al. 2007).

Ferroplasma spp. are frequently detected in various acidic man-made operations like leaching tanks/heaps and also natural habitats like AMD sites, which are considered as hostile environments (Golyshina 2011; Méndez-García et al. 2015). They are considered to be major players in global iron and sulfur cycling (Edwards et al. 2000b; Golyshina and Timmis 2005). The family *Ferroplasmaceae* received scientific attention for its lifestyle in extremely acidic environments and provided new insights into acid and metal tolerance for cells without a protective cell wall. A key explanation for *Ferroplasma* spp. flourishing in acidic environments is their membrane lipids, which are mainly

composed of caldarchaetidylglycerol tetraether-linked monolayers (Macalady et al. 2004). All enzymes analyzed in *F. acidiphilum* were stable *in vitro* in the pH range of 1.7-4.0, and had pH optima much lower than their intracellular pH, estimated to be of ~5.6. This 'pH optimum anomaly' suggests the existence of yet-undetected cellular compartmentalization providing cytoplasmic pH patchiness and low pH environments for the analyzed enzymes (Golyshina et al. 2006). *F. acidiphilum* has a unique iron-protein-dominated cellular machinery. It has been shown that most of the investigated cellular proteins of *F. acidiphilum* are iron-metalloproteins. These include proteins with deduced structural, chaperone and catalytic roles, not described as iron-metalloproteins in any other organism so far investigated. The iron atoms in the proteins seem to organize and stabilize their 3-dimensional structures, to act as 'iron rivets' (Ferrer et al. 2007). *F. acidarmanus* has a minimum inhibitory concentration (MIC) for copper of 312 mM, which is lower than the value for *At. ferrooxidans* (800 mM) but higher than the one for *Sulfolobus metallicus* (200 mM) (Baker-Austin et al. 2005; Orell et al. 2010). It is the most metal (copper)-resistant archaeon to date. It has been shown that *F. acidarmanus* fer1 uses multiple mechanisms e.g. DNA repair and protein chaperones, for resistance against high levels of copper (Baker-Austin et al. 2005). Recently, two respiratory membrane protein complexes were characterized to be involved in iron oxidation respiratory chains, functioning in the uphill and downhill electron flow pathways (Castelle et al. 2015).

Cells of *Ferroplasma* usually promote the growth and metabolic activity of some other leaching bacteria by detoxifying leaching liquors and thus contributing to the maintenance of robust bioleaching microbial communities. Although pyrite leaching by *Leptospirillum ferriphilum* was depressed by *F. acidiphilum* (strain MT17), the inclusion of *Acidithiobacillus caldus* to the mixed cultures of *L. ferriphilum* and *F. acidiphilum* resulted in higher leaching efficiencies compared to pure cultures of *L. ferriphilum* (Okibe and Johnson

2004). Recently, a study also confirmed that the addition of *F. thermophilum* improved copper concentrate dissolution by *A. caldus* and *L. ferriphilum* (Zhang et al. 2015). A metabolic model was constructed for a mixed culture of *F. acidiphilum* and *L. ferriphilum*. This metabolic model, composed of 152 internal reactions and 29 transport reactions, describes the main interactions between these species, assuming that both use iron(II) ions as energy source, and *F. acidiphilum* takes advantage of the organic compounds secreted by *L. ferriphilum* for chemomixotrophic growth (Merino et al. 2014).

1.4.2 The genus *Acidianus*

All strains of *Acidianus* are thermophiles, facultative anaerobes and capable of chemolithoautotrophy and, in some instances, facultative autotrophy. Since the genus *Acidianus* was introduced in 1986 by Segerer and coworkers (1986), seven species have been described up to now (Table 1). The first species *A. brierleyi* was characterized previously as a member of the genus *Sulfolobus* and then re-classified as *Acidianus* (Zillig et al. 1980; Segerer et al. 1986). *A. brierleyi* has an irregular coccoid shape and cell sizes between 1 to 1.5 μm in diameter. It grows between 45 and 75 °C and pH 1 to 6. Its optimum growth, however, occurs at 70 °C and pH 1.5 to 2.0. It appears as yellow-orange under aerobic conditions and greyish-black under anaerobic ones (Segerer et al. 1986). One unique feature of *A. brierleyi* is its ability to live either chemoheterotrophically on yeast extract or chemolithoautotrophically (Larsson et al. 1990). These characteristics make *A. brierleyi* an ideal microorganism for bioleaching and one of the most frequently studied thermoacidophiles for bioleaching.

Although iron oxidation by *A. brierleyi* was shown to be slower than by the mesophile *At. ferrooxidans* (Nemati and Harrison 2000a), bioleaching of pyrite, chalcopyrite or sphalerite by *A. brierleyi* showed higher efficiencies compared to mesophiles (Konishi et al. 1995; Konishi et al. 2001). The presence of *A.*

brierleyi greatly accelerated the leaching of chalcopyrite concentrate (Konishi et al. 1999). This can be due to the fact that *A. brierleyi* possessing high sulfur oxidation activity, which can effectively remove passivating layers of S^0 accumulated on the mineral surface (Zhu et al. 2011; Liang et al. 2012). In addition, temperature effect is another reason because the rate of chemical reactions generally increases with an increase in temperature. Supplementary activated carbon or sodium chloride can accelerate the chalcopyrite dissolution by *A. brierleyi* (Liang et al. 2010; Liang et al. 2012). Yeast extract supplementation also increased the pyrite dissolution rate by *A. brierleyi* (Konishi et al. 1998). UV-induced mutants of *A. brierleyi* have been obtained with an improved bioleaching efficiency for MS (Meng et al. 2007).

A. brierleyi was found to be the dominant thermophile in a bioleaching community processing chalcopyrite concentrates (Dinkla et al. 2009). Recently, *A. brierleyi* was successfully used to leach spent catalyst: apart from removing volatile impurities and increasing the surface, cells could efficiently oxidize MS and achieved a high bioleaching of a coked catalyst. In addition, the importance of the non-contact mechanism in bioleaching of spent catalyst by *A. brierleyi* was highlighted (Bharadwaj and Ting 2013).

In the case of *A. manzaensis*, leaching of chalcopyrite was suggested to occur by the cooperative action of the contact and non-contact mechanisms (Zhang et al. 2010). Cells of *A. manzaensis* grown on solid substrates such as chalcopyrite, pyrite and S^0 showed increased isoelectric points (pH 3.4-3.7) compared to the ones grown on ferrous sulfate (~ pH 2.5). Also, they were more hydrophobic and expressed more surface proteins than ferrous sulfate grown cells (He et al. 2008).

The recent described candidatus *Acidianus copahuensis* showed growth flexibility and physiological versatility (Giaveno et al. 2013). Sulfur oxidation key enzymes like SOR present in *A. brierleyi* (Kletzin et al. 2004) were also detected to be encoded in a draft genome sequence of *A. copahuensis*. Also,

homologous genes of the Fox cluster enzymes, associated with iron oxidation, were found. The presence of *aioAB* genes encoding arsenite oxidase, suggest the ability to utilize arsenite as electron donor (Urbieta et al. 2014). These genes have been reported in *Acidianus hospitalis* and *Sulfolobus tokodaii* genomes, but not in other members of *Sulfolobales*.

1.4.3 The genus *Sulfolobus*

The first species of *Sulfolobus* (*Sulfolobus acidocaldarius*) was isolated from a hot spring at Yellowstone National Park. It is an aerobic and heterotrophic thermophile. Currently, there are 7 described species within the genus *Sulfolobus* (Table 1). Although exhibiting 99.8 % identical 16S rRNA sequences of the *Sulfolobus* species, a small but significant level of genetic differentiation among the populations from Yellowstone National Park, Lassen Volcanic Park (Iceland), Uzon Caldera (Russia), and Mutnovsky Volcano (Russia) has been detected (Whitaker et al. 2003).

S. metallicus is one of the most often used thermophiles for leaching of MS. It is a thermo-acidophilic obligate aerobe with an optimal growth temperature of 65 ˚C and an optimal growth pH of 2-3. It was first isolated from a solfataric field in Krafla, Iceland (Huber and Stetter 1991), and it oxidizes iron(II) ions, reduced inorganic sulfur compounds (RISCs) (e.g. S^0, tetrathionate) and MS. *S. metallicus* is the only species of this genus, which can grow chemolithotrophically using MS or RISCs to sustain growth. Based on 16S rRNA sequences it is classified as a single phylogenetic clade inside the four groups of the genus *Sulfolobus* (Huber and Prangishvili 2006). In addition, compared to the mesophilic and moderately thermophilic archaeal and bacterial counterparts, *S. metallicus* grows at higher temperatures (~ 65 ˚C), leading to increased MS leaching rates.

Bioleaching of pyrite by *S. metallicus* was shown to be influenced by particle size and pulp density. The presence of fine particles (size fraction below 25 μm)

or high pulp density (above 18 %) apparently damaged the structure of the cells, resulting in their inability to oxidize pyrite (Nemati and Harrison 2000b; Nemati et al. 2000).

Bioleaching of chalcopyrite by *S. metallicus* is conducted in a cooperative action between attached cells which can oxidize sulfur-containing surface layers on chalcopyrite, forming thiosulfate, sulfite and bisulfite, and planktonic cells, which further oxidize these intermediate compounds to bisulfate and sulfate. Attached cells play important role in the removal of surface passivating layers. Thus, the oxidative action of iron(III) on chalcopyrite is greatly enhanced (Gautier et al. 2008). In addition, the efficient process of oxidation of residual sulfur compounds, i.e. sulfur and polysulfides, formed during the chemical dissolution of the MS, contributes to a significant increase in copper dissolution rates (Jordan et al. 2006).

1.5 Attachment, EPS and biofilm of acidophiles

Microorganisms are well known for their unique ability to thrive in different lifestyles (e.g. planktonic or sessile) and environments, even within extreme ones. The most common and widespread lifestyle of microbes on earth is in form of biofilms, which are associated colonies of microbes embedded in a matrix of EPS. Biofilms can be found as surface-associated or "floating mats", occurring in air-water interfaces. The biofilm lifestyle protects cells from environmental stress like desiccation, nutrient starvation, radiation and/or oxidative stress (Flemming and Wingender 2010). Biofilm lifestyle generally includes five stages: initial attachment, irreversible attachment, biofilm development, maturation, and dispersal (Fig. 3).
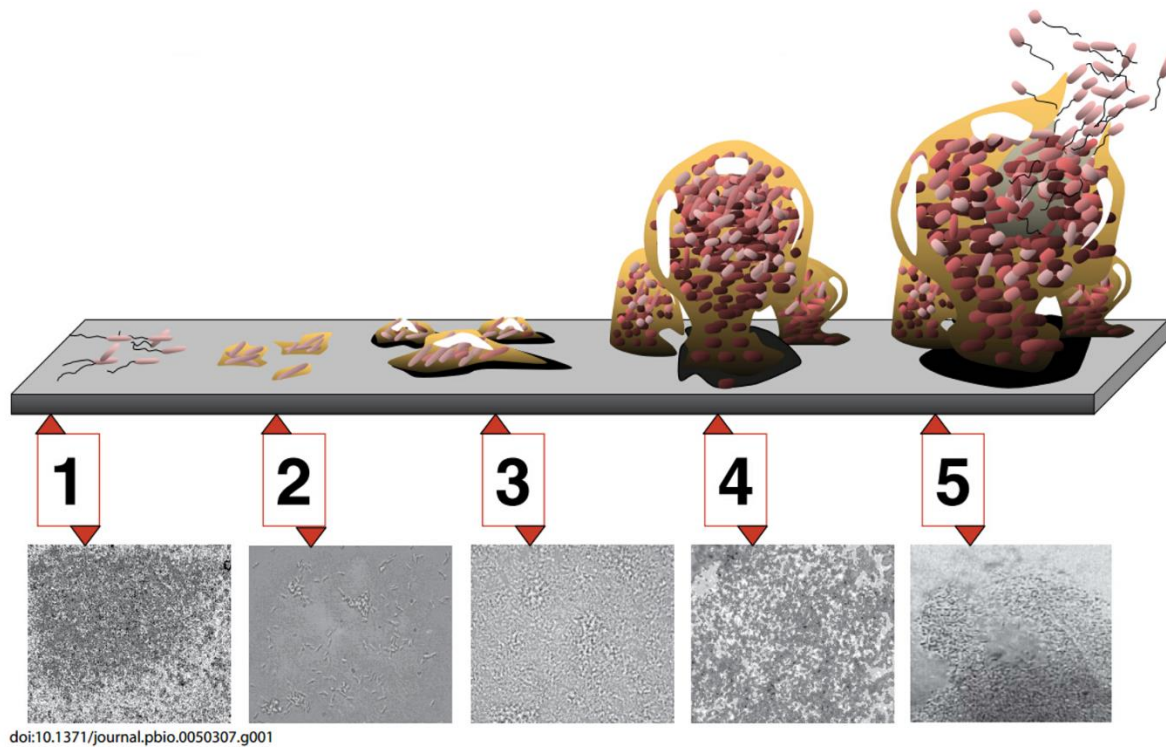
doi:10.1371/journal.pbio.0050307.g001

Figure 3. The five stages of biofilm lifestyle. The current model of biofilm development is a complex developmental process including five distinct stages. Stage 1, initial attachment; stage 2, irreversible attachment; stage 3, maturation I; stage 4, maturation II; stage 5, dispersion. Each stage of development in the diagram is paired with a photomicrograph of a developing *Pseudomonas aeruginosa* biofilm (Monroe 2007).

The EPS matrix is highly hydrated and up to 97 % of biofilm is composed of water (Zhang et al. 1998). It consists of different compounds like proteins, carbohydrates, extracellular DNA (eDNA), detritus or trace amount of metal ions. EPS enable the formation of 3-dimensional biofilm structures. They also play essential roles in mediating cellular attachment and cell-surface connections. The composition varies among different species and growth conditions (Gehrke et al. 1998; Flemming and Wingender 2010).

1.5.1 Attachment of acidophiles to surfaces

It has been shown that attachment of bioleaching microorganisms to MS surface does not occur randomly (Shrihari 1995; Dziurla et al. 1998; Edwards et al. 2001; Gehrke et al. 2001; Noël et al. 2010). Cells of *At. ferrooxidans* and other acidophiles preferentially attach to grain boundaries and sites with visible surface faults e.g. pores, cracks, etc. Cell attachment to pyrite surfaces with a low degree of crystallization seem to be favored, resulting in cell orientation along crystallographic axes, in whose direction oxidation fronts propagate (Sanhueza et al. 1999). *At. ferrooxidans* cells selectively attached to iron containing minerals pyrite or chalcopyrite but not quartz or galena (Ohmura et al. 1993; Harneit et al. 2006). Cell adhesion to pores and scratches may be due to contact area enhancement and protection from weak shear forces. In contrast, cell attachment to areas with low crystallization not often related to changes in surface topography. Therefore, the presence of some attractants may explain attachment to specific sites on the mineral surface. Several strains of *At. ferrooxidans* and *Leptospirillum ferrooxidans* have been shown to possess chemosensory systems (Acuna et al. 1992; Meyer 2002). Chemotaxis and attraction to gradients of iron(II)/(III) ions, thiosulfate and other compounds may occur compulsorily during MS dissolution. Recent work using atomic force microscopy (AFM) equipped with a Kelvin probe indicates that the cells of *L. ferrooxidans* attached to pyrite surfaces which are more negatively charged (about 100-200 mV) than the surrounding areas (Vera et al. 2013b). In a similar case, it was observed that sulfate-reducing bacteria (*Pseudomonas* sp.) attached in the immediate vicinity (nanometer range) of the anode on steel surfaces. The anode was negatively charged until a release of iron(II) ions occurred. As a consequence of bacterial attachment, the anode and the cathode became permanent (manifest), and steel dissolution commenced (Little et al. 2000).

At. ferrooxidans cells cultivated with chalcopyrite showed the strongest interaction forces with the same substrate. Those compared with the ones of

cells cultivated with iron(II) ions or S^0 were considerably lower. Also, chalcopyrite leaching efficiency and initial cell attachment rate were found to be correlated with cell adhesion forces (Zhu et al. 2015). Among the three species *At. ferrooxidans*, *Acidithiobacillus thiooxidans* and *L. ferrooxidans*, the latter one showed the highest adhesion force to chalcopyrite. EPS-deficient cells, obtained after EDTA extraction, exhibited reduced initial attachment rate and adhesion forces to chalcopyrite (Zhu et al. 2012).

It has been shown that in binary species biofilms the presence of active biofilms of iron-oxidizers may influence subsequent cell attachment by other species. *At. thiooxidans* cells attached 40 % more to pyrite precolonized with biofilms of *At. ferrooxidans* or *L. ferrooxidans*. Interestingly, its cell attachment was faster to pyrite precolonized with *L. ferrooxidans* than with *At. ferrooxidans*. As *L. ferrooxidans* leach pyrite more efficiently than *At. ferrooxidans*, the faster attachment observed for *At. thiooxidans* may be related to a chemotactic response towards RISCs like thiosulfate which are known to be released after pyrite leaching (Bellenberg et al. 2014). The analysis of the complete *At. thiooxidans* genome sequence revealed a complete suite of genes for flagellar formation and chemotaxis (Valdes et al. 2011). In contrast, the cell attachment of *At. ferrooxidans* to pyrite grains precolonized with *L. ferrooxidans* was strongly dependent on its pre-cultivation. Thiosulfate-grown cells were positively influenced by the presence of *L. ferrooxidans*, while iron(II)-grown cells were not (Bellenberg et al. 2014). Summarizing, the presence of iron oxidizers, which have been described as primary colonizers in natural AMD biofilms (Wilmes et al. 2009) may be a relevant factor for sulfur-oxidizers to efficiently attach to MS.

1.5.2 Biofilms of acidophiles

In general, acidophilic bacteria and archaea showed preferential attachment to defect sites present on S^0 surface. This has been observed for cells of *At.*

thiooxidans (Schaeffer et al. 1963), *Sulfolobus* sp. (Weiss 1973), *Thiobacillus denitrificans* (Baldensperger et al. 1974) and *At. ferrooxidans* (Espejo and Romero 1987). Cell wall components like a glycocalyx and cell appendages such as pili were found to be involved in connecting cells of *Sulfolobus* sp. and *Thiobacillus albertis* with S^0 (Weiss 1973; Bryant et al. 1983; Bryant et al. 1984; Laishley et al. 1986). Additionally, membrane blebs were visualized and these were hypothesized to aid the cells by overcoming the hydrophobic barrier necessary for their growth on S^0 (Knickerbocker et al. 2000; Crescenzi et al. 2006).

Biofilm formation and EPS production on MS have been studied for acidophilic bacteria and archaea. In general, cells are also forming monolayer biofilms and show selective attachment, preferentially to sites with crystal defects, fractures and pores. Examples of these observations include visualization of cells of *Caldariella* (a thermo-acidophilic archaeon) on pyrite or chalcopyrite (Murr and Berry 1976), *At. ferrooxidans* on pyrite or chalcopyrite (Wakao et al. 1984; Gehrke et al. 1998; Sanhueza et al. 1999; Sampson et al. 2000; Tributsch and Rojas-Chapana 2000; Lei et al. 2009; Noël et al. 2010; Bellenberg et al. 2015), *A. caldus* on pyrite (Edwards et al. 2000a) and enrichment cultures obtained from the Iron Mountain in California on pyrite surfaces (Edwards et al. 1998; Edwards et al. 1999). In contrast, an *in situ* AFM analysis of *Sulfobacillus thermosulfidooxidans* attached to pyrite indicated that cells on the surface were distributed in small clusters instead of forming a continuous biofilm. No evidence was found to suggest a preferential attachment to certain sites or a preferred orientation (Becker et al. 2011). Also, cell attachment of *Metallosphaera sedula* and *S. metallicus* show no preferential orientation. However, pyrite oxidation and pit etching were influenced by surface symmetries (Etzel et al. 2008). Interestingly, two distinct biofilm morphologies were described for an extremely acidophilic archaeon *F. acidarmanus* Fer1. A multilayer biofilm was developed on pyrite surfaces, and up to 5 mm-long

filaments were found on sintered glass spargers taken from gas lift bioreactors (Baker-Austin et al. 2010). Cells of *M. sedula* were found to be wiggling along the metal ore by epifluorescence microscopy (EFM), suggesting that cell appendages were involved in cell attachment to the ore (Huber et al. 1989). Interactions of three axenic cultures of thermophiles *A. brierleyi*, *M. sedula* and *S. metallicus* with pyrite were first documented using SEM and TEM. Several of deposited structures were formed on the pyrite surface, including sub-micron precipitates and disc-shaped structures (Mikkelsen et al. 2007).

The molecular mechanisms controlling biofilm formation in acidophilic metal/sulfur-oxidizing archaea are far less explored (Orell et al. 2013). Preliminary work on crenarchaeal biofilms on other surfaces with respect to their morphology, architecture and chemical components has been done. The first crenarchaeal biofilm analysis was described for three closely related *Sulfolobus* sp. Biofilms with "carpet-like" structures by *S. solfataricus* and *S. tokodaii* and high-density "tower-like" structures by *S. acidocaldarius* were observed (Koerdt et al. 2010). Cell appendages such as pili or flagella were proven to be involved in initial attachment of *S. solfataricus* to various surfaces, including glass, mica, pyrite and carbon-coated gold grids (Zolghadr et al. 2010). Also, three type IV pili-like cell appendages of *S. acidocaldarius* were found to be differently involved in cell colonization and biofilm formation on glass (Henche et al. 2012). The enzyme mannosidase in *S. solfataricus* was found to be important in archaeal biofilm formation and modulation of EPS composition (Koerdt et al. 2012).

Biofilm detachment as well as cell dispersal of acidophilic biofilms is still largely unknown. However, there are observations that acidophiles show such a behavior since footprints have been detected. Microbial footprints are composed mainly of EPS which are left on surfaces due to cell detachment or mechanical removal (Neu and Marshall 1990; Neu and Marshall 1991). Footprints have been described for *Thiobacillus intermedius* on iron (Telegdi et al. 1998), *At.*

ferrooxidans (Rojas-Chapana et al. 1996; Mangold et al. 2008), *Sb. thermosulfidooxidans* (Becker et al. 2011) and a mixed culture of mesoacidophilic chemolithotrophs (Ghorbani et al. 2012). It has been reported that EPS compounds like lipopolysaccharides might detach from biofilms during their maturation (Jiao et al. 2010). Recent work in our laboratory has demonstrated different dynamics of colonization, biofilm formation and cell detachment of iron-oxidizing *Acidithiobacillus* and *Leptospirillum*. In this case the biofilms formed by the latter species are stable for longer incubation periods than the ones formed by iron-oxidizing acidithiobacilli (Bellenberg & Vera, unpublished results). Probably these detachment processes form part of a response to oxidative stress caused by the presence of reactive oxygen species (ROS) (Bellenberg et al. 2015), the increase of the ionic strength and the decrease of the pH.

1.5.3 Extracellular polymeric substances of acidophiles

In case of biofilm forming cells the dissolution process occurs within the EPS layer (Fig. 4), which can be considered a reaction space filling the volume between the outer cell membrane and the surface of the MS. Tributsch and co-workers demonstrated that this distance is 10-100 nm wide (Rodriguez-Leiva and Tributsch 1988). The thickness of *At. ferrooxidans* EPS was estimated for iron(II)-grown cells by *in vivo* AFM to be 28.7 nm (±13.5) (Taylor and Lower 2008). The EPS thickness of S^0- or pyrite-grown cells *in vivo* has not been reported yet. These values probably are higher than the above mentioned ones due to the fact that EPS levels are enhanced when the bacteria are grown with solid substrates (Sand et al. 1998).

The first comprehensive EPS analysis of leaching microorganisms was done for *At. ferrooxidans* strain R1. Pyrite-grown cells had a similar EPS composition compared to iron(II)-grown cells. These EPS consist of the monosaccharides glucose, rhamnose, fucose, xylose, mannose, C12-C20 saturated fatty acids,

glucuronic acid, and iron(III) ions (Gehrke et al. 1998; Gehrke et al. 2001). However, pyrite-grown cells possessed more than ten-fold amount of EPS. The initial attachment is mainly driven by electrostatic interactions (in which most likely 2 moles negatively charged glucuronic acid residues complex 1 mole positively charged iron(III) ions resulting in a net positive charge) with the negatively charged pyrite surface (at pH 2) in sulfuric acid solution (Solari et al. 1992; Blake et al. 1994).

Cells grown on S^0 do not attach well to pyrite, since their EPS composition is different compared to pyrite-grown ones. Their EPS contain considerably less monosaccharides and lack uronic acids, resulting in a complete absence of complexed iron(III) ions or other positively charged ions. However, EPS from S^0-grown cells do possess much more fatty acids than EPS from pyrite-grown cells. Consequently, it seems that hydrophobic interactions are exclusively relevant for attachment of cells of *At. ferrooxidans* to S^0 (Gehrke et al. 1998). Cell surface charge of *At. ferrooxidans* is different from soluble iron(II)-grown cells compared to solid substrate grown ones. Cells possess a higher amount of protein when grown on insoluble substrates such as pyrite or S^0 compared to cells grown with iron(II) ions (Sharma et al. 2003). The formation of capsular polysaccharides (CPS) of *At. ferrooxidans*[T] occurred within the first 24 h of contact with pyrite (Bellenberg et al. 2012).
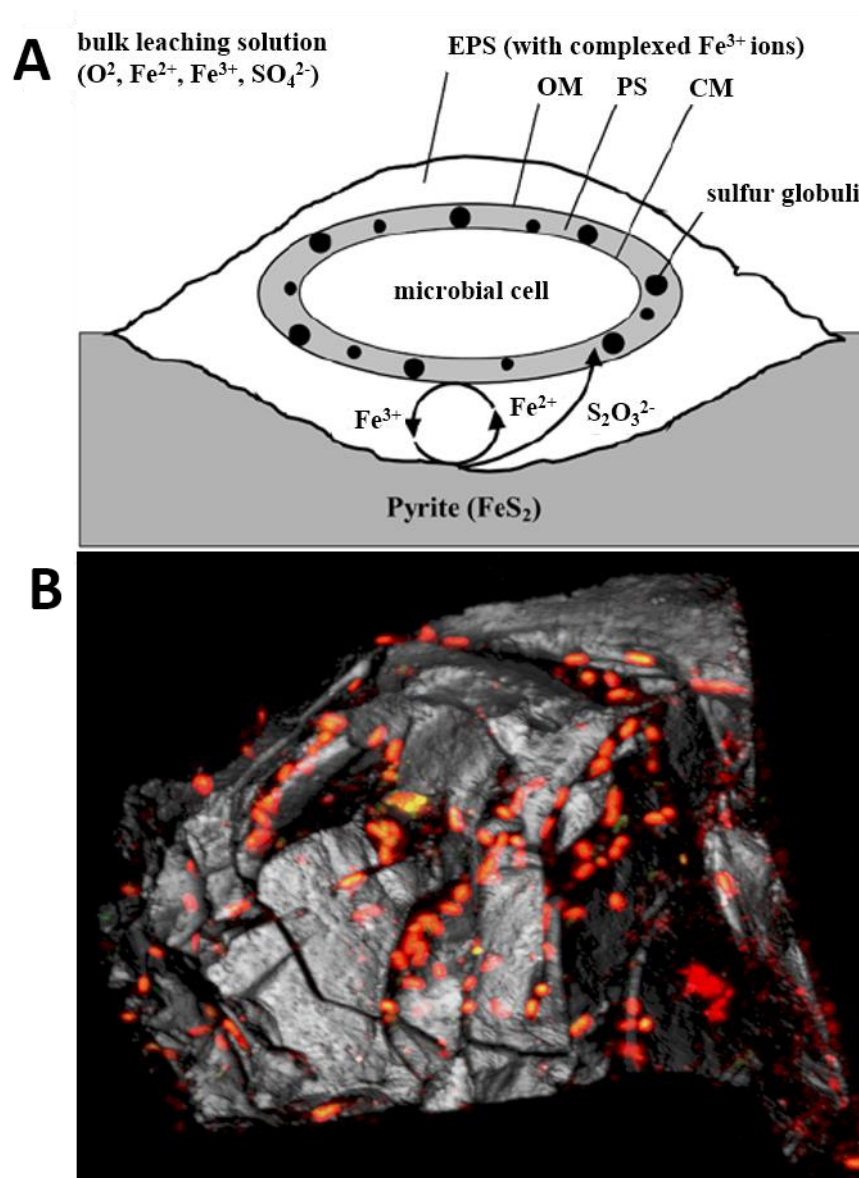
Figure 4. Model for contact leaching catalyzed by a microbial cell (modified from Vera et al. 2013b). A: Overview showing a biofilm cell embedded in the EPS layer attached to pyrite. Compounds like Iron(II)/(III) ions, thiosulfate present during MS dissolution are shown. CM, cytoplasmic membrane; PS, periplasmic space; OM, outer membrane. B: CLSM image showing a 3-D projection of a pyrite grain (50-100 μm) colonized with cells of *At. ferrooxidans*[T]. Cells were stained with Syto 9 (green) for nucleic acids and lectin Con A. Color allocation: green=Syto 9, red=/Con A-tetramethyl rhodamine isothiocyanate (TRITC), grey=reflection. The merged image from all three channels is shown.

There are several methods for extraction of EPS, these comprise physical and chemical ones. Isolation of EPS from *Acidiphilum* 3.2Sup(5) was comparatively

done by using five methods: EDTA, NaOH, ion exchange resin, heating and centrifugation. The extracted EPS mainly contained carbohydrates and proteins regardless of the extraction method. However, higher EPS amounts as well as a less degree of cell lysis were achieved by using EDTA than by the other methods. This study confirmed that both, the amount and the chemical composition of EPS, strongly depend on the applied extraction method (Tapia et al. 2009).

EPS production in stirred reactors processing cobaltiferous pyrite concentrate was studied in order to optimize bioleaching processes. Bacterial attachment and leaching efficiency were both decreased in accordance with reduced levels of EPS production under N limitation. CO_2 limitation caused a significant decrease of exopolysaccharide production (d'Hugues et al. 2008). Analyses of the EPS extracted from several continuously operated bioleaching systems indicated that the EPS consisted mainly of carbohydrates, smaller amount proteins and uronic acids (Govender and Gericke 2011). Characterization of two acidophilic microbial biofilms from Iron Mountain, California showed that their EPS were composed of carbohydrates, metals, proteins and minor quantities of DNA and lipids (Jiao et al. 2010).

Recently, several chemical mapping techniques have been used to *in situ* analyze EPS components of acidophiles. Synchrotron radiation based scanning transmission X-ray microscopy (STXM) imaging and micro X-ray fluorescence (µ-XRF) mapping have been used to study extracellular thiol groups (-SH) of *At. ferrooxidans* cells. It was shown that the -SH content of *At. ferrooxidans* grown on S^0 was four times higher than those contents of iron(II)-grown cells. These data suggest that extracellular -SH groups may play an important role in sulfur activation prior to its oxidation (Xia et al. 2013). STXM has been also used to visually analyze EPS of *At. ferrooxidans* on pyrite. The distribution of polysaccharides and proteins in biofilms was visually correlated with the optical overview. In addition, polysaccharide-rich compounds were often detected at

the pyrite-cell boundaries, while lipid- and protein-rich ones were found in the cell center regions (Mitsunobu et al. 2015).

1.6 Analytical techniques for biofilm and EPS study

1.6.1 Atomic force microscopy

AFM belongs to the group of scanning-probe microscopies (SPMs) which is based on the interactions of electron tunnelling current of a metal tip with surfaces (Binnig et al. 1982). The appearance of AFM was in the mid-1980s (Binnig et al. 1986). During the past of decades, improvement of instrumentation, sample preparation and testing conditions has enabled AFM a powerful tool to explore biological structures like cell surfaces and biological molecules (Dufrêne 2004).

The key feature of an AFM is the cantilever (Fig. 5). AFM operates by sensing the small forces acting between the sample surface and a sharp tip which is fixed on a cantilever. The interaction forces with the sample cause the cantilever to bend and deflect. The deflection of cantilever is detected by a laser beam reflected from the free end of the cantilever into a photodiode. The topographic information collected by photodiode is shown in the imaging mode in computer system with special software (e.g. JPK, Berlin) and a 3D image of the surface architecture with (near) molecular resolution is available. AFM cantilevers and tips are usually made of silicon or silicon nitride using microfabrication techniques. Also, newly developed probes are chemically functionalized, coated with bacteria or biomacromolecules for studying cell-surface interactions (Dorobantu et al. 2012). These AFM probes coated with acidophilic bacteria allow to measure interactive forces between bioleaching microorganisms and mineral surfaces (Zhu et al. 2012; Diao et al. 2014a; Diao et al. 2014b). By combination with other techniques, e.g. a Kelvin probe, relative surface potential differences and charge distributions on the surface can be measured (Vera et al. 2013b).
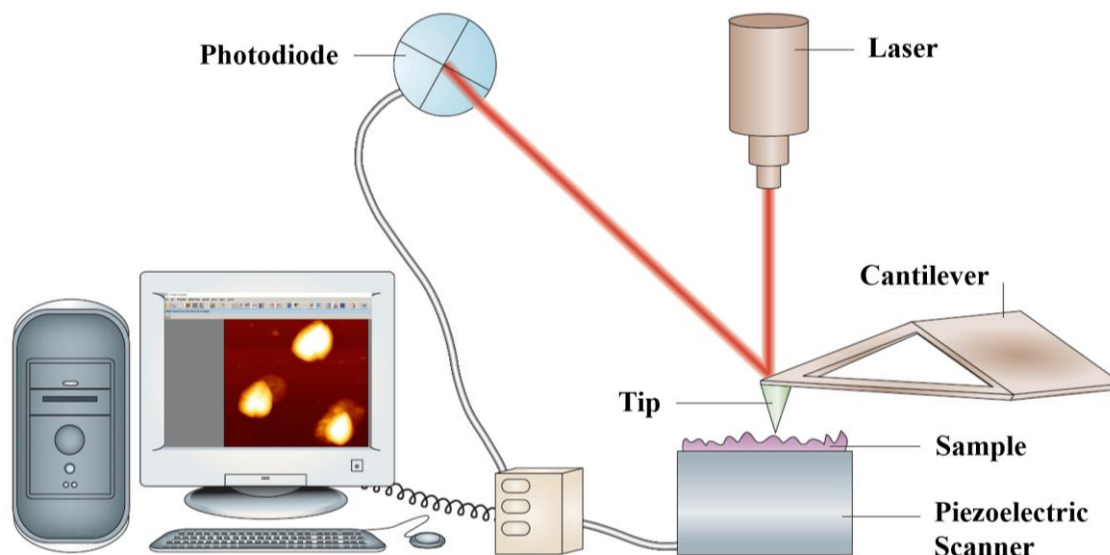
Figure 5. Schematic of AFM working principles (modified from Dufrêne 2004).

The concept of SPMs is the generation of images of surfaces by measuring the physical interaction between a sharp tip and the sample rather than by using an incident beam (light or electrons) as in classical microscopy. The main parts of an atomic force microscope are the sample stage, the cantilever and the optical detection system, which comprises a laser diode and a photodetector. The sample is moved relative to the cantilever in three dimensions using piezoelectric ceramics. The force interacting between the tip and the sample is monitored with pico-newton (10-12 N) sensitivity, by attaching the tip to a soft cantilever, which acts as a spring, and measuring the bending (or deflection) of the cantilever. The cantilever deflection is usually detected by a laser beam focused on the free end of the cantilever and is reflected into a photodiode.

1.6.2 Confocal laser scanning microscopy and Epifluorescence microscopy

CLSM in combination with fluorescent probes provide detailed 3-dimensional structure and compositional information (Lawrence et al. 2003; Neu and Lawrence 2014a). The main advantage of CLSM is its 3-dimensional sectioning capability of fully hydrated, living microbial communities. It allows multi-channel (up to 5) imaging of cellular and EPS constituents in the biofilm matrix. The digital image series or stacks recorded can be used for visualization and

quantification (Neu and Lawrence 2014b). The advantages of CLSM are flexible sample mounting (upright/inverted); high-resolution; optical sectioning; multichannel imaging; sequential/simultaneous; ideal for motile objects and fast processes; options for other light sources; imaging in deep locations; possibility to use excitation of UV fluorochromes and organic substances (Neu and Lawrence 2015).

In CLSM a biological sample is sectioned optically resulting in crisp images without a blurred signal from other optical planes. Single sections, or in most cases series of sections, are recorded as 2-dimensional images that finally will allow 3-dimensional reconstruction with the help of various imaging softwares like IMARIS (Bitplane AG, Zurich) or ImageJ (Abramoff et al. 2004). For this purpose the sample has to be stained with fluorochromes that are specific for certain compounds e.g. glycoconjugates or proteins. In addition, the autofluorescence and the reflection signals may be recorded. This enables to simultaneously visualize different biofilm compounds *in situ*.

A major characteristic of a CLSM set-up is the laser lines available for excitation of fluorochromes. The laser options for excitation include traditional gas lasers (e.g. Ar, He/Ne), laser diodes, two-photon lasers and super-continuum white light sources (Neu and Lawrence 2015). The possible wavelengths range from UV to IR (infra-red). Three laser lines at 488, 561, and 633 nm are usually available. These three lines are sufficient for most samples and cover many of the popular fluorochromes.

The potential of CLSM for complex biofilm visualization was first demonstrated by investigation of *Pseudomonas fluorescens* biofilms. This study showed that quantitative visualizations of 2D (both xy and xz), 3D, and potentially 4D (time course) reconstructions of pure and mixed-species biofilm characteristics were possible (Lawrence et al. 1991). Since then, large amount of publications on biofilm studies are available by using CLSM techniques (Neu and Lawrence 2014b).

EFM is a fast and convenient tool for visualization of complex biological samples like biofilms by fluorescence labelling of DNA, carbohydrates, proteins or lipids. However, like other light microscopes, the resolving power of EFM is limited by diffraction to half the wavelengths of the light used. Therefore, the combination of AFM & EFM takes both advantages that AFM has excellent spatial resolution, whereas EFM offers excellent biological identification properties. The combination of two microscopic techniques can be readily realized by applying a shuttle stage. This shuttle stage carries the actual sample precisely fixed on a glass slide. It could be transferred between the atomic force microscope and the epifluorescence microscope, resulting an exact positioning of the stage on both microscopes. Error of the sample location is no more than 3 to 5 μm (Mangold et al. 2008). The combination of AFM and EFM allows for confirmation of biological or chemical origins of structures at a high resolution (Mangold et al. 2008). Surface properties of minerals and their modification due to microbial activities can be recorded. In addition, the probes used (e.g. fluorescently labeled lectins) can provide additional biochemical information of the biofilm cells. The formation of monolayer biofilms as well as EPS production were found for cells of *Metallosphaera hakonensis* on chalcopyrite (Africa et al. 2013), *At. ferrooxidans* and mixed cultures of *At. thiooxidans* and *At. ferrooxidans* on pyrite (Harneit et al. 2006; Florian et al. 2010; Noël et al. 2010; Florian et al. 2011; Gonzalez et al. 2013). The biofilm formation was accompanied with the production of EPS containing mannose or glucose.

1.6.3 Fluorescence lectin-binding analysis

EPS represent a crucial part of microbial biofilms and a key element in terms of biofilm functionality (Neu and Lawrence 2009). Due to the complexity of EPS, an *in situ* approach to analyze the EPS glycoconjugates by means of fluorescence lectin binding analysis (FLBA) has been developed (Staudt et al. 2003; Peltola et al. 2008; Zippel and Neu 2011; Bennke et al. 2013; Castro et al.

2014). FLBA allows simultaneous visualization and characterization of EPS glycoconjugates based on the lectin specificities. A requirement for FLBA is that lectins shall be tested against a specific biofilm sample (Neu et al. 2001). It is necessary due to the fact that a specific biofilm is stainable only by certain lectins. Normally, this screening allows to select suitable lectins for a particular biofilm sample. Additional EPS components can be visually characterized by combination with other stains specific for proteins, nucleic acids or lipids, among others (Neu and Lawrence 2014a; Neu and Lawrence 2014b). For instance, the Syto and Sypro series are used to detect cells via their nucleic acids and cellular proteins, respectively. FM dyes (FM1-43 and FM4-64) and Nile red are specific to stain membranes and lipophilic compounds. These stains can be used also to stain extracellular compounds in biofilms (Lawrence et al. 2007; Neu and Lawrence 2014a). DDAO (7-hydroxy-9H-1,3-dichloro-9,9-dimethylacridine-2-one) stains nucleic acids and normally does not penetrate cell membranes. Thus, it has been selected as the preferred fluorochrome for staining eDNA (Koerdt et al. 2010). Combination of several types of stains allowed us to get detailed information about biofilms of acidophiles on different energetic substrates.

Lectins are a group of proteins or glycoproteins, which are capable of binding reversibly and specifically to carbohydrates without altering their structures. They are originally called "hemagglutinins", or more commonly as "phytohemagglutinins" duo to the fact that lectins can agglutinate erythrocytes (Sharon and Lis 1972; Lis and Sharon 1973). It is generally believed that Peter Hermann Stillmark first described a lectin in his doctoral thesis presented in 1888 to the University of Dorpat (now Tartu, Estonia). This hemagglutinin named ricin was highly toxic and isolated from seeds of the castor tree (*Ricinus communis*). The sugar specificity of lectins was first demonstrated by sugar inhibition tests. It was found that hemagglutination by Concanavalin A was inhibited by sucrose (Sumner and Howell 1936).

At present, more than 70 lectins are commercially available. These mainly include plant lectins and few other lectins like bacterial lectins, algal lectins, animal lectins, fungal lectins, and virus lectins. More than 200 lectin primary and 3D structures are available in the "Lectin 3D database" (http://glyco3d.cermav.cnrs.fr/search.php?type=lectin).

1.6.4 Fourier transform infrared spectroscopy

Fourier transform infrared (FTIR) spectroscopy is a technique used to obtain an infrared spectrum of absorption, emission, photoconductivity or Raman scattering of a solid, liquid or gas materials. Basically, FTIR spectrum radiation is simultaneously recorded by an interferometric system like Michelson interferometer. The signal measured at the detector which is called interferogram contains all the information of the sample over all wavelengths. The sample-spectrum is then calculated from the interferogram by fast Fourier transform (FT) techniques with elaborated mathematical algorithms.

FTIR spectroscopy offers molecular-scale information on both organic and inorganic constituents for surface characterization. It is widely used to analyze functional groups in environmental samples and also to identify microbes at the strain level according to their specific surface infra-red spectra (Naumann et al. 1991; Schmitt and Flemming 1998; Santos et al. 2010; Alvarez-Ordonez et al. 2011; Liu et al. 2015). In addition, main absorption peak ratios within a defined spectrum of a biological sample can correlate with the composition of biological materials and provide useful information on the composition of environmental biofilm samples (Nichols et al. 1985; Sheng et al. 2006).

For attenuated total reflectance (ATR)-FTIR spectroscopy, IR radiation is multiply reflected on an inner surface (Germanium or diamond) of an internal reflection element (IRE). The radiation penetrates from the IRE into the adjacent environment exponentially decays to zero within approximately 1 μm of the IRE's surface. This radiation termed an evanescent wave can be absorbed

by compounds near the surface, thus producing IR absorption bands. ATR-FTIR spectroscopy has been applied to observe biofilm forming directly on the interface of an ATR crystal. A spectrum is acquired non-destructively, *in situ* and in real time. This method is suitable for fundamental biofilm research, as well as for monitoring of bacterial adhesion and biofilm formation process (Watkinson et al. 1994; Parikh and Chorover 2006; Quilès et al. 2010).

2. Aims of the Study

To date, EPS production and biofilms of archaeal species have been investigated only to a limited extent, especially meso and thermoacidophilic ones. In addition, it is essential to visualize EPS glycoconjugates with regards to i) their identity and ii) their distribution on relevant surfaces. The analysis of EPS chemical composition may contribute to understand their function(s) in bioleaching.

The present work was focused on biofilms of acidophilic archaea with surfaces such as MS (i.e. pyrite or S^0) during bioleaching. Three representative species of iron and/or sulfur-oxidizing archaea, the mesophile *F. acidiphilum* DSM 28986 (former BRGM4), and the thermophiles *S. metallicus* DSM 6482^T and *Acidianus* sp. DSM 29099 (former RZ1), were used.

The study aimed to investigate:

(1) How is their initial attachment behavior to MS such as pyrite or chalcopyrite or S^0?

(2) What are the surface/extracellular compounds involved in the initial attachment?

(3) What are the main features of the archaeal biofilms developed on these surfaces?

(4) Which lectins bind each strain and is it feasible to use a lectin-based approach to distinguish dual-species biofilms?

(5) The composition of the EPS of these strains and how it is influenced by growth conditions e.g. different substrates such as iron(II) ions, pyrite or S^0?

3. Materials and Methods

3.1 Strains and cultivation

F. acidiphilum DSM 28986 (former BRGM4), isolated from a stirred tank reactor (Bryan et al. 2009), was kindly provided by Prof. D. B. Johnson at University of Bangor, UK. *S. metallicus* DSM 6482^T was purchased from Deutsche Sammlung von Mikroorganismen und Zellkulturen GmbH (DSMZ; Braunschweig, Germany). Strain *Acidianus* sp. DSM 29099, an iron- and sulfur-oxidizer, was isolated from a hot spring at Copahue Volcano, Neuquén, Argentina in the autumn of 2011. All strains were cultivated in Mackintosh basal salt medium (MAC) (Mackintosh 1978) containing 0.02 % yeast extract with an initial pH 1.7 for *F. acidiphilum* DSM 28986 or pH 2.5 for *S. metallicus*^{T} and *Acidianus* sp. DSM 29099, respectively. *F. acidiphilum* DSM 28986 was grown at 37 °C with 4 g/L iron(II) ions. *S. metallicus*^{T} and *Acidianus* sp. DSM 29099 were grown at 65 °C with 10 g/L S^0. Cells were cultivated aerobically either in Erlenmeyer flasks under shaking at around 120 rpm or in 5 L bottles with aeration (sterile air; ~15 L/h) and agitation at 180 rpm by placing a magnet bar in the bottle bottom.

3.2 Substratum, biofilm formation and pyrite leaching

Pyrite slices with a size of approx. 1 cm × 1 cm × 2 mm were cut from cubes (origin Navajun, Spain) by using a diamond cut-off wheel (B 127, Ø 127, thickness 0.48, arbor size 12.7 mm) in the laboratory of the Department of Material Science and Engineering. Grains were prepared by crushing and grounding pyrite crystals using a jaw-crusher (BB 1/A, Retsch, Germany) and a disc-swing-mill (HSM 100M, Herzog, 1988) in the laboratory of the Department of Geology. Pyrite grains with a size of 50-100 μm and 200-500 μm were selected by wet sieving using Retsch sieves (Retsch, Germany). Both, slices and grains, were washed with boiling 6 M HCl for 30 min, rinsed twice

with deionized water, and three times with acetone as described previously (Schippers et al. 1996). After cleaning, pyrite was dried at 80 °C for 12 h and sterilized for 24 h at 120 °C under a nitrogen atmosphere.

To produce S^0 prills and cubes, S^0 powder (Carl Roth, Germany) was molten in a glass beaker at 130 °C and poured into ice-cold deionized water with vigorous agitation (250 rpm). S^0 prills with a diameter of 1-3 mm were formed due to rapid cooling. Also, molten S^0 was poured on glass plates to obtain a S^0 layer after its solidification. S^0 coupons with a size of approx. 0.5 cm $\times$ 0.5 cm $\times$ 2 mm were obtained by manually breaking the S^0 layer. Both, S^0 prills and coupons, were autoclaved at 110 °C for 90 min.

For attachment assays, cells were harvested at 8000 rpm (11300 g) for 15 minutes at 20 °C. Cell pellets were washed and resuspended in washing solution (MAC medium supplemented with 0.2 g/L iron(III) ions). This cell suspension was kept at 17 °C for 24 h to replenish EPS. Initial cell number 2-3$\times 10^8$ cells/mL was inoculated with 10 g pyrite or S^0 in 50 mL MAC medium. Cell number was monitored for 6 h. The attached cell number was determined by subtracting the planktonic from the initial cell number. Triplicates were done for the attachment tests.

To allow biofilm formation, 20 g pyrite grains (200-500 μm) or S^0 prills were incubated with pure cultures of test organisms in 300 mL MAC medium (initial cell concentration ~1$\times 10^8$ cells/mL). In case of pyrite or S^0 coupons, 5-10 slices were placed in a 100-mL wide-neck Erlenmeyer flask containing 50 mL MAC medium. Both pyrite and S^0 substrates colonized with cells were withdrawn for staining and microscopic observations (see subchapters 3.5, 3.6 and 3.7).

For bioleaching tests, 300-mL Erlenmeyer flasks containing 5 g of pyrite grains (50-100 μm), 100 mL MAC medium (pH 1.7) and 0.2 g/L yeast extract were inoculated with pure cultures of test organisms at an initial cell number of ~1$\times 10^8$ cells/mL. Abiotic controls were also done. To determine leaching efficiency, iron ions were quantified as described in subchapter 3.3.

3.3 Cell number, pH and iron determination

The cell number in planktonic phase was determined using a Thoma counting chamber (depth = 0.1 mm, area per small square = 0.0025 m^2, Assistant, Germany) and a light microscope (Leica DMLS, Wetzlar GmbH) in phase contrast mode with 400× magnification.

The pH of samples was measured with a digital pH meter (Model pH 537, WTW, in Lab® 422 Combination Semi-micro pH Electrode, Mettler Toledo).

Iron determination was performed according to a "Phenanthroline test" (Tamura et al. 1974). Briefly, iron(II) ions and 1,10-Phenanthroline build a red colour complex, which can be determined spectrophotometrically at 492 nm. Upon addition of hydroxylamine iron(III) ions are reduced to iron(II) ions, whereby the total iron concentration was determined. Samples were measured in triplicate using a UV-VIS spectrophotometer (Cary 50, Varian INC.) equipped with software ADL Shell.

3.4 EPS extraction and chemical analysis

Planktonic cells in late exponential growth phase were separated from pyrite or sulfur prills by filtration through sterile Whatman filter paper. Cells were collected afterwards by centrifugation at 8000 rpm for 15 min. Cell pellets were washed by sterile MAC medium and freeze-dried (ALPHA 2-4 LSC, -80 °C). The supernatant was further filtrated through polycarbonate filters (GTTB, Ø2.5 cm, 0.2 μm pore size, Millipore®) to remove whole cells. These cell-free supernatants (containing "colloidal EPS") were dialyzed using a cellulose membrane (cutoff 3.5 KDa) against deionized water at 4 °C for 48 h. Dialyzed colloidal EPS solutions were further freeze-dried. Capsular EPS were extracted from cell pellets using 20 mM EDTA as described previously (Castro et al. 2014). Sulfur particles were manually milled in a mortar and incubated with 20 mM EDTA at 4 °C and shaking at 180 rpm for 4 h to extract EPS from biofilm cells. Pyrite grains were directly incubated with 20 mM EDTA to extract EPS

from biofilm cells. The extraction was repeated three times and the resulting solutions were centrifuged, filtered and dialyzed as described above.

Phenol–sulfuric acid method was used for carbohydrate determination with glucose as a standard (Dubois et al. 1956). Protein concentration was analyzed with bovine serum albumin (BSA) standard (Bradford 1976). DNA was determined using DNA from salmon sperm as a standard (Burton 1956). Cell lysis was estimated by measuring glucose-6-phosphate dehydrogenase (G6PDH) activity (Ng and Dawes 1973).

3.5 Staining

The cell biomass and spatial distribution within the biofilms on pyrite or S^0 were visualized after staining with the nucleic acid stains: DAPI (diamidino-2-phenylindole), Syto 9, Syto 61, Syto 64, SybrGreen (Invitrogen, Germany) and DDAO (7-hydroxy-9H-1,3-dichloro-9,9-dimethylacridin-2-one; Invitrogen, Germany). The detailed information of these stains are shown in subchapters 4.2 and 4.3. The cell-permeant Syto 64, a fluorescent nucleic acid stain, exhibits bright red fluorescence upon binding to nucleic acids. Pyrite or S^0 samples with attached cells were washed three times with filter-sterilized tap water. Neutralized samples were mounted in a Petri dish or in a CoverWell chamber of 20 mm in diameter with 0.5 mm spacer (Invitrogen, Germany). DDAO was incubated with samples for 20 min before CLSM observation. All other dyes were added to the washed samples and directly visualized. Direct light exposure was avoided. Stains specific for proteins, lipophilic compounds and β-polysaccharides were also tested to characterize biofilm components.

3.6 Fluorescence lectin-binding assays

Pyrite or S^0 samples were neutralized with filter-sterilized tap water and incubated with 0.1 mg/mL lectins for 20 min at room temperature in the dark. Lectin staining was done in a Petri dish or in a CoverWell chamber of 20 mm in

diameter with 0.5 mm spacer (Invitrogen, Germany). Afterwards, stained samples were washed three times with filter-sterilized tap water in order to remove unbound lectins. More than three pyrite grains or S^0 prills were checked by eye under microscope to make a decision whether a lectin bound or not bound to biofilm cells. In case of counter staining, lectin stained samples were incubated with nucleic acid/protein/lipid stains and directly observed using CLSM without any further treatment.

For staining cells from the planktonic phase, 1 mL of cultures grown for 4 days were filtered on polycarbonate filters (GTTB, Ø2.5 cm, 0.2 µm pore size, Millipore®) as described previously (Bellenberg et al. 2012) and incubated with fluorescent lectins for 20 min. After staining, cells were washed three times with filter-sterilized tap water. Filters with stained cells were then mounted using an anti-fading agent (Citifluor, Ltd. AF2) and covered by a coverslip prior to CLSM observation.

3.7 Confocal laser scanning microscopy

Examination of stained samples was performed using a TCS SP5X AOBS (Leica, Heidelberg, Germany), controlled by the LASAF 2.4.1 build 6384. The system was equipped with an upright microscope and a super continuum light source (470-670 nm) as well as a 405 nm pulsed laser diode. Images were collected with a 63× water immersion lens with a numerical aperture (NA) of 1.2 and a 63× water immersible lens with a NA of 0.9. Details of fluorescent dyes along with excitation and emission filters used are shown in subchapter 4.2. CLSM data sets were recorded in sequential mode to avoid cross talk of the fluorochromes between two different channels. Surface topography and texture of the pyrite as well as of the S^0 surface were recorded by using the CLSM in reflection mode.

3.8 Atomic force microscopy and Epifluorescence microscopy

The BioMaterial Workstation (JPK Instruments, Germany), a combination of a NanoWizard II atomic force microscope (JPK Instruments, Germany) with an upright epifluorescence microscope (AxioImager A1m, Zeiss, Germany), was used to visualize cell and EPS distribution on surfaces. For AFM imaging, a silicon cantilever CSC37-A (Mikromasch, Estonia) with the following features was used: typical length, 250 μm; width, 35 μm; thickness, 2 μm; resonance frequency, 41 kHz; and nominal force/spring constant, 0.65 N/m. Each AFM image consists of 512 by 512 or 1024 by 1024 pixels. AFM imaging was performed in contact mode in air. For visualization of morphology of planktonic cells, 20 μL of cell suspension were spread on a glass slide and cells were fixed by evaporation. For visualization of biofilm cells and EPS on pyrite slices or S^0 coupons, samples were washed three times with filter-sterilized tap water prior to staining. Cells and their EPS were stained by Syto 9 and TRITC labeled Con A, respectively as mentioned above. By using a shuttle stage, the same surface area of samples was both visualized by EFM and AFM with an error below 2 μm (Mangold et al. 2008). At least three different spots (around 100 by 100 μm) from each sample were checked and recorded by combined AFM and EFM.

3.9 Fourier transform infrared spectroscopy

Powdered cell pellets, colloidal EPS, and EPS extracted planktonic or biofilm cells were spread on a diamond attenuated total reflectance (ATR) apparatus (Pike Technologies, USA), separately attached to the FTIR. The spectra were recorded using an FTIR 430 spectrometer (JASCO, Japan). The baseline shift of blank spectra was corrected using Spectra Manager (JASCO, Japan). At least 64 scans, with a resolution of 4 cm^{-1}, were collected for all samples using the Happ-Genzel apodization function. Two measurements were done for each sample. As all cellular components possess characteristic absorbance

frequencies and primary molecular vibrations between 4000-550 wave numbers (Naumann et al. 1991), the FTIR scan was carried out in this region.

3.10 Digital image analysis

Fluorescence images were analyzed using an extended version of software ImageJ (http://imagej.nih.gov/ij/).

Maximum intensity (MIP), isosurface and XYZ projections of 3-dimensional data sets were produced with the software IMARIS version 7.3.1 (Bitplane AG, Zurich, Switzerland). In some cases, deconvolution of 3-dimensional data sets was processed to enhance the clarity of the images using Huygens ver. 14.06 (SVI, The Netherlands).

4. Results and Discussion

This part is divided into three sections according to the single publications generated within this thesis. At the beginning of each subchapter, a short interpretation of the section is given.

4.1 Biofilm formation by the extremely acidophilic archaeon *F. acidiphilum*

The genus *Ferroplasma* receives great interest with respect to their special physicological properties, e.g. extremely acidophilic and cell wall-lacking. Microbial attachment to solid substrates of acidophiles and cell surface propterties are of great importance for manipulation of bioleaching both in nature and in anthropogenic processes. In this work, we applied floating filter cultivation technique and microscopical techniques e.g. CLSM, AFM & EFM and SEM to investigate the biofilm development of *F. acidiphilum*. CLSM studies showed that biofilms were heterogeneously distributed on floating filters over time, and varied within the different growth conditions such as supplementation with glucose. Cells formed a monolayer biofilm on pyrite and were preferably attached to its surface imperfections such as cracks/defects. Biofilm and planktonic cells exhibited significant morphological differences as visualized by AFM.

Contents lists available at ScienceDirect

Hydrometallurgy

journal homepage: www.elsevier.com/locate/hydromet

CrossMark

Colonization and biofilm formation of the extremely acidophilic archaeon *Ferroplasma acidiphilum*

Ruiyong Zhang [a], Sören Bellenberg [a], Laura Castro [b], Thomas R. Neu [c], Wolfgang Sand [a], Mario Vera [a,*]

[a] Aquatische Biotechnologie, Biofilm Centre, Universität Duisburg-Essen, 45141 Essen, Germany
[b] Department of Material Science and Metallurgical Engineering, Complutense University of Madrid, Av. Complutense s/n, 28040 Madrid, Spain
[c] Department of River Ecology, Helmholtz Centre for Environmental Research-UFZ, 39114 Magdeburg, Germany

ARTICLE INFO

ABSTRACT

Ferroplasma spp. are widely distributed in acid mine drainage (AMD) and biomining environments at mesophilic and moderately elevated temperatures, at low pH and high concentrations of iron and other metal ions. Microbial attachment and biofilm formation on metal sulfides are of great importance during bioleaching. In this work, several cultivation and microscopical techniques were applied to investigate the biofilm development of *Ferroplasma acidiphilum*. Biofilms were heterogeneously distributed on filters over time, and varied within the different growth conditions such as supplementation with glucose. Additionally, cell distribution, biofilm formation as well as EPS production of *F. acidiphilum* cells forming biofilms on pyrite were observed by confocal laser scanning microscopy (CLSM), scanning electron microscopy (SEM) and atomic force microscopy (AFM) combined with epifluorescence microscopy (EFM). Cells formed a monolayer biofilm and were preferably attached to the cracks/defects of pyrite surfaces. Biofilm and planktonic cells exhibited significant morphological differences. Capsular EPS were observed in both biofilm and planktonic cells.

© 2014 Elsevier B.V. All rights reserved.

1. Introduction

The mobilization of metal cations from often almost insoluble ores by biological oxidation and complexation processes is referred to as bioleaching (Rohwerder et al., 2003). The recovery of heavy metals such as zinc, cobalt, copper and nickel by an application of microorganisms is now a widely used technique (Rawlings and Johnson, 2007). Around 20% of copper production worldwide was done by biohydrometallurgical operations in 2010 (Schippers et al., 2013). However, bioleaching can occur spontaneously in nature and cause serious environmental problems like acid mine drainage (AMD) (Hallberg, 2010). There are many species of prokaryotes that have been reported in AMD and relevant environments (Johnson and Hallberg, 2003; Schippers et al., 2010). Acidophilic archaea belonging to *Thermoplasmatales* including *Thermoplamsa, Picrophilus, Ferroplasma* and *Acidiplasma* are the most common acidophiles of all known microorganisms.

Ferroplasma acidiphilum was first isolated from a semi-industrial bioleaching reactor processing arsenopyrite in Kazakhstan (Golyshina et al., 2000). *Ferroplasma* spp. are present in various acidic man-made operations such as leaching tanks/heaps and also natural habitats, which are considered as hostile environments. The family *Ferroplasmaceae* received

scientific attention for its lifestyle in extremely acidic environments and new insights into acid and metal tolerance for cells without a protective cell wall. A key explanation for *Ferroplasma* spp. flourishing in acidic environments are their membrane lipids which are mainly composed of caldarchaetidylglycerol tetraether-linked monolayers (Macalady et al., 2004). *Ferroplasma* spp. are considered to be major players in global iron and sulfur cycling (Edwards et al., 2000; Golyshina, 2011).

Biofilms are communities of microorganisms attached to a surface embedded in extracellular polymeric substances (EPS). EPS mainly contain carbohydrates, proteins, lipids, nucleic acids and complexed metal ions (Flemming and Wingender, 2010). Attachment of microorganisms to mineral surfaces is of great importance for the process of mineral dissolution (Vera et al., 2013). Evidence showed that attachment of cells of *Acidithiobacillus ferrooxidans* to pyrite correlated with the degree of pyrite crystallization (Sanhueza et al., 1999). EPS mediate the contact between cells and metal sulfide (MS) and help to facilitate the dissolution of a MS due to ferric iron complexation, thus providing a reaction space for the chemical attack on a MS (Sand and Gehrke, 2006). EPS of *At. ferrooxidans* contain the carbohydrates glucose, rhamnose, fucose, xylose, mannose, C12–C20 saturated fatty acids, glucuronic acid, and Fe(III) ions (Gehrke et al., 1998). More than 80% of bacterial cells were attached to the non-limiting surfaces within 24 h, although less than 5% of the available surface area was colonized (Sand et al., 1998).

Archaeal biofilms are a common phenomenon and as complex as bacterial ones (Fröls, 2013; Orell et al., 2013). Some data have shown characteristics of attachment, biofilms and EPS composition of

* Corresponding author at: Universität Duisburg-Essen, Fakultät für Chemie, Biofilm Centre, Aquatic Biotechnology., Universitätsstr. 5, 45141 Essen, Germany. Tel.: +49 201 1837080; fax: +49 201 1837090.
E-mail address: mario.vera@uni-due.de (M. Vera).

Sulfolobus spp. (Koerdt et al., 2010, 2012). However, in these studies cells were grown with organic substrates and no applicable data are available for bioleaching processes. A biofilm of *Sulfolobus metallicus* was reported to develop on the support of a biotrickling filter during hydrogen sulfide/sulfur oxidation (Morales et al., 2011). A genome analysis indicated that several genes may be involved in adhesion and biofilm formation in *Metallosphaera sedula* (Auernik et al., 2008). Cells of *M. hakonensis* adhered to different MS and have maximum surface coverage at their optimal growth temperature. In addition, cells showed selective attachment to different sulfide minerals (Africa et al., 2013).

Although archaea are almost ubiquitously present in biomining ecosystems, very few investigations on acidophilic archaea for their role in bioleaching and AMD have been conducted (Brune and Bayer, 2012). In this study biofilm development of *F. acidiphilum* was examined in order to get an improved knowledge of the interaction of iron-oxidizing archaea and surfaces as well as colonization and growth on pyrite. Several microscopical techniques, including confocal laser scanning microscopy (CLSM), scanning electron microscopy (SEM) and atomic force microscopy (AFM) combined with epifluorescence microscopy (EFM) as well as the floating filter technique were used.

2. Materials and methods

2.1. Strain and cultivation

F. acidiphilum BRGM4 (DSM 28986) was isolated from a pilot-scale bioreactor (d'Hugues et al., 2008). 16S rRNA gene sequence analysis demonstrated that strain BRGM4 (GenBank accession no. KJ847278) showed sequence identity of 99% with the type strain *F. acidiphilum* Y (Golyshina et al., 2000). *F. acidiphilum* BRGM4 was cultivated in Mackintosh (MAC) medium (Mackintosh, 1978). Cells were grown at an initial pH of 1.7 in 5 L bottles containing 4 g/L iron (II) ions and 0.2 g/L yeast extract at 37 °C with agitation and aeration. For bioleaching, attachment and floating filter experiments, cells in late exponential phase were harvested by centrifugation at 8000 rpm for 15 min.

2.2. Pyrite preparation

Pyrite coupons with a size of approx. 1 cm × 1 cm × 2 mm were cut from cubes (origin Navajun, Spain). Grains with a size of 50–200 μm were selected after grinding and sieving. Both, slices and grains, were washed with boiling 6 M HCl for 30 min, rinsed with deionized water until neutral pH and three times with acetone. After cleaning, pyrite was dried at 80 °C for 12 h and sterilized for 24 h at 120 °C under a nitrogen atmosphere.

2.3. Leaching experiments

300-mL Erlenmeyer flasks containing 5 g of pyrite grains (50–100 μm grain sizes) and 100 mL of MAC medium (pH 1.7) and 0.2 g/L yeast extract were inoculated with *F. acidiphilum* BRGM4 at an initial cell number of 1.2×10^8 cells/mL. Abiotic controls were also done. Cell numbers were determined by direct microscopic counts and pH of the leachates was measured using a digital pH meter (Model pH 537, WTW). Iron ions were quantified using the phenanthroline method (according to DIN 38406-1).

2.4. Floating filter technique and CLSM

5×10^7 cells were filtered on autoclaved polycarbonate filters (GTTB, Ø 2.5 cm, 0.2 μm pore size, Millipore®) and immediately transferred to MAC medium containing 5 g/L iron (II) ions coupled with additional conditions. These included glucose supplementation (1 g/L) and P_i starvation (by incubation in MAC medium prepared without P_i). Cells grown on filters or pyrite were stained by 4′,6-diamidino-2-phenylindole (DAPI) or Sypro Red (Invitrogen). Polysaccharide moieties

were observed by using the fluorescently labeled lectins Concanavalin A (Con A) or *Limulus polyphemus* agglutinin (LPA) (EY Laboratories), respectively. The staining of biofilms on filters was conducted as previously described (Bellenberg et al., 2012). A similar procedure was applied for pyrite samples, except that samples were stained in a coverwell chamber of 20 mm in diameter and 0.5 mm in depth (Invitrogen). Freshly-stained pyrite samples were visualized by CLSM using a TCS SP5X, controlled by the LASAF 2.4.1 build 6384 (Leica, Heidelberg, Germany). The system was equipped with an upright microscope and a super continuum light source (470–670 nm) as well as a 405 nm laser diode. Images were collected with a 63× water immersion lens with a numerical aperture (NA) of 1.2 and a 63× water immersible lens with a NA of 0.9. CLSM data sets were recorded in sequential mode in order to avoid interference of the fluorochrome emission signals between two different channels. Surface topography and texture of the pyrite surface were recorded by using CLSM in reflection mode.

2.5. AFM & EFM

Pyrite slices were rinsed with sterile MAC medium and deionized water. Cells attached on pyrite coupons and their EPS were stained by Syto 9 (Invitrogen) and fluorescently labeled Con A, respectively as mentioned in Section 2.4. Stained samples were dried at room temperature and visualized by EFM (Zeiss, Germany) combined with AFM (BioMaterial™Workstation, JPK Instruments) for the investigation of cell morphology and distribution on the surfaces of pyrite coupons as described previously (González et al., 2012; Mangold et al., 2008).

2.6. SEM observations

Pyrite slices incubated with cells were rinsed with deionized water and then successively dehydrated with increasing concentrations of acetone (60%, 80% and 90%) and stored overnight at 4 °C in 90% acetone. Samples were subjected to critical-point drying and coated with graphite and gold. Specimens were examined with a JEOL JSM-6330F microscope, FE-SEM at 10 kV.

3. Results and discussion

3.1. Effects of substrates on cell morphology

Comparative studies on the cell morphology of *F. acidiphilum*, grown on iron (II) sulfate and yeast extract with or without glucose over time, were performed. Cells showed morphological variability and thus responded to defined growth conditions. As shown in Fig. 1, young cultures (3 days, early exponential phase) grown on iron (II) sulfate were characterized by irregularly shaped spherical cells. In contrast, cells taken from early stationary phase cultures (7 days) were pleomorphic. A substantial proportion of cells showed extensions with a size of 0.3–0.4 μm. These occurred more abundant in cells taken from stationary phase cultures, as compared to those cells from exponential phase cultures. With the addition of glucose (1 g/L), cells appeared to be also pleomorphic and accumulated in chains containing several cells/buds (Fig. 1b). This preference to form aggregates was possibly due to an enhanced EPS production because of glucose supplementation. A similar phenomenon of increased EPS production has been observed in *At. ferrooxidans* after addition of glucose or galactose (Bellenberg et al., 2012). *F. acidiphilum* proliferates via budding (Golyshina et al., 2000). Buds were observed in both, planktonic and biofilm cells. Iron (II) sulfate grown cells in the exponential phase varied from 1.1 to 2.5 μm with bud sizes ranging from 0.3 to 0.6 μm, while cells in stationary phase were between 0.3 and 2.8 μm, with bud sizes ranging from 0.3 to 0.8 μm. Pyrite-attached cells showed morphological differences compared to planktonic cells (Fig. 2). They were slightly rod-shaped with an approximate size of 0.7 × 1.2 μm. *Ferroplasma*, *Acidiplasma* and *Thermoplasma*, unlike other archaeal genera, lack a cell wall (Albers
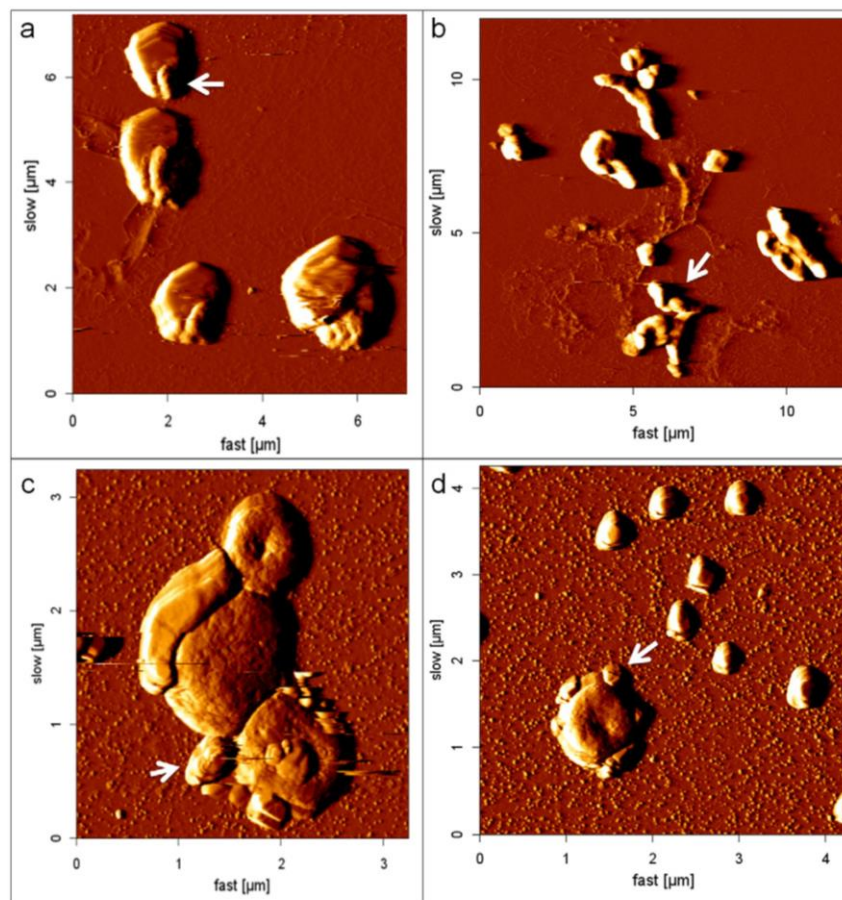
Fig. 1. Planktonic cells of *F. acidiphilum* grown on iron (II) ions visualized by AFM on glass (a, 3 days. b, 3 days, addition of glucose. c and d, 7 days). Arrows show cell buds.

and Meyer, 2011; Golyshina et al., 2009). Their cytoplasmic membrane is the only structural barrier against the surrounding environment. Consequently, environmental influences, such as variations in pH value and ion concentrations, directly affect the cell membrane. In addition, due to the fluidity of lipid membranes it is not surprising that cells of *F. acidiphilum* exhibit pleomorphy in planktonic state, when grown with different energy sources. Simultaneously, it is likely that biofilm cells displayed relatively homogeneous morphology on pyrite due to the support of the solid surface for maintenance of cell structures. Interferences on the AFM images were observed in the case of scanning cells from 7 days old cultures or cells grown with addition of glucose to the medium (Fig. 1b and c). These distortions are normally observed if high amounts of EPS are surrounding the cells (Mangold et al., 2008). This result seems to indicate that iron grown cells in the early stationary phase or with glucose supplementation produce more EPS than cells in early exponential phase. This finding also agrees with early reports that archaeal cells of *Haloferax* and *Sulfolobus* produce increased amounts of EPS over time (Antón et al., 1988; Nicolaus et al., 1993). EPS from cell-wall lacking archaea relevant to bioleaching have not been reported. N-glycosylation of surface proteins in acidophilic archaea is essential for these organisms to survive in the extremely acidic conditions. N-linked glycans and glycoproteins are key surface components of *T. acidophilum* (Vinogradov et al., 2012). *F. acidiphilum* BRGM4 might possess such functional groups (e.g. glycans) covalently attached to the proteinaceous layer or their membrane and the production of

these extracellular components might be dependent on substrate availability. In addition, it has been shown that cell appendages (e.g. pili or flagella) are involved in *S. solfataricus* attachment to surfaces (Zolghadr et al., 2010). However, with the techniques applied we could not obtain clear evidences of the presence of similar cell appendages in *F. acidiphilum* BRGM4.

3.2. Bioleaching of pyrite

Strains of *Ferroplasma* have been shown to oxidize MS (e.g. pyrite or chalcopyrite) in pure culture (Okibe et al., 2003; Zhou et al., 2008) in the presence of trace amounts of yeast extract. Since cells of *F. acidiphilum* BRGM4 are not able to grow on 0.02% yeast extract as unique energy source (not shown), we tested growth on pyrite plus 0.02% yeast extract as energy source (Fig. 3). In the non-inoculated cultures (sterile control), around 0.06 g/L of total iron was measured at the end of the experiments (Fig. 3). Obviously, pyrite dissolution was accelerated by strain BRGM4. However, a low overall pyrite oxidation was observed, with 0.9 g/L of total iron ions released and a final pH of 1.2 after 45 days, although cell numbers reached 10^9 cells/mL. By comparison, cells of *F. acidiphilum* BRGM4 had approximately 20 or 29 times lower pyrite oxidation rates than the ones for the iron-oxidizing bacterium *Leptospirillum ferriphilum* (Florian et al., 2011; Zhang et al., 2010) or the thermoacidophilic archaeon *Acidianus* RZ1 (unpublished results), respectively. *Ferroplasma* spp. need to consume considerable metabolic resources in order to
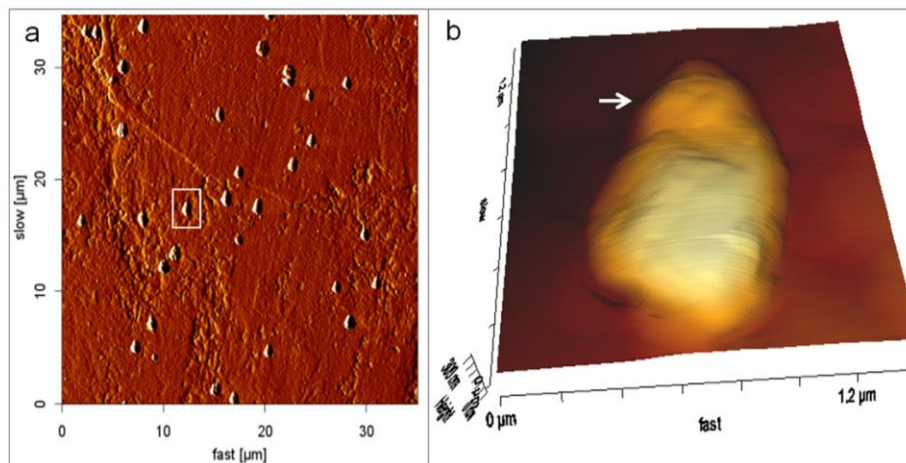
Fig. 2. Biofilm cells of *F. acidiphilum* on pyrite visualized using AFM (a, an overview of cells attached to pyrite; b, 3-D image of a single cell corresponding to the white frame in a). The arrow in (b) shows a cell bud.

survive in extremely acidic environments (Golyshina et al., 2006). The observed linear increase in cell numbers suggests that the attached cell population was actively dividing. As *F. acidiphilum* cannot oxidize the reduced inorganic sulfur compounds (RISCs), the planktonic cell subpopulation may have a reduced metabolic activity. However, this assumption needs further biochemical evidence.

Field emission SEM (FESEM) observations showed that the pyrite surfaces had rough areas and flat surfaces (Fig. S1). These rough surfaces are probably caused by the attack from ferric iron ions complexed in the EPS of *F. acidiphilum* BRGM4 cells and bulk solution. In contrast, the grains which appeared as not degraded by cells showed a relatively high light reflection by means of CLSM (not shown). Heterogeneous dissolution of pyrite by *At. ferrooxidans* was observed in the previous studies using SEM (Bennett and Tributsch, 1978; Edwards et al., 2001).

3.3. Biofilm formation on polycarbonate filters

Cells of *F. acidiphilum* grown on polycarbonate filters were visualized by CLSM combined with fluorescent probes for staining nucleic acids or glycoconjugates of their EPS. Cells were distributed relatively homogeneously on the filters (not shown) and were, due to the pore size, not able to penetrate through filters into the bulk solution. The spatial development of biofilm over time is shown in Fig. 4. The lectin Con A, recognizing ß-(1,3)-linked mannose and glucose residues of polysaccharides, was used to stain glycoconjugates as a major part of the EPS of *F. acidiphilum* BRGM4. After 1 day of incubation, cells showed Con A signal overlapping with DAPI signal. Thus, cells showed an EPS production at the early stage of biofilm formation, probably due to the contact with surfaces. Multilayered biofilms with a thickness of up to 20 µm were observed after 5 days of incubation. In contrast to the reports on *At. ferrooxidans* (Bellenberg et al., 2012), an enhancement of biofilm formation under Pi starvation was not observed (Fig. 4d). Mechanisms of response to Pi starvation have been described in *At. ferrooxidans* (Vera et al., 2003). As a canonical Pho regulon is absent in archaea, it is unclear how *Ferroplasma* spp. cells respond to Pi starvation. Interestingly, aggregates/microcolonies of approximately 20 µm in diameter were observed, when glucose was added (Fig. 4e). In the case of biofilms on filters, Con A signals were not only observed for the cells but also extended around the cells on the filters. In contrast, the Con A signal was restricted only to cell shapes of *F. acidiphilum* on pyrite surfaces (Figs. 2 and 6). This suggests that cells of *F. acidiphilum* are able to modify their biofilm formation and EPS production patterns in response to energy substrates. As CLSM
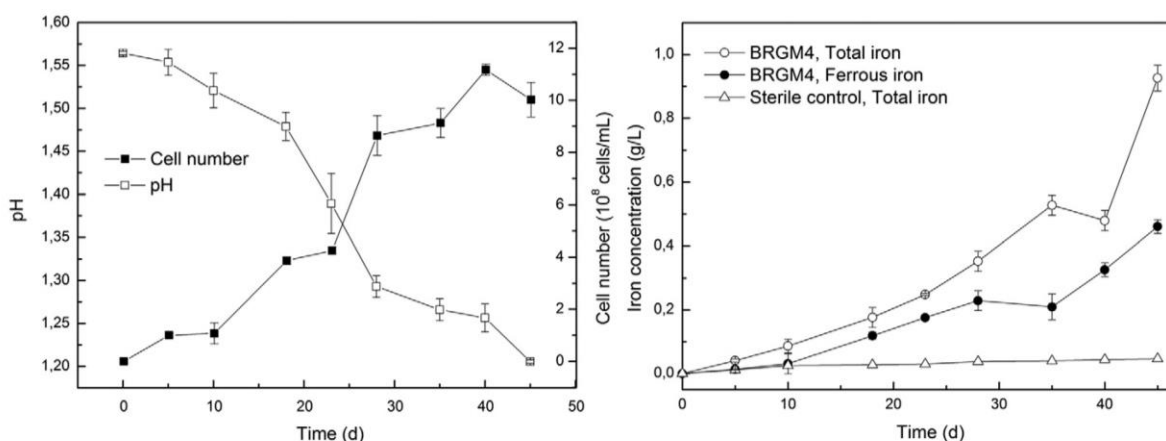

Fig. 3. Bioleaching of pyrite by cells of *F. acidiphilum*. Changes in pH and cell growth over time in flask cultures (left) and concentration of Fe(II) and Fe total dissolved over time (right). All measurements were performed in triplicate.
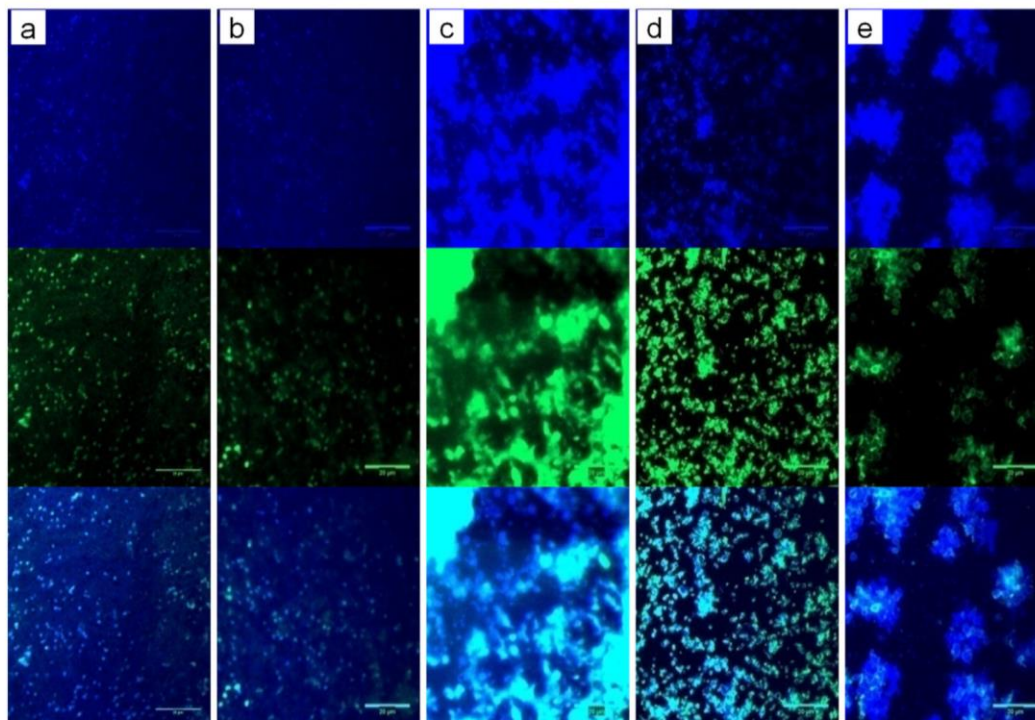
Fig. 4. Biofilms of *F. acidiphilum* on polycarbonate filters visualized by CLSM. In the upper and middle row of images, the signals from DAPI (blue) and Con A (green) are shown, while the images in the bottom row represent the merged images from both channels. Pictures a, b and c show cells after 1, 2 and 5 days of incubation on iron (II) sulfate. Cells grown under P_i starvation (d) and cells grown mixotrophically with glucose supplementation (1 g/L) (e) are shown. Bars represent 20 μm.

can collect 3 dimensional image series of a fully hydrated sample, information on the EPS production of cells at different locations becomes available (Neu et al., 2010). The upper layer of biofilm cells on floating filters showed a considerable reduced Con A signal compared to the ones in contact with the surface, as indicated in Fig. 5. Thus, it is apparent that cells synthesize more EPS when they are exposed to surfaces. Within the multilayered biofilms on polycarbonate filters or monolayered biofilms on pyrite, polymers containing mannose and glucose were present. *F. acidiphilum* was first described to be an obligately

chemoautotrophic archaeon capable of oxidizing iron (II) ions. However, yeast extract and/or some vitamins are required for the cell growth. Later studies indicated that all *Ferroplasma* strains can grow heterotrophically, consequently they have to be considered as mixotrophs (Dopson et al., 2004). After several transfers to a medium with decreased iron (II) concentrations and increased sugar amounts we were able to obtain heterotrophically growing *F. acidiphilum* BRGM4 cultures. They utilized glucose as energy source and cell numbers reached 4×10^8 cells/mL in 8 days. In addition, cells were 2–3 times larger than iron (II) ion-grown ones (not
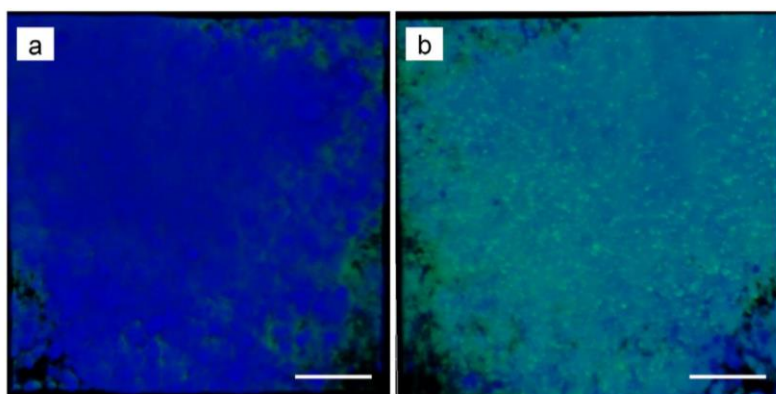

Fig. 5. CLSM images of biofilms of *F. acidiphilum* grown on iron (II) sulfate for 5 days on polycarbonate filters. Samples were stained by DAPI and fluorescently labeled Con A, respectively. Merged channels from both DAPI (blue) and Con A (green) are shown. (a) View from the upper layer biofilms facing air. (b) View from the underlayer biofilms in contact with polycarbonate surface. Bar represents 20 μm.

shown). There is evidence from *At. ferrooxidans* that glucose and galactose can be incorporated into capsular polysaccharides and cause an increased biofilm formation (Barreto et al., 2005; Bellenberg et al., 2012). In the case of cells of *F. acidiphilum* BRGM4, glucose may be used for the production of EPS to allow the cells to adsorb to polycarbonate surfaces. Bacteria produce diffusible extracellular signaling molecules, e.g., N-acylhomoserine lactones (AHLs) and oligopeptides, to monitor their own population density and to coordinate the expression of specific sets of genes in response to the cell density. The communication in biomining bacteria via AHLs is thought to be a widespread phenomenon and involved in cell-mineral interactions and biofilm formation (González et al., 2012; Ruiz et al., 2008). As expected, we did not detect any AHLs in pure culture of *F. acidiphilum* BRGM4 (not shown). This agrees with the previous findings in *F. acidarmanus* (Baker-Austin et al., 2010).

3.4. Attachment to and biofilm formation on pyrite

A combination of AFM and EFM has been used for visualization of surfaces with the advantage of high resolution and of identification of biological specimens (Mangold et al., 2008). As shown in Fig. 6, after attachment of cells to a pyrite surface a monolayer biofilm was formed. A similar behavior has been reported previously for acidophilic bacteria (Mangold et al., 2008; Noël et al., 2010). Biofilms formed by heterotrophic prokaryotes or phototrophs usually consist of dynamic, multilayer structures that can grow to three-dimensional macro-communities (Stoodley et al., 2002). In contrast, leaching
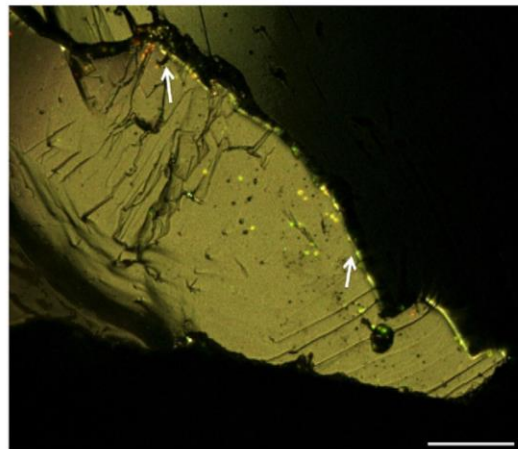
Fig. 7. CLSM image showing a maximum projection of a pyrite grain (200–500 mesh) colonized with cells of *F. acidiphilum* after 7 days of incubation. Cells were double stained with SyproRed (red) specific for proteins and fluorescent labeled LPA (green) specific for sialic acid residues in polysaccharides. Signals from both fluorescent channels plus light reflection (to image the pyrite grain surface) were recorded; the merged image from all three channels is shown. As indicated by arrows, the cell colonization pattern strongly correlates with surface imperfections/topographic defects. Bar represents 10 μm.
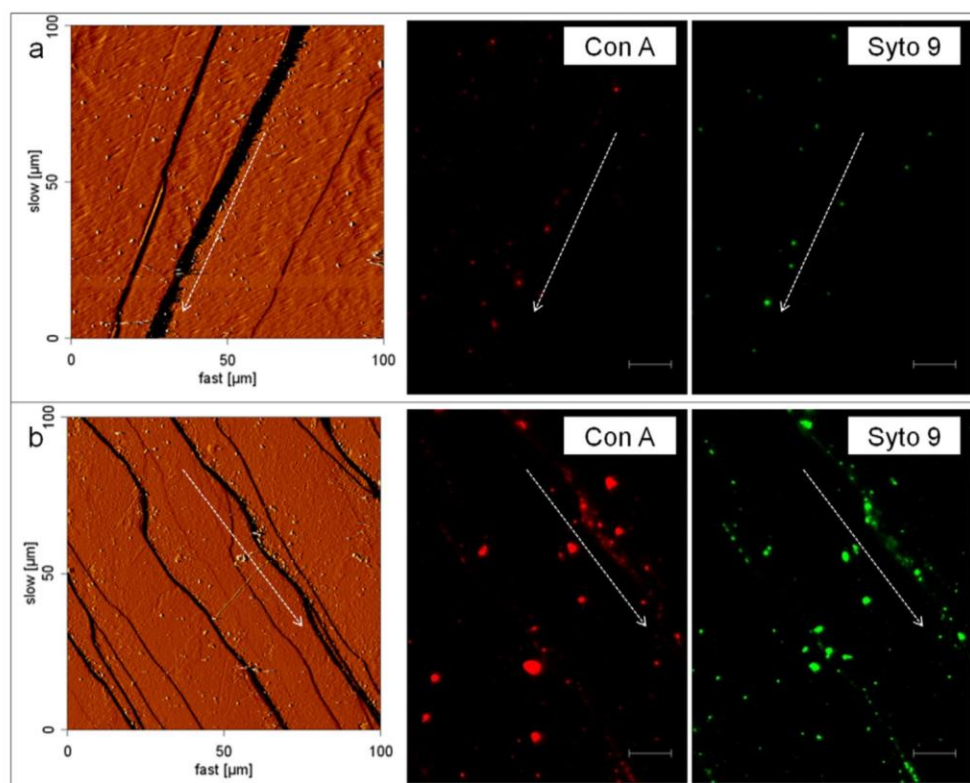
Fig. 6. Biofilm cells of *F. acidiphilum* on pyrite (a, 5 h and b, 7 days) visualized by AFM (left) and EFM (Con A and Syto 9 staining, right). Arrows show cell attachment to cracks or imperfections. Bars represent 10 μm.
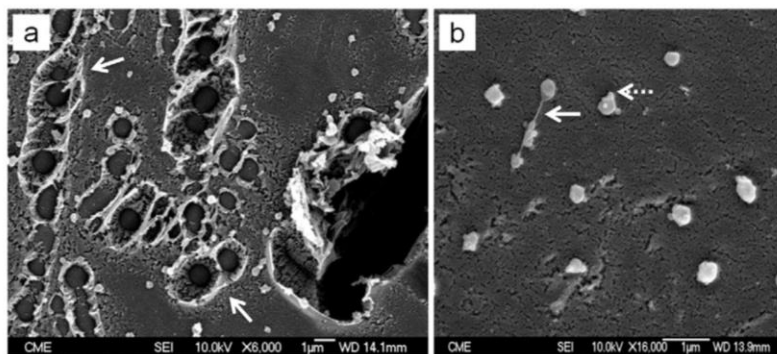
Fig. 8. SEM images of surfaces of a pyrite slice after 1 month of bioleaching with *F. acidiphilum*. Arrows in the left image (a) show isolated or connected pits. Arrows in the right image (b) show threads connecting cells (solid arrow) and cell buds (dash arrow), respectively.

microorganisms mainly develop monolayer biofilms on MS surfaces. These microbes attach to the surface of a MS in order to obtain energy by metabolizing compounds released during the dissolution of mineral substrates. Two distinct biofilm morphologies were described in *F. acidarmanus* Fer1: A multilayer film was formed on pyrite surfaces after 38 days and up to 5 mm-long filaments were found on the sintered glass spargers in the gas lift bioreactors (Baker-Austin et al., 2010). Thus, the attachment of *Ferroplasma* spp. to surfaces and the subsequent biofilm formation vary among the species, as described for other leaching bacteria (Ghauri et al., 2007).

Cells started colonizing pyrite within the first 5 h of incubation (Fig. 6a) and showed overlapping Syto 9 and Con A signals. This suggests that glycoconjugates were produced by the attached cells. Preferential attachment was observed along topographical faults/cracks of the pyrite surface (Fig. 6, arrows), a phenomenon also described for other leaching bacteria (Florian et al., 2010; Mangold et al., 2008; Noël et al., 2010). CLSM data of fully hydrated samples confirmed this phenomenon (Fig. 7). Obviously, large parts of the pyrite surfaces ($\geq$80%) remained free of cells. Low coverage of pyrite with *F. acidiphilum* cells seems to be correlated to their limited pyrite leaching ability.

SEM was also applied to investigate the distribution of cells of *F. acidiphilum* on pyrite. As shown in Fig. 8, after 1 month of cultivation few cells were attached to pyrite. Extensive pits were found, which were heterogeneously distributed over the pyrite surface and often cell-shaped (1–2 μm in diameters). These pits were either isolated or connected to form long chains of pits. Similar dissolution patterns of pyrite have been reported in the previous studies (Edwards et al., 2001; Rodriguez-Leiva and Tributsch, 1988).

Biofilm formation and propagation occur by three different mechanisms: (1) the redistribution of surface-attached but motile cells, (2) the multiplication of attached cells and (3) attachment of cells from the bulk aqueous phase (Stoodley et al., 2002). Attached cells with buds were visible, as indicated in Fig. 8b (dash arrow). In addition, threads connecting cells, which probably correspond to shrunken EPS due to the dehydration during sample preparation (e.g. acetone treatment) were also evident (Fig. 8b, solid arrow). The production of EPS by *F. acidiphilum* BRGM4 was observed by fluorescent lectin-binding analysis (FLBA) and various glycoconjugates in biofilm cells were detected (unpublished data). The lectins showing a positive signal had specificities for e.g. mannose and glucose. These sugar monomers have been found also in EPS of other acidophilic bacteria (Gehrke et al., 1998; Harneit et al., 2006). In case of SEM observations, cells seem to appear slightly deformed and contracted to relatively small sizes (0.3–0.5 μm) (Fig. 8). Hence, various combined microscopical techniques are needed to reveal details of the complex interfacial interactions between archaeal cells and surfaces.

4. Conclusions

This study aimed at providing a better understanding of interfacial interactions between cells of the acidophilic archaeon *F. acidiphilum* and surfaces. Attachment and subsequent biofilm formation were investigated on polycarbonate and pyrite surfaces by various microscopical techniques. Cells of *F. acidiphilum* BRGM4 grew heterogeneously on filters over time and seem to modify their biofilms according to the substrate (e.g. glucose supplementation). EPS were evident in *F. acidiphilum* BRGM4 biofilms on pyrite and polycarbonate filters. Low coverage of the pyrite surface by cells seems to correlate with their low leaching ability. Bioleaching conducted by *F. acidiphilum* occurs possibly via combined contact and non-contact mechanisms.

Supplementary data to this article can be found online at http://dx.doi.org/10.1016/j.hydromet.2014.07.001.

References

Africa, C.J., van Hille, R.P., Sand, W., Harrison, S.T., 2013. Investigation and in situ visualisation of interfacial interactions of thermophilic microorganisms with metal-sulphides in a simulated heap environment. Miner. Eng. 48, 100–1017.
Albers, S.-V., Meyer, B.H., 2011. The archaeal cell envelope. Nat. Rev. Microbiol. 9, 414–426.
Antón, J., Meseguer, I., Rodriguez-Valera, F., 1988. Production of an extracellular polysaccharide by *Haloferax mediterranei*. Appl. Environ. Microbiol. 54, 2381–2386.
Auernik, K.S., Maezato, Y., Blum, P.H., Kelly, R.M., 2008. The genome sequence of the metal-mobilizing, extremely thermoacidophilic archaeon *Metallosphaera sedula* provides insights into bioleaching-associated metabolism. Appl. Environ. Microbiol. 74, 682–692.
Baker-Austin, C., Potrykus, J., Wexler, M., Bond, P.L., Dopson, M., 2010. Biofilm development in the extremely acidophilic archaeon 'Ferroplasma acidarmanus' Fer1. Extremophiles 14, 485–491.
Barreto, M., Gehrke, T., Harneit, K., Sand, W., Jedlicki, E., Holmes, D., 2005. Unexpected insights into biofilm formation by *Acidithiobacillus ferrooxidans* revealed by genome analysis and experimental approaches. In: Harrison, S.T.L., Rawlings, D.E., Petersen, J. (Eds.), Proceedings of the 16th International Biohydrometallurgy Symposium. Compress, Cape Town, South Africa, pp. 25–29.
Bellenberg, S., Leon-Morales, C.F., Sand, W., Vera, M., 2012. Visualization of capsular polysaccharide induction in *Acidithiobacillus ferrooxidans*. Hydrometallurgy 129–130, 82–89.
Bennett, J., Tributsch, H., 1978. Bacterial leaching patterns on pyrite crystal surfaces. J. Bacteriol. 134, 310–317.
Brune, K.D., Bayer, T.S., 2012. Engineering microbial consortia to enhance biomining and bioremediation. Front. Microbiol. 3, 203.
d'Hugues, P., Joulian, C., Spolaore, P., Michel, C., Garrido, F., Morin, D., 2008. Continuous bioleaching of a pyrite concentrate in stirred reactors: population dynamics and exopolysaccharide production vs. bioleaching performance. Hydrometallurgy 94, 34–41.

Dopson, M., Baker-Austin, C., Hind, A., Bowman, J.P., Bond, P.L., 2004. Characterization of *Ferroplasma* isolates and *Ferroplasma acidarmanus* sp. nov., extreme acidophiles from acid mine drainage and industrial bioleaching environments. Appl. Environ. Microbiol. 70, 2079–2088.

Edwards, K.J., Bond, P.L., Gihring, T.M., Banfield, J.F., 2000. An archaeal iron-oxidizing extreme acidophile important in acid mine drainage. Science 287, 1796–1799.

Edwards, K.J., Hu, B., Hamers, R.J., Banfield, J.F., 2001. A new look at microbial leaching patterns on sulfide minerals. FEMS Microbiol. Ecol. 34, 197–206.

Flemming, H.C., Wingender, J., 2010. The biofilm matrix. Nat. Rev. Microbiol. 8, 623–633.

Florian, B., Noël, N., Sand, W., 2010. Visualization of initial attachment of bioleaching bacteria using combined atomic force and epifluorescence microscopy. Miner. Eng. 23, 532–535.

Florian, B., Noël, N., Thyssen, C., Felschau, I., Sand, W., 2011. Some quantitative data on bacterial attachment to pyrite. Miner. Eng. 24, 1132–1138.

Fröls, S., 2013. Archaeal biofilms: widespread and complex. Biochem. Soc. Trans. 41, 393–398.

Gehrke, T., Telegdi, J., Thierry, D., Sand, W., 1998. Importance of extracellular polymeric substances from *Thiobacillus ferrooxidans* for bioleaching. Appl. Environ. Microbiol. 64, 2743–2747.

Ghauri, M.A., Okibe, N., Johnson, D.B., 2007. Attachment of acidophilic bacteria to solid surfaces: the significance of species and strain variations. Hydrometallurgy 85, 72–80.

Golyshina, O.V., 2011. Environmental, biogeographic, and biochemical patterns of archaea of the family *Ferroplasmaceae*. Appl. Environ. Microbiol. 77, 5071–5078.

Golyshina, O.V., Pivovarova, T.A., Karavaiko, G.I., Kondratéva, T.F., Moore, E., Abraham, W.-R., Lünsdorf, H., Timmis, K.N., Yakimov, M.M., Golyshin, P., 2000. *Ferroplasma acidiphilum* gen. nov., sp. nov., an acidophilic, autotrophic, ferrous-iron-oxidizing, cell-wall-lacking, mesophilic member of the *Ferroplasmaceae* fam. nov., comprising a distinct lineage of the Archaea. Int. J. Syst. Evol. Microbiol. 50, 997–1006.

Golyshina, O.V., Golyshin, P.N., Timmis, K.N., Ferrer, M., 2006. The 'pH optimum anomaly' of intracellular enzymes of *Ferroplasma acidiphilum*. Environ. Microbiol. 8, 416–425.

Golyshina, O.V., Yakimov, M.M., Lünsdorf, H., Ferrer, M., Nimtz, M., Timmis, K.N., Wray, V., Tindall, B.J., Golyshin, P.N., 2009. *Acidiplasma aeolicum* gen. nov., sp. nov., a euryarchaeon of the family *Ferroplasmaceae* isolated from a hydrothermal pool, and transfer of *Ferroplasma cupricumulans* to *Acidiplasma cupricumulans* comb. nov. Int. J. Syst. Evol. Microbiol. 59, 2815–2823.

González, A., Bellenberg, S., Mamani, S., Ruiz, L., Echeverría, A., Soulère, L., Doutheau, A., Demergasso, C., Sand, W., Queneau, Y., 2012. AHL signaling molecules with a large acyl chain enhance biofilm formation on sulfur and metal sulfides by the bioleaching bacterium *Acidithiobacillus ferrooxidans*. Appl. Microbiol. Biotechnol. 97, 3729–3737.

Hallberg, K., 2010. New perspectives in acid mine drainage microbiology. Hydrometallurgy 104, 448–453.

Harneit, K., Göksel, A., Kock, D., Klock, J.H., Gehrke, T., Sand, W., 2006. Adhesion to metal sulfide surfaces by cells of *Acidithiobacillus ferrooxidans*, *Acidithiobacillus thiooxidans* and *Leptospirillum ferrooxidans*. Hydrometallurgy 83, 245–254.

Johnson, D.B., Hallberg, K.B., 2003. The microbiology of acidic mine waters. Res. Microbiol. 154, 466–473.

Koerdt, A., Gödeke, J., Berger, J., Thormann, K.M., Albers, S.V., 2010. Crenarchaeal biofilm formation under extreme conditions. PLoS ONE 5 (11), e14104. http://dx.doi.org/10.1371/journal.pone.0014104.e14104.

Koerdt, A., Jachlewski, S., Ghosh, A., Wingender, J., Siebers, B., Albers, S.V., 2012. Complementation of *Sulfolobus solfataricus* PBL2025 with an α-mannosidase: effects on surface attachment and biofilm formation. Extremophiles 16, 115–125.

Macalady, J.L., Vestling, M.M., Baumler, D., Boekelheide, N., Kaspar, C.W., Banfield, J.F., 2004. Tetraether-linked membrane monolayers in *Ferroplasma* spp: a key to survival in acid. Extremophiles 8, 411–419.

Mackintosh, M.E., 1978. Nitrogen fixation by *Thiobacillus ferrooxidans*. J. Gen. Microbiol. 105, 215–218.

Mangold, S., Harneit, K., Rohwerder, T., Claus, G., Sand, W., 2008. Novel combination of atomic force microscopy and epifluorescence microscopy for visualization of leaching bacteria on pyrite. Appl. Environ. Microbiol. 74, 410–415.

Morales, M., Arancibia, J., Lemus, M., Silva, J., Gentina, J.C., Aroca, G., 2011. Bio-oxidation of H_2S by *Sulfolobus metallicus*. Biotechnol. Lett. 33, 2141–2145.

Neu, T.R., Manz, B., Volke, F., Dynes, J.J., Hitchcock, A.P., Lawrence, J.R., 2010. Advanced imaging techniques for assessment of structure, composition and function in biofilm systems. FEMS Microbiol. Ecol. 72, 1–21.

Nicolaus, B., Manca, M.C., Ramano, I., Lama, L., 1993. Production of an exopolysaccharide from two thermophilic archaea belonging to the genus *Sulfolobus*. FEMS Microbiol. Lett. 109, 203–206.

Noël, N., Florian, B., Sand, W., 2010. AFM & EFM study on attachment of acidophilic leaching organisms. Hydrometallurgy 104, 370–375.

Okibe, N., Gericke, M., Hallberg, K.B., Johnson, D.B., 2003. Enumeration and characterization of acidophilic microorganisms isolated from a pilot plant stirred-tank bioleaching operation. Appl. Environ. Microbiol. 69, 1936–1943.

Orell, A., Fröls, S., Albers, S.V., 2013. Archaeal biofilms: the great unexplored. Annu. Rev. Microbiol. 67, 337–354.

Rawlings, D.E., Johnson, D.B., 2007. The microbiology of biomining: development and optimization of mineral-oxidizing microbial consortia. Microbiology 153, 315–324.

Rodriguez-Leiva, M., Tributsch, H., 1988. Morphology of bacterial leaching patterns by *Thiobacillus ferrooxidans* on synthetic pyrite. Arch. Microbiol. 149, 401–405.

Rohwerder, T., Gehrke, T., Kinzler, K., Sand, W., 2003. Bioleaching review part A. Appl. Microbiol. Biotechnol. 63, 239–248.

Ruiz, L.M., Valenzuela, S., Castro, M., Gonzalez, A., Frezza, M., Soulère, L., Rohwerder, T., Queneau, Y., Doutheau, A., Sand, W., 2008. AHL communication is a widespread phenomenon in biomining bacteria and seems to be involved in mineral-adhesion efficiency. Hydrometallurgy 94, 133–137.

Sand, W., Gehrke, T., 2006. Extracellular polymeric substances mediate bioleaching/biocorrosion via interfacial processes involving iron (III) ions and acidophilic bacteria. Res. Microbiol. 157, 49–56.

Sand, W., Gehrke, T., Hallmann, R., Schippers, A., 1998. Towards a novel bioleaching mechanism. Min. Pro. Ext. Met. Rev. 19, 97–106.

Sanhueza, A., Ferrer, I., Vargas, T., Amils, R., Sánchez, C., 1999. Attachment of *Thiobacillus ferrooxidans* on synthetic pyrite of varying structural and electronic properties. Hydrometallurgy 51, 115–129.

Schippers, A., Breuker, A., Blazejak, A., Bosecker, K., Kock, D., Wright, T., 2010. The biogeochemistry and microbiology of sulfidic mine waste and bioleaching dumps and heaps, and novel Fe(II)-oxidizing bacteria. Hydrometallurgy 104, 342–350.

Schippers, A., Hedrich, S., Vasters, J., Drobe, M., Sand, W., Willscher, S., 2013. Biomining: metal recovery from ores with microorganisms. In: Schippers, A., Glombitza, F., Sand, W. (Eds.), Advances in Biochemical Engineering/Biotechnology. Geobiotechnology Springer, Berlin. http://dx.doi.org/10.1007/10_2013_216.

Stoodley, P., Sauer, K., Davies, D., Costerton, J.W., 2002. Biofilms as complex differentiated communities. Annu. Rev. Microbiol. 56, 187–209.

Vera, M., Guiliani, N., Jerez, C.A., 2003. Proteomic and genomic analysis of the phosphate starvation response of *Acidithiobacillus ferrooxidans*. Hydrometallurgy 71, 125–132.

Vera, M., Schippers, A., Sand, W., 2013. Progress in bioleaching: fundamentals and mechanisms of bacterial metal sulfide oxidation—part A. Appl. Microbiol. Biotechnol. 97, 7529–7541.

Vinogradov, E., Deschatelets, L., Lamoureux, M., Patel, G.B., Tremblay, T.-L., Robotham, A., Goneau, M.-F., Cummings-Lorbetskie, C., Watson, D.C., Brisson, J.-R., 2012. Cell surface glycoproteins from *Thermoplasma acidophilum* are modified with an N-linked glycan containing 6-C-sulfofucose. Glycobiology 22, 1256–1267.

Zhang, R.Y., Xia, J.L., Peng, J.H., Zhang, Q., Zhang, C.G., Nie, Z.Y., Qiu, G.Z., 2010. A new strain *Leptospirillum ferriphilum* YTW315 for bioleaching of metal sulfides ores. T. Nonferr. Metal. Soc. 20, 135–141.

Zhou, H., Zhang, R., Hu, P., Zeng, W., Xie, Y., Wu, C., Qiu, G., 2008. Isolation and characterization of *Ferroplasma thermophilum* sp. nov., a novel extremely acidophilic, moderately thermophilic archaeon and its role in bioleaching of chalcopyrite. J. Appl. Microbiol. 105, 591–601.

Zolghadr, B., Klingl, A., Koerdt, A., Driessen, A.J., Rachel, R., Albers, S.-V., 2010. Appendage-mediated surface adherence of *Sulfolobus solfataricus*. J. Bacteriol. 192, 104–110.

- 49 -

Supplementary data

Fig. S1 SEM of *F. acidiphilum* cells on pyrite grains after 14 days of bioleaching (1, flat surfaces. 2, crude surfaces). Arrows show cells attached to surfaces.
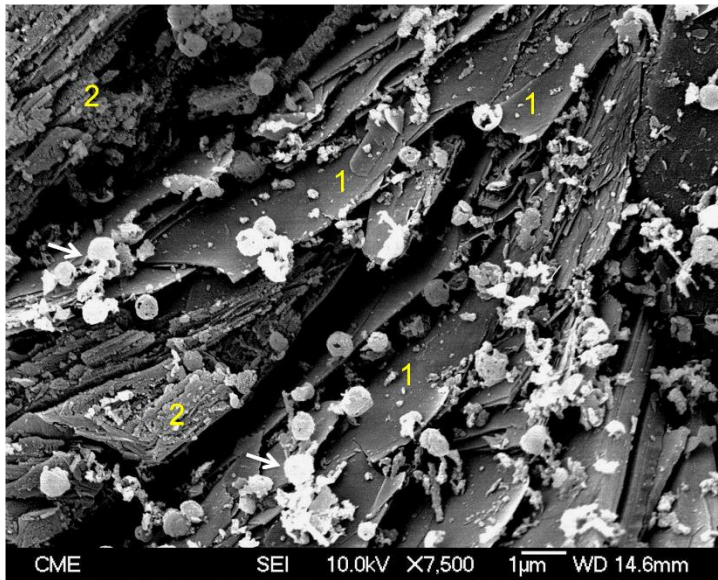
4.2 Visualization of acidophilic archaeal biofilms on pyrite and S^0

In order to investigate EPS glycoconjugates, a major part of the EPS, during biofilm formation/bioleaching by archaea on pyrite, FLBA has been performed. Three representative archaeal species, *F. acidiphilum* DSM 28986, *S. metallicus*^{T} and a novel isolate *Acidianus* sp. DSM 29099 were selected. Also, *Acidianus* sp. DSM 29099 biofilms on S^0 were studied. More than 20 lectins bound to archaeal biofilms on pyrite and to *Acidianus* sp. DSM 29099 biofilms on S^0. The major binding patterns, e.g. tightly bound EPS and loosely bound EPS, were detected on both substrates. The three archaeal species produced various EPS glycoconjugates containing sugar moieties like glucose, galactose, mannose, GlcNAc, GalNAc, sialic acid, and fucose. Additionally, the substratum induced different EPS glycoconjugates and biofilm structures for cells of *Acidianus* sp. DSM 29099.

This is the first study of glycoconjugates in acidophilic archaea using FLBA technique. The selected lectins are currently used in our laboratory for assessment of interactions between various members of microbial bioleaching communities, especially to elucidate the role of archaea.

microbial biotechnology

Open Access

Use of lectins to in situ visualize glycoconjugates of extracellular polymeric substances in acidophilic archaeal biofilms

R. Y. Zhang,[1] T. R. Neu,[2] S. Bellenberg,[1] U. Kuhlicke,[2] W. Sand[1] and M. Vera[1]*

[1]Aquatische Biotechnologie, Biofilm Centre, Universität Duisburg – Essen, Universitätsstraße 5, 45141 Essen, Germany.
[2]Department of River Ecology, Helmholtz Centre for Environmental Research-UFZ, Brueckstrasse 3A, 39114 Magdeburg, Germany.

Summary

Biofilm formation and the production of extracellular polymeric substances (EPS) by meso- and thermoacidophilic metal-oxidizing archaea on relevant substrates have been studied to a limited extent. In order to investigate glycoconjugates, a major part of the EPS, during biofilm formation/bioleaching by archaea on pyrite, a screening with 75 commercially available lectins by fluorescence lectin-binding analysis (FLBA) has been performed. Three representative archaeal species, *Ferroplasma acidiphilum* DSM 28986, *Sulfolobus metallicus* DSM 6482[T] and a novel isolate *Acidianus* sp. DSM 29099 were used. In addition, *Acidianus* sp. DSM 29099 biofilms on elemental sulfur were studied. The results of FLBA indicate (i) 22 lectins bound to archaeal biofilms on pyrite and 21 lectins were binding to *Acidianus* sp. DSM 29099 biofilms on elemental sulfur; (ii) major binding patterns, e.g. tightly bound EPS and loosely bound EPS, were detected on both substrates; (iii) the three archaeal species produced various EPS glycoconjugates on pyrite surfaces. Additionally, the substratum induced different EPS glycoconjugates and biofilm structures of cells of *Acidianus* sp. DSM 29099. Our data provide new insights into interactions between acidophilic

archaea on relevant surfaces and also indicate that FLBA is a valuable tool for in situ investigations on archaeal biofilms.

Introduction

Microbial leaching of metal sulfides (MS) is an expanding biotechnology (Brierley and Brierley, 2013). However, it can also occur as an unwanted natural process called acid rock drainage or acid mine drainage (AMD). This process is accompanied by acidification and heavy metal pollution of water bodies and can cause serious environmental problems (Kalin *et al.*, 2006; Sand *et al.*, 2007). Acidophilic archaea including genera such as *Ferroplasma*, *Acidianus*, *Sulfolobus* and *Metallosphera* play important roles in bioleaching and AMD systems, and have received significant attention for commercial applications (Olson *et al.*, 2003; Golyshina and Timmis, 2005; Rawlings and Johnson, 2007).

The genera *Acidianus* and *Sulfolobus* are thermoacidophiles found in hydrothermal vents or bioleaching systems at temperatures above 60°C. They are capable of oxidizing both iron(II) ions and reduced inorganic sulfur compounds (RISCs). Biological ferric iron regeneration and acidic conditions are crucial for the dissolution of MS (Schippers and Sand, 1999; Sand *et al.*, 2001). Under thermophilic conditions, iron oxidation is accelerated, and the passivation of chalcopyrite ($CuFeS_2$) surfaces by RISCs is nearly eliminated, which has significant importance in the biomining industry.

The mesophilic archaeon *Ferroplasma acidiphilum* was first isolated from a semi-industrial bioleaching reactor processing arsenopyrite in Kazakhstan (Golyshina *et al.*, 2000). It oxidizes iron(II) ions or pyrite in the presence of trace amounts of yeast extract. In addition, all isolated strains of *Ferroplasma* spp. can grow heterotrophically (Dopson *et al.*, 2004). *Ferroplasma* is frequently detected in biomining ecosystems and is considered to be a major player in global iron and sulfur cycles in highly acidic environments (Edwards *et al.*, 2000; Golyshina and Timmis, 2005; Chen *et al.*, 2014).

Biofilms are defined as interface-associated communities of microorganisms embedded in extracellular polymeric substances (EPS). The EPS usually consist of polysaccharides, proteins, lipids and DNA. They are

generally subdivided into two types: 'capsular EPS' are tightly bound to cells, while 'colloidal EPS' are loosely bound to cells and can be easily released (e.g. by centrifugation or washing) into the solution (Nielsen and Jahn, 1999). EPS are essential for biofilm structure and function due to their involvement in cellular associations, nutrition exchange and interactions of microorganisms with their bio-physicochemical environment (Wolfaardt *et al.*, 1999; Neu and Lawrence, 2009). EPS are also involved in the attachment and biofilm formation of leaching microorganisms to surfaces of MS, which is an essential step at the start of the leaching process (Vera *et al.*, 2013). Biofilms formed by heterotrophic prokaryotes or phototrophs are usually dynamic structures that can grow to thick three-dimensional macro-communities (Stoodley *et al.*, 2002). In contrast, the majority of metal-oxidizing microorganisms attach directly to the surface of MS, forming monolayer biofilms. By this lifestyle, cells can obtain energy from Iron(II) ions or RISCs, which are released during the dissolution of the MS. Interestingly, two distinct biofilm morphologies were described for *Ferroplasma acidarmanus* Fer1: A multilayer film was formed on pyrite surfaces after 38 days of incubation, and up to 5 mm-long filaments were found on sintered glass spargers in gas lift bioreactors (Baker-Austin *et al.*, 2010).

Few studies have shown biofilms of archaea, including thermoacidophiles, halophiles and methanogens. The first archaeal biofilm was described for the hyperthermophilic *Thermococcus litoralis*, which developed in rich media on polycarbonate filters and glass surfaces (Rinker and Kelly, 1996). *Pyrococcus furiosus* and *Methanobacter thermoautotrophicus* developed monospecies biofilms on solid surfaces (Näther *et al.*, 2006; Thoma *et al.*, 2008). Bi-species biofilm development of *P. furiosus* and *Methanopyrus kandlerii* was shown to be established within less than 24 h on abiotic surfaces (Schopf *et al.*, 2008). Biofilm analysis of three *Sulfolobus* spp. showed that their structures were different, ranging from simple carpet-like structures in *Sulfolobus solfataricus* and *Sulfolobus tokodaii* to high density tower-like structures in *Sulfolobus acidocaldarius* in static systems. All three species produced EPS containing glucose, galactose, mannose and N-acetylglucosamine (GlcNAc) once biofilm formation was initiated (Koerdt *et al.*, 2010). Biofilm formation by methanogenic archaea under static conditions was studied by confocal laser scanning microscopy (CLSM) and scanning electron microscopy. The three species, *Methanosphaera stadtmanae*, *Methanobrevibacter smithii* and *Methanosarcina mazei* strain Gö1, formed mainly bilayer biofilms on mica surfaces. Nevertheless, the development of multilayer biofilms was also observed (Bang *et al.*, 2014). Biofilm formation of haloarchaea, including species of *Halobacterium*, *Haloferax* and *Halorubrum*, was investigated by a

fluorescence-based live cell adhesion assay. Cellular appendages were speculated to be involved in the initial attachment (Fröls *et al.*, 2012). Two types of biofilm structures were detected including carpet-like multilayers and large aggregates adhering to glass surfaces. Similar as occurring in the acidophilic archaea such as *Sulfolobus* and *Ferroplasma* (Baker-Austin *et al.*, 2010; Koerdt *et al.*, 2010; Zhang *et al.*, 2014), biofilm development occurs in a surprisingly wide variety in haloarchaea. In addition, EPS like eDNA and various glycoconjugates were found to be present in these biofilms (Fröls *et al.*, 2012).

Lectins are proteins or glycoproteins capable of binding reversibly and specifically to carbohydrates without altering their structures. Fluorescence lectin-binding analysis (FLBA) represents the only option for non-destructive and in situ glycoconjugate analysis and, therefore, is widely used in glycoconjugate/biofilm analysis in combination with other fluorochromes, e.g. specific for nucleic acids (Zippel and Neu, 2011; Bennke *et al.*, 2013; Castro *et al.*, 2014). Furthermore, their multivalency ensures high-affinity binding to the cell surface and biofilm structures containing various glycoconjugates. Only a few lectins combined with nucleic acid dyes have been used in investigations on acidophilic biofilms related to bioleaching and AMD systems. The most frequently used lectin is Concanavalin A (Con A) from the jack-bean, *Canavalia ensiformis*, binding to mannose and glucose residues (Goldstein *et al.*, 1965). Con A has been used to visualize various acidophilic archaeal and bacterial biofilm cells, e.g. *Sulfolobus* (Koerdt *et al.*, 2010; Zolghadr *et al.*, 2010; Bellenberg *et al.*, 2012), *F. acidiphilum* (Zhang *et al.*, 2014) and *Metallosphaera hakonensis* (Africa *et al.*, 2013). As EPS are complex mixtures consisting of many types of macromolecules, it is impossible to address their complexity with a single staining approach. Even for the similar glycoconjugates, multiple lectin probes have to be used (Neu and Lawrence, 2009). Thus, it is necessary to screen a library of lectins in order to find the ones binding to the glycoconjugates in a particular biofilm (Peltola *et al.*, 2008; Zippel and Neu, 2011; Bennke *et al.*, 2013).

To date, EPS production and biofilms of archaeal species have been investigated only to a limited extent, especially concerning the ones growing in acidic environments (Orell *et al.*, 2013). Nevertheless, it is essential to visualize EPS glycoconjugate identity and distribution on relevant surfaces together with analysis of their chemical composition to understand their function(s) in bioleaching. In the present study, three representative archaeal strains – a euryarchaeote *F. acidiphilum* DSM 28986 and two crenarchaeota, *Sulfolobus metallicus* DSM 6482^T and *Acidianus* sp. DSM 29099 – were selected for FLBA of their EPS glycoconjugates and biofilm structures during bioleaching of pyrite as well as on elemental sulfur in case of *Acidianus* sp. DSM 29099. In order to image EPS

450   *R. Y. Zhang et al.*

glycoconjugates in these biofilms, 75 commercially available lectins were tested for applicability. This is the first report of EPS glycoconjugate probing by means of FLBA for archaeal biofilms in situ during bioleaching.

Results and discussion

Visualization of attached archaea and biofilms

In previous reports, acridine orange (Fröls *et al.*, 2012), fluorescein (Baker-Austin *et al.*, 2010) and DAPI (Henche *et al.*, 2012; Koerdt *et al.*, 2012) have been used for staining acidophilic archaeal species. In order to display the distribution of archaeal cells as well as to visualize EPS including proteins, nucleic acids and lipophilic compounds in biofilms on pyrite surfaces, six fluorochromes including SybrGreen (Invitrogen, Carlsbad, CA, USA), Syto 9 (Invitrogen), Syto 64 (Invitrogen), SyproRed (Invitrogen), SyproOrange (Invitrogen) and FM4-64 (Invitrogen) were selected to evaluate their potential suitability (Table 1). Sypro stains like SyproRed and SyproOrange were originally developed for measuring protein concentrations in solution or in gels. Later, they were used for flow cytometry studies (Zubkov *et al.*, 1999) and finally for staining the biofilm matrix for CLSM examination (Neu and Lawrence, 1999a; Lawrence *et al.*, 2003). FM-dyes (FM4-64 and FM1-43) are widely used to study endocytosis, vesicle trafficking and organelle organization in living eukaryotic cells (Bolte *et al.*, 2004).

Archaeal cells and biofilms on pyrite. As negative control, the abovementioned dyes including fluoroconjugated lectins were selected randomly to stain sterile pyrite for evaluation of their unspecific binding. Surface structures of sterile, cleaned pyrites showed no unspecific binding of dyes when examined by CLSM (not shown). As shown in Fig. 1A–C, cells of *F. acidiphilum* DSM 28986 attached to pyrite were successfully stained by SybrGreen, Syto 9 and Syto 64. Similarly, cells of *Acidianus* sp. DSM 29099 and *S. metallicus*^{T} were also clearly visualized by staining with these dyes (Fig. 2A, B, D and E). In addition, SyproRed stained cells of *F. acidiphilum* DSM 28986

(Fig. 1D), *Acidianus* sp. DSM 29099 (Fig. 2C) and *S. metallicus*^{T} (Fig. 2E). FM4-64 stained cells of the *Sulfolobales* (not shown) and *F. acidiphilum* DSM 28986 (Fig. 1E). SyproRed and FM4-64 staining gave clear cell-corresponding signals. Therefore, these fluorochromes were used for counter staining in the following tests for cell localization.

In this study, Sypro was used in order to examine archaeal cell surfaces as well as extracellular features. *Ferroplasma*, *Acidiplasma* and *Thermoplasma*, unlike other Archaea, lack a cell wall (Golyshina *et al.*, 2000; 2009). It has been shown that the cytoplasmic membrane of *F. acidiphilum* is covered with a thin layer of an amorphous, electron-dense surface matrix (Golyshina and Timmis, 2005). The positive Sypro staining indicates that the thin layer of electron-dense material observed could be a proteinaceous layer, although there is no surface layer (S-layer) characterized in *Ferroplasma*. Another explanation could be that Sypro interacts with membrane proteins. In contrast to *F. acidiphilum*, *Acidianus* sp. DSM 29099 and *S. metallicus*^{T} possess a cell wall, which is mainly composed of S-layer proteins and anchored by their carboxyl-terminal transmembrane domains to the cytoplasmic membrane (Albers and Meyer, 2011). Obviously, S-layer proteins of these two thermophilic archaeal strains were recognized by SyproRed (Fig. 2C and E).

Besides cell visualization, these protein-, lipid- and nucleic acid-specific dyes should also allow the detection of proteins, lipids and DNA as part of the EPS in biofilms (Neu and Lawrence, 2014). In this study, staining of three archaeal strains by abovementioned fluorochromes was mostly restricted to cells, as no smear or diffuse signals around cells were visible (Figs 1 and 2). This indicates that the EPS components including proteins, lipids and eDNA were not present in colloidal fractions or below their detection limit if assessed by means of CLSM. These findings are in good agreement with the EPS analysis by colorimetric methods. The colloidal EPS of *F. acidiphilum* DSM 28986 as well as *Acidianus* sp. DSM 29099 grown on pyrite mainly contained polysaccharides. In contrast, capsular EPS contained both polysaccharides and pro-

Table 1. List of dyes and their Ex and Em wavelengths and associated binding targets.

Dyes	Specificity	Ex/Em wavelength (nm)	Company
SYTO 9	NA	483/478–488, 500–560	Invitrogen
SYTO 64	NA	483, 599/475–489, 625–700	Invitrogen
SybrGreen	NA	483/475–489, 500–560	Invitrogen
FM4-64	Lipid-rich domain	483, 506/650–790	Invitrogen
SyproRed	Proteins	475, 500/470–480, 580–680	Invitrogen
SyproOrange	Proteins	475/470–480, 520–620	Invitrogen
TRITC or Alexa 488-conjugated lectins	EPS glycoconjugates	490/505–545	EY Laboratories, Inc.
FITC-conjugated lectins	EPS glycoconjugates	490/485–495, 510–600	Sanbio Laboratory/ EY Laboratories, Inc.

Em, emission; Ex, excitation; FITC, fluorescein isothiocyanate; NA, nucleic acids; TRITC, tetramethyl rhodamine isothiocyanate.
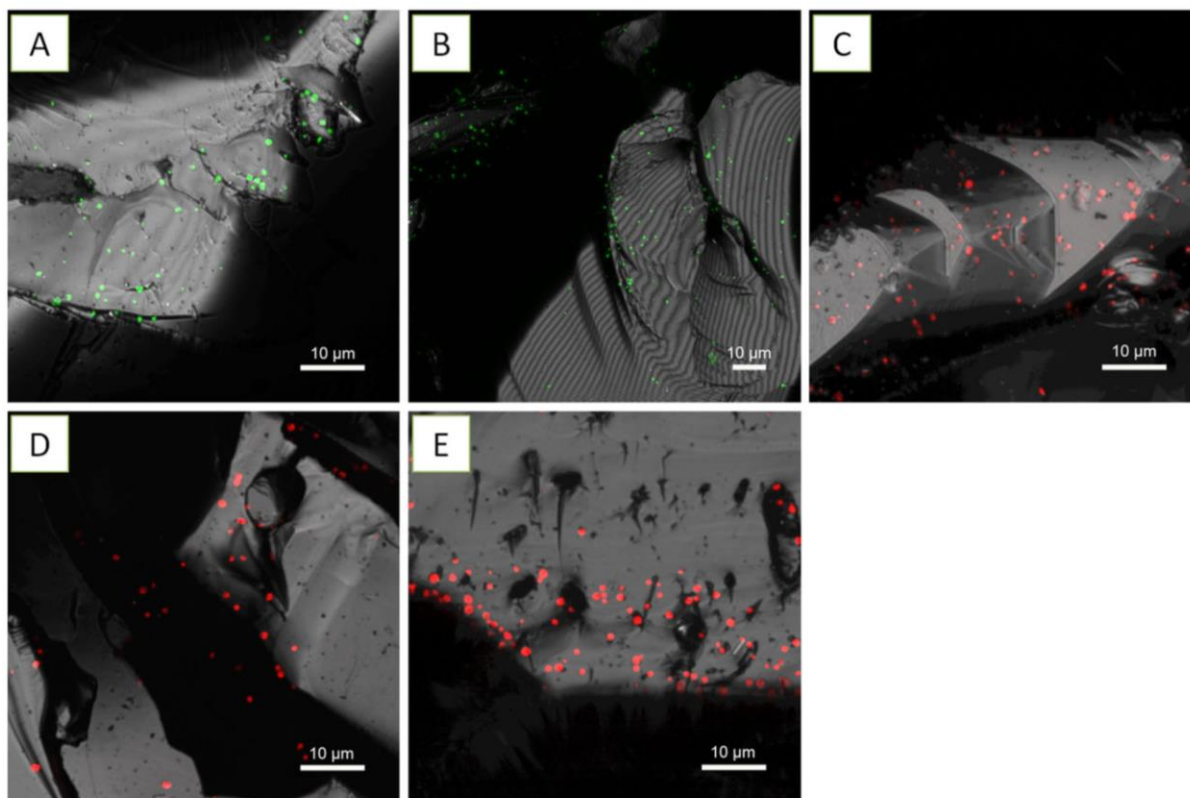
Fig. 1. Maximum intensity projections of *F. acidiphilum* DSM 28986 biofilms on pyrite stained by SybrGreen (A), Syto 9 (B), Syto 64 (C), SyproRed (D) and FM4-64 (E). Color allocation: green = SybrGreen/Syto 9, red = SyproRed/FM4-64. The pyrite surface is shown in reflection mode (= grey).

teins (R. Y. Zhang, unpublished). In this context, extracellular proteins on cell surface were also stained by SyproRed (Figs 1D, 2C and E). We did not detect eDNA in both cases. It is widely accepted that eDNA has a crucial role in biofilm development and dynamics (Whitchurch *et al.*, 2002; Karatan and Watnick, 2009). However, as DNA is a costly molecule for the cell to synthesize, it is reasonable to assume that the chemolithotrophic organisms tested, which obtain little energy by oxidation of pyrite, are not excreting measurable amounts of DNA.

In general, cells of the three species were heterogeneously distributed and developed monolayer biofilms on pyrite surfaces. Large pyrite areas remained uncolonized (~ 90%). Nevertheless, two levels of spatial organization were observed: cells and small clusters of cells (Figs 1 and 2). These results were confirmed by atomic force microscopy (AFM) combined with epifluorescence microscopy (EFM) (Supporting Information Fig. S1). It must be noted that cell attachment by the strains to pyrite did not occur randomly. Cells of *Acidianus* sp. DSM 29099 and *S. metallicus*[T] preferentially colonized surface locations with defects (Fig. 2). During the examination of pyrite grains, it became obvious that highly colonized grains

exhibited more scratches, microcracks or grooves as compared with the less colonized ones. More pits were observed when pyrite was leached by cells of *Acidianus* sp. DSM 29099 or *S. metallicus*[T] as compared with *F. acidiphilum* DSM 28986 (Figs 1 and 2). *Acidianus* sp. DSM 29099 and *S. metallicus*[T], due to their increased growth temperature and their ability to oxidize RISCs arising from pyrite dissolution, have a much higher pyrite leaching capacity than *F. acidiphilum* DSM 28986 (approximately 25 times, Table 2). In a previous report, cells of *Metallosphaera* and *Sulfolobus* spp. did not exhibit any preferential orientation when they attached to pyrite (Etzel *et al.*, 2008). This maybe ascribed to the use of

Table 2. Comparison of pyrite leaching activities the strains used after 20 days of cultivation.

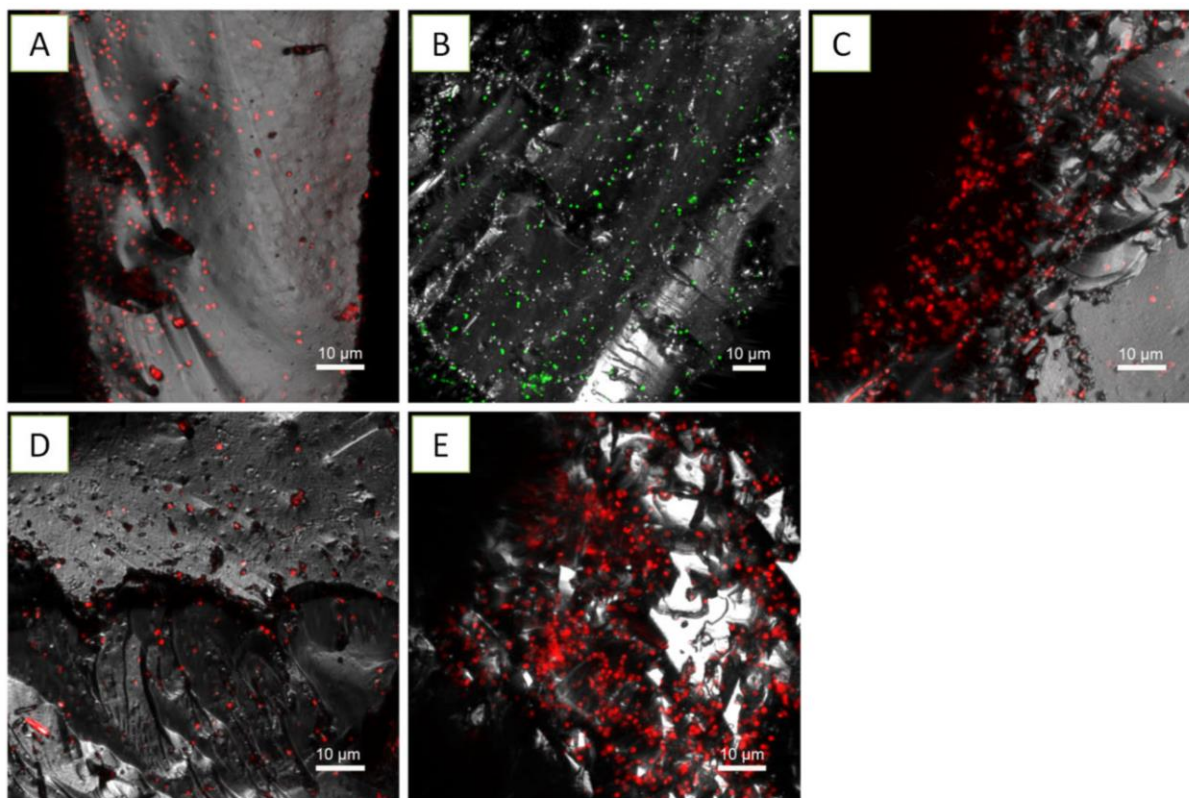| Strain	Fe total (mg l⁻¹)	Fe III/ Fe II ratio	Temperature
Ferroplasma acidiphilum DSM 28986	255	0.4	37°C
Sulfolobus metallicus[T]	6353	6	65°C
Acidianus sp. DSM 29099	5913	2.7	65°C

Fig. 2. Maximum intensity projections of *Acidianus* sp. DSM 29099 biofilms on pyrite stained by Syto 64 (A), SybrGreen (B) and SyproRed (C). *Sulfolobus metallicus*[T] biofilms on pyrite stained by Syto 64 (D) and SyproRed (E). Color allocation: green = SybrGreen, red = Syto 64/SyproRed, grey = reflection.

different pyrite qualities having different surface properties (e.g. crystallographic orientation).

Acidianus sp. DSM 29099 on elemental sulfur. The first observation of acidophilic microbes attached to elemental sulfur was described for *Acidithiobacillus thiooxidans* by means of electron microscopy (Schaeffer *et al.*, 1963). The attachment of sulfur-oxidizing microbes to sulfur surfaces has been shown to be favoured by the presence of pili, filamentous or glycoglyx materials (Weiss, 1973; Bryant *et al.*, 1984; Blais *et al.*, 1994). These studies focused mainly on bacteria, and usually, samples were pre-fixed by glutaraldehyde and dehydrated before visualization. By directly applying different stains including SybrGreen, Syto 64 and SyproRed, biofilm cells of *Acidianus* sp. DSM 29099 were clearly visualized on elemental sulfur under fully hydrated conditions, as shown in Fig. 3. Biofilms were heterogeneously distributed and characterized as individual groups of cells, thin but large colonies with up to 50 μm in diameter. Cells formed large aggregates or dense biofilms, in particular, on some sites with cracks and grooves. These cell distribution patterns suggest that adhesion does not occur randomly, and

biofilm formation does not proceed uniformly at the sulfur surface. In this case, the presence of cell aggregates suggest that the physical contact of *Acidianus* cells with sulfur is a necessary step for sulfur solubilization, while the upper cells in the aggregates could be oxidizing soluble RISCs.

FLBA of biofilms on pyrite and elemental sulfur

The application of FLBA usually includes a screening of all commercially available lectins for probing their reaction with glycoconjugates of (archaeal) biofilms. With the most suitable lectins (for acidophilic archaea), the production of glycoconjugates during biofilm formation may be monitored. In combination with nucleic acid-specific fluorochromes, samples can be analyzed by multichannel CLSM, which has several advantages in analyzing structuring features of hydrated biofilms (Stewart *et al.*, 1995; Lawrence *et al.*, 1998; Neu and Lawrence, 1999b; 2002). As shown in Table 3, pyrite-grown cells of the three species tested were stainable by 22 (eight for *F. acidiphilum* DSM 28986, eight for *Acidianus* sp. DSM 29099 and 14 for *S. metallicus*[T]) out of 75 lectins. In
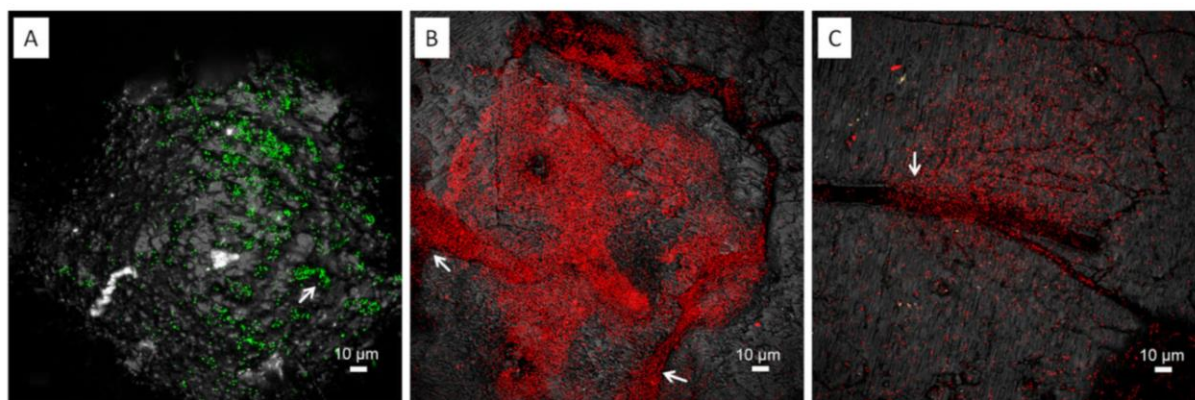
Fig. 3. Maximum intensity projections of biofilms from *Acidianus* sp. DSM 29099 on elemental sulfur. Samples were stained by SybrGreen (A), SyproOrange (B) and Syto 64 (C). Color allocation: green = SybrGreen, red = Syto 64/SyproOrange, grey = reflection. Cells formed a thin biofilm in shallow regions, cracks or holes when sulfur prills were used (A). A clear
tendency of cells to attach to physical defects on sulfur coupons is also evident (B and C). Arrows show preferential attachment sites with distortions.

addition, three binding patterns of lectins to EPS glycoconjugates on pyrite surfaces could be differentiated (Table 3). As indicated in Fig. 4A–C (see also Supporting Information Fig. S2), Con A bound to the cell surface of *Acidianus* sp. DSM 29099. Pyrite surfaces free of cells showed no Con A binding, indicating that Con A only reacted with tightly bound EPS of *Acidianus* sp. DSM 29099.

The lectins *Aleuria aurantia* lectin (AAL) and *Limulus polyphemus* agglutinin (LPA) stained biofilm cells of *Acidianus* sp. DSM 29099 (Fig. 4D and E) and *F. acidiphilum* DSM 28986 as well as their surrounding sites (Fig. 5). Unlike the binding of Con A to cells on pyrite surface, these lectins also bound to cell-free EPS on pyrite surfaces. This 'colloidal' EPS binding pattern may allow us to speculate that capsular EPS are probably involved in the initial attachment, and consequently, more EPS were produced in form of colloidal EPS by cells building biofilms on pyrite. Thus, as ocurring in bioleaching bacteria, large areas of the surface may actually be devoid of cells but may be covered by 'colloidal' EPS (Sand *et al.*, 2001). In this context, it has been reported that *T. litoralis* excretes exopolysaccharides into the growth medium and that these may cause a conditioning layer on surfaces (Rinker and Kelly, 1996).

Fig. 6 shows that the cell surfaces of *Acidianus* sp. DSM 29099 and *S. metallicus*[T] clearly reacted with the lectin *Griffonia simplicifolia* lectin (GS-I). Within stained biofilms, GS-I signals mostly covered the cells but also filled the space between cells and pyrite surfaces. This cell-associated binding pattern indicates the potential complexity of biofilm structures. It can be concluded that the lectins showing cell-associated binding patterns

reacted with relatively more biofilm components than the ones present just in capsular or colloidal EPS.

Glycoconjugates produced on pyrite. The glycoconjugates present in biofilms of the three archaeal species on pyrite are listed in Table 3. Based on lectin specificity, fucose, glucose, N-acetylgalactosamine (GalNAc), galactose and mannose were found in the three tested species.

Acidianus sp. DSM 29099 and *S. metallicus*[T] biofilms on pyrite were shown to possess similar glycoconjugates including fucose, GlcNAc, GalNAc, galactose, mannose and glucose. Both GalNAc and GlcNAc are present in archaeal cell walls. As *Ferroplasma* lacks a cell wall, it is not surprising that we did not detect GlcNAc in these archaea. The binding of the lectin LPA to biofilm cells strongly suggest *F. acidiphilum* DSM 28986 to possess sialic acid residues. Sialic acids are a family of about 50 derivatives of *N*-acetyl or *N*-glycolyl neuraminic acids. They typically occupy the distal end of glycan chains, which makes them suitable for interaction with other cells or with environmental constituents and interfaces. Sialic acids are mainly found in animals and their pathogens, and in certain bacteria (Angata and Varki, 2002; Vimr *et al.*, 2004). They are important components of glycoproteins and glycolipids in animal cell membranes. Studies concerning the presence of sialic acid in archaea are rare (Angata and Varki, 2002; Lewis *et al.*, 2009). By applying reverse-phase high-performance liquid chromatography combined with a fluorescent labelling method using 1,2-diamino-4,5-methylenedioxybenzene dihydrochloride to label the sialic acids (Hara *et al.*, 1989), we were able to confirm the presence of sialic acids in cells of *F. acidiphilum* DSM 28986 (R. Y. Zhang & V. Blanchard, unpublished). Additionally, planktonic cells of this micro-

454 *R. Y. Zhang* et al.

Table 3. Results of lectin binding assays to extracellular glycoconjugates of three archaeal strains on pyrite.

Lectins[a]	Specificities	*Ferroplasma acidiphilum* DSM 28986	*Acidianus* sp. DSM 29099	*Sulfolobus metallicus*[T]
AAL	Fuc	+ Cell-associated structures	+ Colloidal	+ Cell-associated structures
AIA	Gal; GalNAc	+ Capsular	−	−
Con A	Man; Glc	+ Capsular	+ Capsular	+ Capsular
DGL	Man; Glc	+ Colloidal	−	−
GNA	Man	−	+ Capsular	+ Colloidal
GS-I	Gal; GalNAc	−	+ Cell-associated structures	+ Cell-associated structures
HHA	Man	−	−	+ Capsular
HPA	GalNAc	+ Capsular	+ Colloidal	−
IAA	GalNAc	−	−	+ Cell-associated structures
LEA	GlcNAc	−	+ Cell-associated structures	−
LPA	Sia	+ Colloidal	−	−
MNA-G	Gal	−	−	+ Capsular
MPA	GalNAc	−	+ Colloidal	−
PA-I	Gal	+ Capsular	−	−
PHA-E	Man	+ Colloidal	−	+ Capsular
PHA-L	GalNAc	−	−	+ Capsular
PMA	Man	−	+ Capsular	−
PSA	Man	−	−	+ Capsular
SJA	GalNAc	−	−	+ Colloidal
STA	GluNAc			Capsular
VVA	GalNAc	−	−	+ Cell-associated structures
WFA	GalNAc	−	−	+ Capsular

a. The details of all lectins used in this study are shown in Supporting Information Table S1. Staining and visualization procedures are described in the section Experimental procedures.
+, lectin binding; −, no binding; AIA, *Artocarpus integrifolia* agglutinin; DGL, *Dioclea grandiflora* lectin; GNA, *Galanthus nivalis* agglutinin; HHA, Amaryllis lectin; HPA, *Helix pomatia* agglutinin; IAA, *Iberis amara* agglutinin; LEA, *Lycopersicon esculentum* agglutinin; MNA-G, Morniga G; MPA, *Maclura pomifera* agglutinin; PA-I, *Pseudomonas aeruginosa* lectin I; PHA-E, *Phaseolus vulgaris* agglutinin E; PHA-L, *Phaseolus vulgaris* agglutinin L; PMA, *Polygonatum multiflorum* agglutinin; PSA, *Pisum sativum* agglutinin; SJA, *Sophora japonica* agglutinin; STA, *Solanum tuberosum* agglutinin; VVA, *Vicia villosa* agglutinin; WFA, *Wisteria floribunda* agglutinin.

organism were not stained by LPA. As sialic acid residues are mostly present in biofilms of *F. acidiphilum* DSM 28986 grown on pyrite, it can be assumed that these residues play an important role in attachment and presumably also in the biologically accelerated oxidation of pyrite. Consequently, these results indicate that acidophilic leaching archaea might use different surface compounds (i.e. sialic acids in case of *F. acidiphilum*) for mediating cell–mineral interactions compared with bacterial ones. These are considered to be established by uronic acids complexing iron(III) ions, which are mediating cell attachment by electrostatic interactions and increase the concentration of the pyrite oxidizing agent iron(III) ions (Sand *et al.*, 2001).

A few lectins including Con A, GS-I, GS-II and WGA have been applied to stain and visualize EPS of *Sulfolobus* spp. WGA was first reported to stain *S. acidocaldarius* and *Sulfolobus shibatae* on polycarbonate membrane filters (Fife *et al.*, 2000). In our assays, this lectin did not bind to any of the strains tested. The lectins Con A, GS-I and GS-II have been used in studies on *S. acidocaldarius*, *S. solfataricus* and
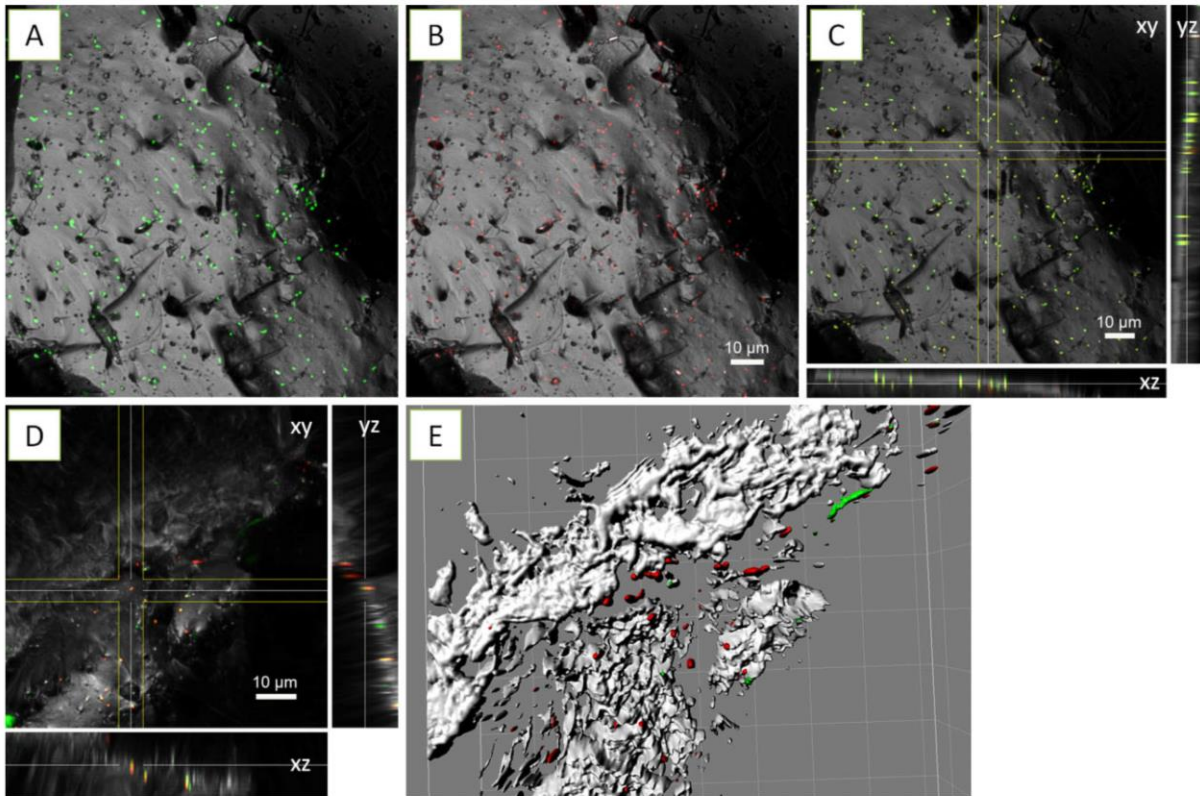
Fig. 4. Maximum intensity projections (A, B), XYZ projection (C, D) and isosurface projection (E) of *Acidianus* sp. DSM 29099 biofilms on pyrite stained by Con A (B) and AAL (D, E), and counter stained by and SybrGreen (A) and Syto 64 (D, E). Color allocation: green = SybrGreen/AAL-fluorescein isothiocyanate (FITC), red = Syto 64/Con A-tetramethyl rhodamine isothiocyanate (TRITC), grey = reflection.
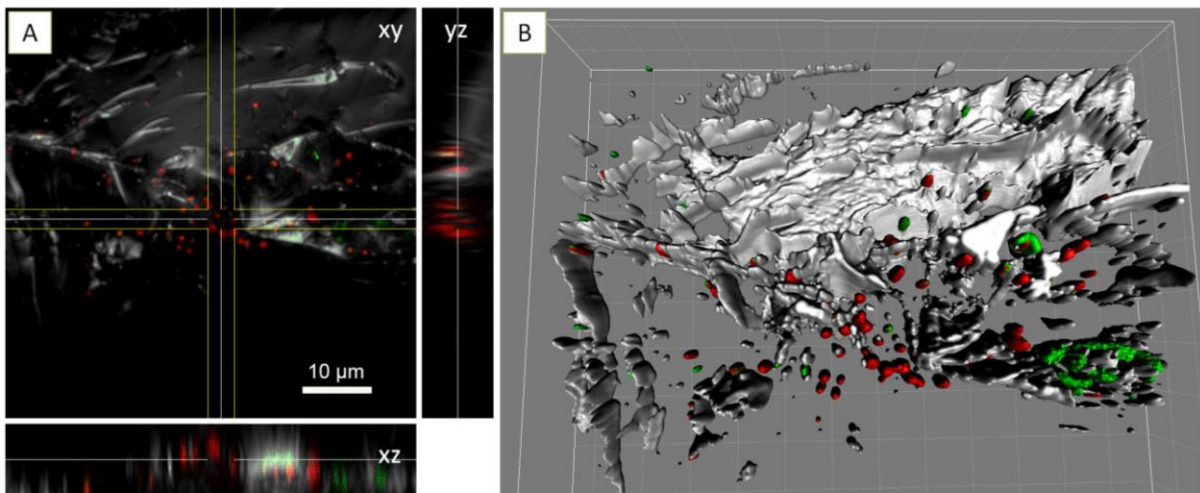

Fig. 5. XYZ projection (A) and isosurface projection (B) of *F. acidiphilum* DSM 28986 biofilms on pyrite stained by LPA-fluorescein isothiocyanate (FITC) and counter stained by FM4-64. Color allocation: green = LPA-FITC, red = FM4-64, grey = reflection. Grid size in B = 10 μm.
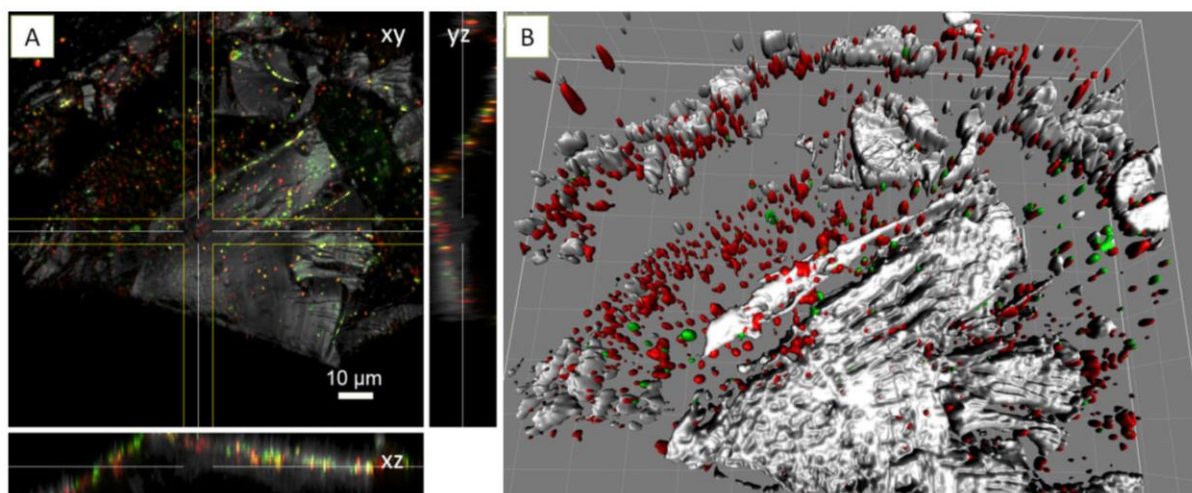
Fig. 6. XYZ projection (A) and isosurface projection (B) of *Acidianus* sp. DSM 29099 biofilms on pyrite stained by GS-I-fluorescein isothiocyanate (FITC) and counter stained by Syto64. Color allocation: green = GS-I-FITC, red = Syto 64, grey = reflection. Grid size in B = 10 μm.

S. tokodaii, including some *S. solfataricus* mutants defective in biofilm formation and production of cell surface appendages (Koerdt *et al.*, 2010; 2012; Zolghadr *et al.*, 2010; Henche *et al.*, 2012). The reaction of these lectins with *Acidianus* sp. DSM 29099 and *S. metallicus*[T] (Tables 3 and 4) strongly indicates that especially Con A and GS-I can be used to monitor biofilm formation of *Sulfolobales*. However, it is important to remark that the abovementioned species are normally grown in complex media (e.g. 0.1% tryptone or 0.2% maltose), while in our experiments, we have used pyrite or elemental sulfur (in case of *Acidianus* sp. DSM 29099) as energy sources. Under these conditions, most of the carbon for biosynthesis must be fixed from CO_2. Control experiments showed no significant cell growth of *Acidianus* sp. DSM 29099 with 0.02% yeast extract as sole energy source (not shown). As we focused on biofilm formation on pyrite or sulfur surfaces, we cannot rule out that under presence of sufficient amounts of organic carbon, *Acidianus* sp. DSM 29099 may build structurally more complex biofims as described for other *Sulfolobales* (Koerdt *et al.*, 2010).

The lectins AAL and Con A stained cells of the three species used in this study, which is consistent with previous reports that these two lectins have the potential to stain various kinds of biofilms (Neu and Lawrence, 2002; Neu *et al.*, 2002; Strathmann *et al.*, 2002; Staudt *et al.*, 2003; Bellenberg *et al.*, 2012). The monomers glucose, mannose and fucose were also found in EPS fractions of *Acidithiobacillus ferrooxidans* (Gehrke *et al.*, 1998). Thus, leaching bacteria and archaea may have similarities in their EPS composition.

Glycoconjugates produced on elemental sulfur. Twenty-one lectins were shown to bind EPS glycoconjugates of *Acidianus* sp. DSM 29099 (Table 4). In addition, two major binding patterns became evident. Five lectins showed signals covering cells and an extended area around them, indicating their binding to colloidal or loosely bound EPS. In contrast, 16 lectins showed a 'capsular binding pattern', in which signals were only restricted to cells (Fig. 7 and Supporting Information Fig. S2). Among these 21 lectins, only AAL, Con A and GS-I stained EPS glycoconjugates of *Acidianus* sp. DSM 29099 on pyrite (Tables 3 and 4). It indicates that the glycoconjugates, which these three

Table 4. Results of lectin binding assays to extracellular glycoconjugates of *Acidianus* sp. DSM 29099 on elemental sulfur.

Lectins	Binding pattern	Lectins	Binding pattern
AAA	Capsular	AAL	Capsular/cell-associated structures
Con A	Capsular/cell-associated structures	DBA	Capsular
ECA	Colloidal	EEA	Capsular
GHA	Capsular	GS-I	Colloidal/cell-associated structures
HHA	Colloidal	HMA	Colloidal
IAA	Colloidal	IRA	Capsular
LAL	Capsular	LBA	Capsular
LcH	Capsular	MOA	Colloidal
PNA	Capsular	PSA	Capsular
SJA	Capsular	TL	Capsular
VGA	Capsular		

DBA, *Dolichos biflorus* agglutinin; ECA, *Erythrina cristagalli* agglutinin; EEA, *Euonymus europaeus* agglutinin; GHA, *Glechoma hederacea* agglutinin; HMA, *Homarus americanus* agglutinin; IRA, *Iris hybrid* agglutinin; LAL, *Laburnum anagyroides* lectin; LBA, *Phaseolus lunatus* agglutinin; LcH, *Lens culinaris* haemagglutinin; MOA, *Marasmium oreades* agglutinin; PNA, Peanut agglutinin; TL, *Tulipa* sp. agglutinin; VGA, *Vicia graminea* agglutinin.
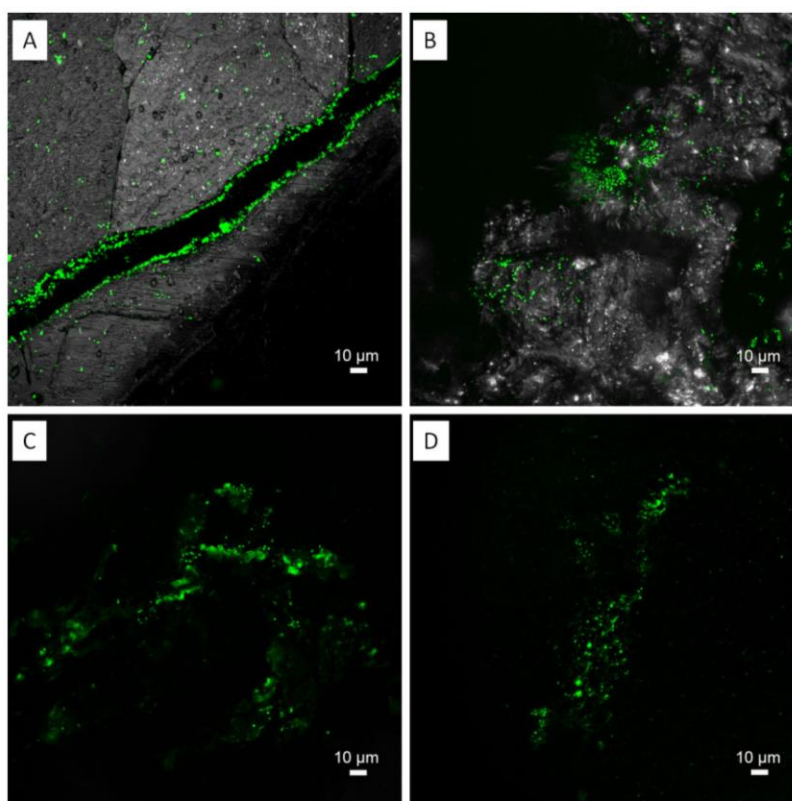
Fig. 7. Maximum intensity projections of biofilms from *Acidianus* sp. DSM 29099 on elemental sulfur. Samples were stained by lectins AAL-Alexa488 (A), Peanut agglutinin (PNA)-fluorescein isothiocyanate (FITC) (B), *Erythrina cristagalli* agglutinin (ECA)-FITC (C) and GS-I (D). Two distinguished lectin binding patterns became visible, tightly bound "capsular" EPS staining (A and B) and loosely bound "colloidal" (C and D). Color allocation: green = lectins, grey = reflection.

lectins recognized (i.e. glucose, mannose, GalNAc and galactose), are common components of *Acidianus* sp. DSM 29099 attached on pyrite and sulfur surfaces. From another point of view, *Acidianus* cells may express different glycoconjugates which correlate with their energy sources. In addition, extracellular proteins of *Sulfolobales* are highly glycosylated. N-glycans usually consist of glucose, mannose, GalNAc and GlcNAc. The high glycosylation density in S-layers could represent an adaptation of these organisms to the high temperature and acidic environment that they naturally encounter (Meyer and Albers, 2013). It has been shown that the loss of one terminal hexose of the N-glycan has effects on cell growth and motility (Jarrell *et al.*, 2014). We suggest that some of the lectins bound also to the N-glycans from the S-layer, which are probably differentially expressed between pyrite and sulfur-grown cells in biofilms of *Acidianus* sp. DSM 29099.

Conclusions

We studied a library of lectins for their potential to visualize and characterize glycoconjugates in acidophilic archaeal

biofilms. The lectin binding tests provided the first hint for the distribution of glycoconjugates that are involved in biofilm formation on pyrite as well as on elemental sulfur. By FLBA, the glycoconjugates in acidophilic archaeal biofilms were characterized as polymers containing sugar moieties like glucose, galactose, mannose, GlcNAc, GalNAc, sialic acid and fucose. Twenty-two lectins were shown to be useful for the study of EPS glycoconjugates of acidophilic archaea during pyrite dissolution. These lectins may be used in future studies for assessment of interactions between various members of microbial bioleaching communities, especially in order to elucidate the role of archaea in detail. In addition, lectins which are species or strain specific (e.g. LPA staining *F. acidiphilum*) may be used as probes to differentiate a target archaeon from others in multi-species biofilm studies.

Experimental procedures

Archaeal strains and cultivation

Ferroplasma acidiphilum DSM 28986 = JCM 30201 (former BRGM4) was isolated from a stirred tank reactor (Bryan

458   *R. Y. Zhang* et al.

et al., 2009). *Sulfolobus metallicus* DSM 6482^T was purchased from DSMZ. Strain *Acidianus* sp. DSM 29099 = JCM 30227, an iron- and sulfur-oxidizer, was isolated from a hot spring at Copahue Volcano, Neuquén, Argentina (R. Y. Zhang & W. Sand, unpublished). All strains were cultivated in MAC medium (Mackintosh, 1978) containing 0.02% yeast extract with an initial pH 1.8 for *F. acidiphilum* DSM 28986 or pH 2.5 for *S. metallicus*^{T} and *Acidianus* sp. DSM 29099 respectively. *Ferroplasma acidiphilum* DSM 28986 was grown at 37°C with 4 g l^{-1} iron(II) ions. *Sulfolobus metallicus*^{T} and *Acidianus* sp. DSM 29099 were grown at 65°C with 10 g l^{-1} elemental sulfur.

Substratum, biofilm formation and pyrite leaching

Pyrite grains with a size of 200–500 μm were selected after grinding and sieving of pyrite cubes from Rioja (Spain). They were cleaned and sterilized as described (Schippers *et al.*, 1996; Schippers and Sand, 1999). For cell attachment assays, 20 g of sterile pyrite grains were incubated with pure cultures of each strain in 300 ml Mac (initial cell concentration 10^8 cells/ml) to allow biofilm development and pyrite dissolution. Iron ions were quantified by the phenanthroline method (Tamura *et al.*, 1974).

Sulfur powder (Roth, Germany) was molten and poured into deionized water with agitation. Sulfur prills with a diameter of 1–3 mm were formed due to rapid cooling. A plate covered with aluminium was used to get a sulfur layer after solidification. Sulfur coupons with a size of approximately 0.5 cm × 0.5 cm × 2 mm were obtained by breaking the sulfur layer. Both sulfur prills and coupons were sterilized at 110°C for 90 min.

Staining

Cell distribution was observed after nucleic acid staining with Syto 9, Syto 64 or SybrGreen. In addition, SyproRed, binding to cellular proteins, or FM4-64, binding to lipid-rich domains (Bolte *et al.*, 2004), were used for counter staining. For glycoconjugate staining, biofilms of each cell population were assayed with lectins conjugated with fluorescein isothiocyanate, Alexa 488 or tetramethyl rhodamine isothiocyanate (Supporting Information Table S1). Briefly, samples were washed with filter-sterilized tap water and incubated with 0.1 mg ml^{-1} lectins for 20 min at room temperature. Afterwards, stained samples were washed three times with filter-sterilized tap water in order to remove unbound lectins. Direct light exposure was avoided. Counter staining was done in a coverwell chamber of 20 mm in diameter with 0.5 mm spacer (Invitrogen). Counter-stained samples were directly observed using CLSM without any further treatment.

CLSM

Examination of stained biofilms was performed by CLSM using a TCS SP5X (Leica, Heidelberg, Germany), controlled by the LASAF 2.4.1 build 6384. The system was equipped with an upright microscope and a super continuum light source (470–670 nm) as well as a 405 nm laser diode. Images were collected with a 63 × water immersion lens with a numerical

aperture (NA) of 1.2 and a 63 × water immersible lens with an NA of 0.9. The details of fluorescent dyes along with excitation and emission filters are shown in Table 1. CLSM data sets were recorded in sequential mode in order to avoid cross talk of the fluorochromes between two different channels. Surface topography and texture of the pyrite as well as of the elemental sulfur surface were recorded by using the CLSM in reflection mode.

AFM and EFM

Pyrite slices were rinsed with sterile MAC medium and deionized water. Cells attached to pyrite coupons and their EPS were stained by Syto 9 and by fluorescently labelled Con A. Stained samples were dried at room temperature and visualized by EFM (Zeiss, Germany) combined with AFM (BioMaterial™Workstation, JPK Instruments) for the investigation of cell morphology and distribution of cells on the surfaces of pyrite coupons (Zhang *et al.*, 2014).

Digital image analysis

Fluorescence images were analyzed using an extended version of software IMAGEJ (Abràmoff *et al.*, 2004). Maximum intensity and XYZ projections of three-dimensional data sets were produced with the software IMARIS version 7.3.1 (Bitplane AG, Zurich, Switzerland).

Conflict of interest

None declared.

References

Abràmoff, M.D., Magalhães, P.J., and Ram, S.J. (2004) Image processing with ImageJ. *Biophotonics International* **11:** 36–43.

Africa, C.J., van Hille, R.P., Sand, W., and Harrison, S.T.L. (2013) Investigation and *in situ* visualisation of interfacial interactions of thermophilic microorganisms with metalsulphides in a simulated heap environment. *Miner Eng* **48:** 100–107.

Albers, S.V., and Meyer, B.H. (2011) The archaeal cell envelope. *Nat Rev Microbiol* **9:** 414–426.

Angata, T., and Varki, A. (2002) Chemical diversity in the sialic acids and related α-keto acids: an evolutionary perspective. *Chem Rev* **102:** 439–470.

Baker-Austin, C., Potrykus, J., Wexler, M., Bond, P.L., and Dopson, M. (2010) Biofilm development in the extremely acidophilic archaeon 'Ferroplasma acidarmanus' Fer1. *Extremophiles* **14:** 485–491.

Bang, C., Ehlers, C., Orell, A., Prasse, D., Spinner, M., Gorb, S.N., *et al.* (2014) Biofilm formation of mucosa-associated methanoarchaeal strains. *Front Microbiol* **5:** 353.

Bellenberg, S., Leon-Morales, C.F., Sand, W., and Vera, M. (2012) Visualization of capsular polysaccharide induction in *Acidithiobacillus ferrooxidans*. *Hydrometallurgy* **129:** 82–89.

Bennke, C.M., Neu, T.R., Fuchs, B.M., and Amann, R. (2013) Mapping glycoconjugate-mediated interactions of marine *Bacteroidetes* with diatoms. *Syst Appl Microbiol* **36:** 417–425.

Blais, J.-F., Tyagi, R., Meunier, N., and Auclair, J. (1994) The production of extracellular appendages during bacterial colonization of elemental sulphur. *Process Biochem* **29:** 475–482.

Bolte, S., Talbot, C., Boutte, Y., Catrice, O., Read, N., and Satiat-Jeunemaitre, B. (2004) FM-dyes as experimental probes for dissecting vesicle trafficking in living plant cells. *J Microsc* **214:** 159–173.

Brierley, C.L., and Brierley, J.A. (2013) Progress in bioleaching: part B: applications of microbial processes by the minerals industries. *Appl Microbiol Biotechnol* **97:** 7543–7552.

Bryan, C.G., Joulian, C., Spolaore, P., Challan-Belval, S., El Achbouni, H., Morin, D.H.R., and D'Hugues, P. (2009) Adaptation and evolution of microbial consortia in a stirred tank reactor bioleaching system: indigenous population versus a defined consortium. *Adv Mat Res* **71:** 79–82.

Bryant, R., Costerton, J., and Laishley, E. (1984) The role of *Thiobacillus albertis* glycocalyx in the adhesion of cells to elemental sulfur. *Can J Microbiol* **30:** 81–90.

Castro, L., Zhang, R., Muñoz, J.A., González, F., Blázquez, M.L., Sand, W., and Ballester, A. (2014) Characterization of exopolymeric substances (EPS) produced by *Aeromonas hydrophila* under reducing conditions. *Biofouling* **30:** 501–511.

Chen, Y., Li, J., Chen, L., Hua, Z., Huang, L., Liu, J., *et al.* (2014) Biogeochemical processes governing natural pyrite oxidation and release of acid metalliferous drainage. *Environ Sci Technol* **48:** 5537–5545.

Dopson, M., Baker-Austin, C., Hind, A., Bowman, J.P., and Bond, P.L. (2004) Characterization of *Ferroplasma* isolates and *Ferroplasma acidarmanus* sp. nov., extreme acidophiles from acid mine drainage and industrial bioleaching environments. *Appl Environ Microbiol* **70:** 2079–2088.

Edwards, K.J., Bond, P.L., Gihring, T.M., and Banfield, J.F. (2000) An archaeal iron-oxidizing extreme acidophile important in acid mine drainage. *Science* **287:** 1796–1799.

Etzel, K., Klingl, A., Huber, H., Rachel, R., Schmalz, G., Thomm, M., and Depmeier, W. (2008) Etching of {111} and {210} synthetic pyrite surfaces by two archaeal strains, *Metallosphaera sedula* and *Sulfolobus metallicus*. *Hydrometallurgy* **94:** 116–120.

Fife, D.J., Bruhn, D.F., Miller, K.S., and Stoner, D.L. (2000) Evaluation of a fluorescent lectin-based staining technique for some acidophilic mining bacteria. *Appl Environ Microbiol* **66:** 2208–2210.

Fröls, S., Dyall-Smith, M., and Pfeifer, F. (2012) Biofilm formation by haloarchaea. *Environ Microbiol* **14:** 3159–3174.

Gehrke, T., Telegdi, J., Thierry, D., and Sand, W. (1998) Importance of extracellular polymeric substances from *Thiobacillus ferrooxidans* for bioleaching. *Appl Environ Microbiol* **64:** 2743–2747.

Goldstein, I., Hollerman, C., and Merrick, J.M. (1965) Protein-carbohydrate interaction I. The interaction of polysaccharides with concanavalin A. *BBA-Gen Subjects* **97:** 68–76.

Golyshina, O.V., and Timmis, K.N. (2005) *Ferroplasma* and relatives, recently discovered cell wall-lacking archaea making a living in extremely acid, heavy metal-rich environments. *Environ Microbiol* **7:** 1277–1288.

Golyshina, O.V., Pivovarova, T.A., Karavaiko, G.I., Kondratéva, T.F., Moore, E., Abraham, W.R., *et al.* (2000) *Ferroplasma acidiphilum* gen. nov., sp. nov., an acidophilic, autotrophic, ferrous-iron-oxidizing, cell-wall-lacking, mesophilic member of the *Ferroplasmaceae* fam. nov., comprising a distinct lineage of the Archaea. *Int J Syst Evol Microbiol* **50:** 997–1006.

Golyshina, O.V., Yakimov, M.M., Lünsdorf, H., Ferrer, M., Nimtz, M., Timmis, K.N., *et al.* (2009) *Acidiplasma aeolicum* gen. nov., sp. nov., a euryarchaeon of the family *Ferroplasmaceae* isolated from a hydrothermal pool, and transfer of *Ferroplasma cupricumulans* to *Acidiplasma cupricumulans* comb. nov. *Int J Syst Evol Microbiol* **59:** 2815–2823.

Hara, S., Yamaguchi, M., Takemori, Y., Furuhata, K., Ogura, H., and Nakamura, M. (1989) Determination of mono-*O*-acetylated *N*-acetylneuraminic acids in human and rat sera by fluorometric high-performance liquid chromatography. *Anal Biochem* **179:** 162–166.

Henche, A.L., Koerdt, A., Ghosh, A., and Albers, S.V. (2012) Influence of cell surface structures on crenarchaeal biofilm formation using a thermostable green fluorescent protein. *Environ Microbiol* **14:** 779–793.

Jarrell, K.F., Ding, Y., Meyer, B.H., Albers, S.-V., Kaminski, L., and Eichler, J. (2014) N-Linked glycosylation in archaea: a structural, functional, and genetic analysis. *Microbiol Mol Biol Rev* **78:** 304–341.

Kalin, M., Fyson, A., and Wheeler, W.N. (2006) The chemistry of conventional and alternative treatment systems for the neutralization of acid mine drainage. *Sci Total Environ* **366:** 395–408.

Karatan, E., and Watnick, P. (2009) Signals, regulatory networks, and materials that build and break bacterial biofilms. *Microbiol Mol Biol Rev* **73:** 310–347.

Koerdt, A., Gödeke, J., Berger, J., Thormann, K.M., and Albers, S.V. (2010) Crenarchaeal biofilm formation under extreme conditions. *PLoS ONE* **5:** e14104.

Koerdt, A., Jachlewski, S., Ghosh, A., Wingender, J., Siebers, B., and Albers, S.-V. (2012) Complementation of *Sulfolobus solfataricus* PBL2025 with an α-mannosidase: effects on surface attachment and biofilm formation. *Extremophiles* **16:** 115–125.

Lawrence, J., Neu, T., and Swerhone, G. (1998) Application of multiple parameter imaging for the quantification of algal,

460 *R. Y. Zhang* et al.

bacterial and exopolymer components of microbial biofilms. *J Microbiol Methods* **32:** 253–261.

Lawrence, J., Swerhone, G., Leppard, G., Araki, T., Zhang, X., West, M., and Hitchcock, A. (2003) Scanning transmission X-ray, laser scanning, and transmission electron microscopy mapping of the exopolymeric matrix of microbial biofilms. *Appl Environ Microbiol* **69:** 5543–5554.

Lewis, A.L., Desa, N., Hansen, E.E., Knirel, Y.A., Gordon, J.I., Gagneux, P., *et al.* (2009) Innovations in host and microbial sialic acid biosynthesis revealed by phylogenomic prediction of nonulosonic acid structure. *Proc Natl Acad Sci* **106:** 13552–13557.

Mackintosh, M.E. (1978) *Nitrogen fixation by* Thiobacillus ferrooxidans. *J Gen Microbiol* **105:** 215–218.

Meyer, B.H., and Albers, S.-V. (2013) Hot and sweet: protein glycosylation in Crenarchaeota. *Biochem Soc Trans* **41:** 384–392.

Näther, D.J., Rachel, R., Wanner, G., and Wirth, R. (2006) Flagella of *Pyrococcus furiosus*: multifunctional organelles, made for swimming, adhesion to various surfaces, and cell-cell contacts. *J Bacteriol* **188:** 6915–6923.

Neu, T., and Lawrence, J. (2009) Extracellular polymeric substances in microbial biofilms. In *Microbial Glycobiology: Structures, Relevance and Applications*. Moran, A., Brennan, P., Holst, O., and von Itzstein, M. (eds). San Diego, CA, USA: Elsevier, pp. 735–758.

Neu, T.R., and Lawrence, J.R. (1999a) In situ characterization of extracellular polymeric substances (EPS) in biofilm systems. In *Microbial Extracellular Polymeric Substances: Characterization, Structure and Function*. Wingender, J., Neu, T.R., and Flemming, H.-C. (eds). Berlin, Germany: Springer, pp. 21–47.

Neu, T.R., and Lawrence, J.R. (1999b) Lectin-binding analysis in biofilm systems. *Methods Enzymol* **310:** 145–152.

Neu, T.R., and Lawrence, J.R. (2002) Laser scanning microscopy in combination with fluorescence techniques for biofilm study. In *Encyclopedia of Environmental Microbiology*. Bitton, G. (ed.). New York, USA: Wiley, pp. 1772–1788.

Neu, T.R., and Lawrence, J.R. (2014) Advanced techniques for in situ analysis of the biofilm matrix (structure, composition, dynamics) by means of laser scanning microscopy. In *Microbial Biofilms: Methods and Protocols, Methods*. In *Molecular Biology*. Donelli, G. (ed.). New York, USA: Springer, pp. 43–64.

Neu, T.R., Kuhlicke, U., and Lawrence, J.R. (2002) Assessment of fluorochromes for two-photon laser scanning microscopy of biofilms. *Appl Environ Microbiol* **68:** 901–909.

Nielsen, P.H., and Jahn, A. (1999) Extraction of EPS. In *Microbial Extracellular Polymeric Substances: Characterization, Structure and Function*. Wingender, J., Neu, T.R., and Flemming, H.-C. (eds). Berlin, Germany: Springer, pp. 49–72.

Olson, G., Brierley, J., and Brierley, C. (2003) Bioleaching review part B. *Appl Microbiol Biotechnol* **63:** 249–257.

Orell, A., Fröls, S., and Albers, S.-V. (2013) Archaeal biofilms: the great unexplored. *Annu Rev Microbiol* **67:** 337–354.

Peltola, M., Neu, T.R., Raulio, M., Kolari, M., and Salkinoja-Salonen, M.S. (2008) Architecture of

Deinococcus geothermalis biofilms on glass and steel: a lectin study. *Environ Microbiol* **10:** 1752–1759.

Rawlings, D.E., and Johnson, D.B. (2007) The microbiology of biomining: development and optimization of mineral-oxidizing microbial consortia. *Microbiology* **153:** 315–324.

Rinker, K.D., and Kelly, R.M. (1996) Growth physiology of the hyperthermophilic archaeon *Thermococcus litoralis*: development of a sulfur-free defined medium, characterization of an exopolysaccharide, and evidence of biofilm formation. *Appl Environ Microbiol* **62:** 4478–4485.

Sand, W., Gehrke, T., Jozsa, P.G., and Schippers, A. (2001) Bio) chemistry of bacterial leaching – direct vs. indirect bioleaching. *Hydrometallurgy* **59:** 159–175.

Sand, W., Jozsa, P.-G., Kovacs, Z.-M., Săsăran, N., and Schippers, A. (2007) Long-term evaluation of acid rock drainage mitigation measures in large lysimeters. *J Geochem Explor* **92:** 205–211.

Schaeffer, W., Holbert, P., and Umbreit, W. (1963) Attachment of *Thiobacillus thiooxidans* to sulfur crystals. *J Bacteriol* **85:** 137–140.

Schippers, A., and Sand, W. (1999) Bacterial leaching of metal sulfides proceeds by two indirect mechanisms via thiosulfate or via polysulfides and sulfur. *Appl Environ Microbiol* **65:** 319–321.

Schippers, A., Jozsa, P., and Sand, W. (1996) Sulfur chemistry in bacterial leaching of pyrite. *Appl Environ Microbiol* **62:** 3424–3431.

Schopf, S., Wanner, G., Rachel, R., and Wirth, R. (2008) An archaeal bi-species biofilm formed by *Pyrococcus furiosus* and *Methanopyrus kandleri*. *Arch Microbiol* **190:** 371–377.

Staudt, C., Horn, H., Hempel, D., and Neu, T. (2003) Screening of lectins for staining lectin-specific glycoconjugates in the EPS of biofilms. In. In *Biofilms in Medicine, Industry and Environmental Technology*. Lens, P., O'Flaherty, V., Moran, A.P., Stoodley, P., and Mahony, T. (eds). London, UK: IWA Publishing, pp. 308–327.

Stewart, P.S., Murga, R., Srinivasan, R., and de Beer, D. (1995) Biofilm structural heterogeneity visualized by three microscopic methods. *Water Res* **29:** 2006–2009.

Stoodley, P., Sauer, K., Davies, D., and Costerton, J.W. (2002) Biofilms as complex differentiated communities. *Annu Rev Microbiol* **56:** 187–209.

Strathmann, M., Wingender, J., and Flemming, H.-C. (2002) Application of fluorescently labelled lectins for the visualization and biochemical characterization of polysaccharides in biofilms of *Pseudomonas aeruginosa*. *J Microbiol Methods* **50:** 237–248.

Tamura, H., Goto, K., Yotsuyanagi, T., and Nagayama, M. (1974) Spectrophotometric determination of iron (II) with 1, 10-phenanthroline in the presence of large amounts of iron (III). *Talanta* **21:** 314–318.

Thoma, C., Frank, M., Rachel, R., Schmid, S., Näther, D., Wanner, G., and Wirth, R. (2008) The Mth60 fimbriae of *Methanothermobacter thermoautotrophicus* are functional adhesins. *Environ Microbiol* **10:** 2785–2795.

Vera, M., Schippers, A., and Sand, W. (2013) Progress in bioleaching: fundamentals and mechanisms of bacterial metal sulfide oxidation – part A. *Appl Microbiol Biotechnol* **97:** 7529–7541.

A lectin study of archaeal glycoconjugates during bioleaching 461

Vimr, E.R., Kalivoda, K.A., Deszo, E.L., and Steenbergen, S.M. (2004) Diversity of microbial sialic acid metabolism. *Microbiol Mol Biol Rev* **68:** 132–153.

Weiss, R. (1973) Attachment of bacteria to sulphur in extreme environments. *J Gen Microbiol* **77:** 501–507.

Whitchurch, C.B., Tolker-Nielsen, T., Ragas, P.C., and Mattick, J.S. (2002) Extracellular DNA required for bacterial biofilm formation. *Science* **295:** 1487–1487.

Wolfaardt, G.M., Lawrence, J.R., and Korber, D.R. (1999) Function of EPS. In *Microbial Extracellular Polymeric Substances: Characterization, Structure and Function.* Wingender, J., Neu, T.R., and Flemming, H.-C. (eds). Berlin, Germany: Springer, pp. 171–200.

Zhang, R., Bellenberg, S., Castro, L., Neu, T.R., Sand, W., and Vera, M. (2014) Colonization and biofilm formation of the extremely acidophilic archaeon *Ferroplasma acidiphilum.* *Hydrometallurgy* doi: 10.1016/j.hydromet .2014.07.001.

Zippel, B., and Neu, T. (2011) Characterization of glycoconjugates of extracellular polymeric substances in tufa-associated biofilms by using fluorescence lectin-binding analysis. *Appl Environ Microbiol* **77:** 505–516.

Zolghadr, B., Klingl, A., Koerdt, A., Driessen, A.J., Rachel, R., and Albers, S.-V. (2010) Appendage-mediated surface adherence of *Sulfolobus solfataricus. J Bacteriol* **192:** 104–110.

Zubkov, M.V., Fuchs, B.M., Eilers, H., Burkill, P.H., and Amann, R. (1999) Determination of total protein content of bacterial cells by SYPRO staining and flow cytometry. *Appl Environ Microbiol* **65:** 3251–3257.

Supporting information

Additional Supporting Information may be found in the online version of this article at the publisher's web-site:

Fig. S1. Biofilm cells of *Acidianus* sp. DSM 29099 visualized by atomic force microscope (AFM) combined with epifluorescence microscope (EFM), exhibiting preferential attack on the pyrite lattice along planes. A and B show EFM images of *Acidianus* sp. DSM 29099 biofilms stained by Syto 9 (green) and TRITC-conjugated Con A (red), respectively. C shows AFM scanning corresponding to EFM (A and B). White arrows show a cell cluster. Bars represent 10 μm.

Fig. S2. Biofilm cells of *Acidianus* sp. DSM 29099. A, cells grown on pyrite and stained by TRITC-conjugated Con A (red) and Syto 9 (green), respectively. B, cells grown on elemental sulfur and stained by FITC-conjugated Con A (green). Con A stained cell surfaces and gave a clear 'capsular binding' pattern. Arrows show cell surfaces. Bars represent 5 μm.

Table S1. List of fluorescent labeled lectins used for staining of archaeal biofilms and their binding target.

Supplementary Material

Use of lectins to in situ visualize glycoconjugates of extracellular polymeric substances in acidophilic archaeal biofilms

R.Y. Zhang[1], T. R. Neu[2], S. Bellenberg[1], U. Kuhlicke[2], W. Sand[1] and M. Vera[1*]

[1]Universität Duisburg – Essen, Biofilm Centre, Aquatische Biotechnologie, Universitätsstraße 5, 45141, Essen, Germany

[2]Helmholtz Centre for Environmental Research-UFZ, Department of River Ecology, Brueckstrasse 3A, 39114, Magdeburg, Germany
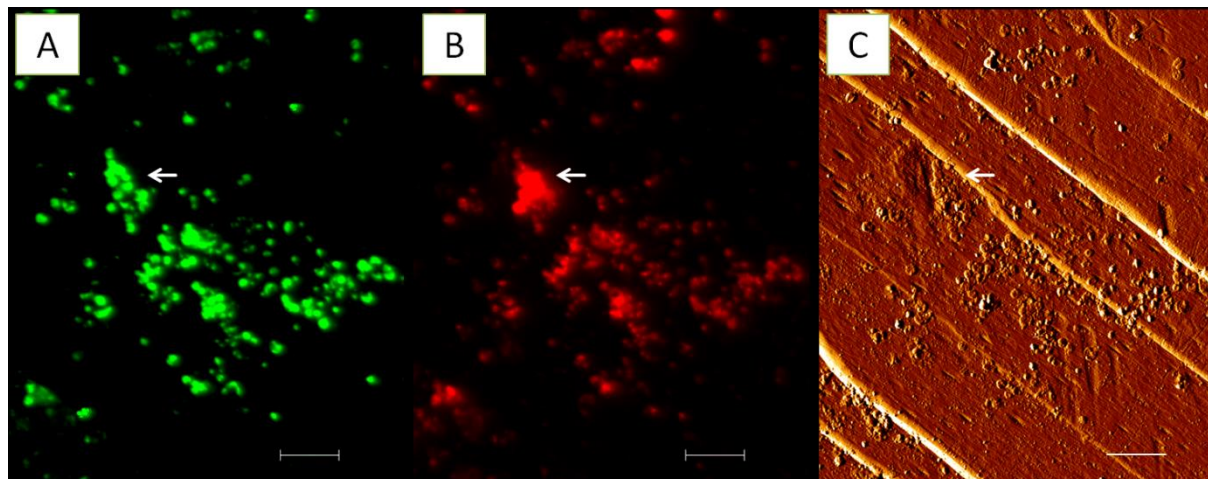
*Corresponding Author

E-mail: mario.vera@uni-due.de

Tel: + 49 0201/183 7080

Fax: + 49 0201/183 7088

Running title: A lectin study of archaeal glycoconjugates during bioleaching

Keywords Bioleaching · Biofilm · Archaea · Lectin

Supplementary Fig. S1. Biofilm cells of *Acidianus* sp. DSM 29099 visualized by atomic force microscope (AFM) combined with epifluorescence microscope (EFM), exhibiting preferential attack on the pyrite lattice along planes. A and B show EFM images of *Acidianus* sp. DSM 29099 biofilms stained by Syto 9 (green) and TRITC-conjugated Con A (red), respectively. C shows AFM scanning corresponding to EFM (A and B). White arrows show a cell cluster. Bars represent 10 μm. For details of the AFM & EFM visualization procedure, see the section Experimental procedures and Mangold *et al*., 2008.
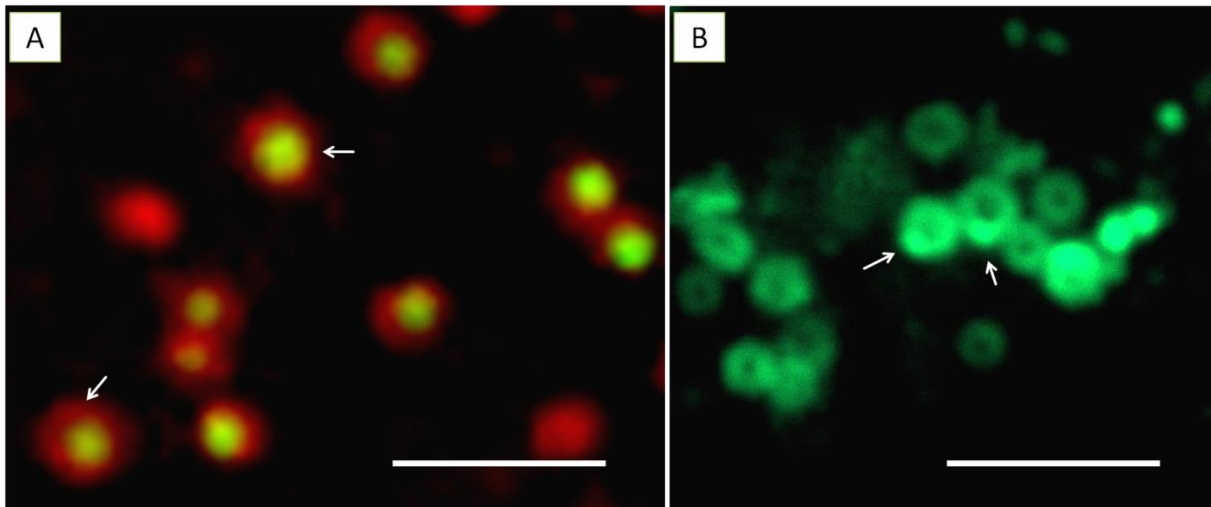
Supplementary Fig. S2. Biofilm cells of *Acidianus* sp. DSM 29099. A, cells grown on pyrite and stained by TRITC-conjugated Con A (red) and Syto 9 (green), respectively. B, cells grown on elemental sulfur and stained by FITC-conjugated Con A (green). Con A stained cell surfaces and gave a clear 'capsular binding' pattern. Arrows show cell surfaces. Bars represent 5 µm.

Supplementary Table S1. List of fluorescent labeled lectins used for staining of archaeal biofilms and their binding target

Name and abbreviation*	Source	Specificity	Lectin group[#]
FITC labeled lectins			
Anguilla anguilla agglutinin, AAA	Eel serum (*Anguilla anguilla*)	Fuc	Animal
Agaricus bisporus agglutinin, ABA/ABL	Edible mushroom (*Agaricus bisporus*)	GalNAc; Gal	Fungi
Amaranthin, ACA/ACL	*Amaranthus caudatus*	GalNAc	Plant
Artocarpus integrifolia agglutinin, AIA	*Artocarpus integrifolia*	GalNAc; Gal	Plant
Arum maculatum agglutinin, AMA	*Arum maculatum*	Man	Plant
Aegopodium podagraria lectin, APP	*Aegopodium podagraria*	GalNAc	Plant
Allium sativum agglutinin, ASA	Garlic (*Allium sativum*)	Man	Plant
Bryonia dioica agglutinin, BDA	*Bryonia dioica*	GalNAc	Plant
Bauhinia purpurea agglutinin, BPA	*Bauhinia purpurea*	GalNAc	Plant
Colchicum autumnale lectin, CA	Meadow saffron (*Colchicumautumnale*)	Lac; GalNAc; Gal	Plant
Caragana aborescens agglutinin, CAA	*Caragana arborescens*	GalNAc	Plant
*Calystegia sepium*lectin, Calsepa	Hedge bindweed (*Calystegia sepium*)	Man/Mal	Plant
Concanavalin A, Con A	Jackbean (*Canavallaensiformis*)	Glc, Man	Plant
Cicer arietinum agglutinin, CPA	Chick pea (*Cicer arietinum*)	Complex	Plant

Cytisus scoparius agglutinin, CSA	Scotchbroom (*Cytisusscoparius*)	GalNAc; Gal	Plant
Dolichos biflorus agglutinin, DBA	*Dolichos biflorus*	GalNAc	Plant
Dioclea grandiflora lectin, DGL	*Dioclea grandiflora*	Glc, Man	Plant
*Datura stramonium*agglutinin, DSA	*Datura stramonium*	GlcNAc	Plant
Erythrina cristagalli agglutinin, ECA	*Erythrina cristagalli*	GalNAc; Gal	Plant
Euonymus europaeus agglutinin, EEA	*Euonymus europaeus*	Gal	Plant
Glechoma hederacea agglutinin, GHA	Ivy (*Glechoma lederacea*)	GalNAc	Plant
Galanthus nivalis agglutinin, GNA	Snowdrop (*Galanthus nivalis*)	Man	Plant
Griffonia simplicifolia lectin, GS-I	*Griffonia simplicifolia*	GalNAc; Gal	Plant
Helix aspersa agglutinin, HAA	Snail (*Helix aspersa*)	GalNAc	Animal
Amaryllis lectin, HHA	Amaryllis (*Hippeastrum hybrid*)	Man	Plant
Homarus americanus agglutinin, HMA	Lobster (*Homarus americanus*)	Sia	Animal
Helix pomatia agglutinin, HPA	Edible snail (*Helix pomatia*)	GalNAc	Animal
Iris hybrid agglutinin, IRA	Dutch iris (*Iris hybrid*)	GalNAc	Plant
Laburnum alpinum agglutinin, LAA	*Laburnum alpinum*	Gal	Plant
Laburnum anagyroides lectin, LAL	*Laburnum anagyroides*	Fuc	Plant
Phaseolus lunatus agglutinin, LBA	Lima bean (*Phaseolus lunatus*)	GalNAc	Plant
Lens culinaris haemagglutinin,	Lentil (*Lens culinaris*)	Glc, Man	Plant

LcH

Lycopersicon esculentum agglutinin, LEA	Tomato (*Lycopersicon esculentum agglutinin*)	GlcNAc	Plant
Limax flavus agglutinin, LFA	Slug (*Limax flavus*)	Sia	Animal
Tetragonolobus purpurea lectin, Lotus	*Tetragonolobus purpurea*	Fuc	Plant
Limulus polyphemus agglutinin, LPA	Horseshoe crab (*Limulus polyphemus*)	Sia	Animal
Maackia amurensis agglutinin, MAA	*Maackia amurensis*	Sia	Plant
Morniga G, MNA-G	*Morus nigra*	Gal	Plant
Marasmium oreades agglutinin, MOA	Mushroom (*Marasmium oreades*)	Gal	Fungi
Maclura pomifera agglutinin, MPA	*Maclura pomifera*	GalNAc	Plant
Narcissus pseudonarcissus agglutinin, NPA	*Narcissus pseudonarcissus*	Man	Plant
*Phaseolus vulgaris*agglutinin E, PHA-E	*Phaseolus vulgaris*	Man	Plant
*Phaseolus vulgaris*agglutinin E, PHA-L	*Phaseolus vulgaris*	GalNAc	Plant
Polygonatum multiflorum agglutinin, PMA	*Polygonatum multiflorum*	Man	Plant
Peanut agglutinin, PNA	Peanut (*Arachis hypogea*)	Gal	Plant
Pisum sativum agglutinin, PSA	*Pisum sativum*	Man	Plant
Polyporus squamosus lectin, PSL	Polypore mushroom (*Polyporus squamosus*)	Sia	Fungi
Psophocarpus tetragonolobus agglutinin, PTA	*Psophocarpus tetragonolobus*	GalNAc	Plant
Phytolacca americana agglutinin, PWA	Pokeweed (*Phytolacca americana*)	GlcNAc	Plant

Robinia pseudoaccacia agglutinin, RPA	Black locust (*Robinia pseudacacia*)	GalNAc	Plant
Soybean agglutinin, SBA	Soybean (*Glycine max*)	GalNAc; Gal	Plant
Sophora japonica agglutinin, SJA	Japanese pagoda tree (*Sophora japonica*)	GalNAc	Plant
Sambucus nigra agglutinin, SNA	Elderberry (*Sambucus nigra*)	GalNAc; Gal	Plant
Solanum tuberosum agglutinin, STA	*Solanum tuberosum*	GlcNAc	Plant
Trichosanthes kirilowii agglutinin, TKA	*Trichosanthes kirilowii*	Gal	Plant
Tulipa sp. agglutinin, TL	*Tulipa* sp.	GalNAc	Plant
Urtica dioica agglutinin, UDA	*Urtica dioica*	GalNAc	Plant
Ulex europaeus I, UEA I	Furze gorse (*Ulex europaeus*)	Fuc	Plant
Vicia faba agglutinin, VFA	*Vicia faba*	Glc	Plant
Vicia graminea agglutinin, VGA	*Vicia graminea*	GlcNAc	Plant
Vigna radiata agglutinin, VRA	*Vigna radiata*	Gal	Plant
Vicia villosa agglutinin, VVA	*Vicia villosa*	GalNAc	Plant
Wisteria floribunda agglutinin, WFA	*Wisteria floribunda*	GalNAc	Plant
Wheat germ agglutinin, WGA	*Triticum vulgaris*	GlcNAc	Plant
Alexa488 labeled lectins			
Aleuria aurantia lectin, AAL	*Aleuria aurantia*	Fuc	Fungi
Cancer antennarius agglutinin, CCA	Marine crab (*Cancer antennarius*)	Sia	Animal
Codium fragile lectin, Co	*Codium fragile*	GalNAc	Alga
Erythrina corallodendron lectin, Ecor	*Erythrina corallodendron*	Gal	Plant
Homarus americanus agglutinin,	Lobster(*Homarus americanus*)	Sia	Animal

Iberis amara agglutinin, IAA	*Iberis amara*	GalNAc	Plant
Mangifera indica agglutinin, MIA	*Mangifera indica*	ND	Plant
Perseau americana agglutinin, PAA	*Perseau americana*	GlcNAc	Plant
Pseudomonas aeruginosa lectin I, PA-I	*Pseudomonas aeruginosa*	Gal	Bacteria
Ptilota plumosa agglutinin, PPA	*Ptilota plumosa*	Gal	Alga
Trifolium repens agglutinin, RTA	*Trifolium repens*	GlcA	Plant
Tritrichomonas mobilensis lectin, TML	*Tritrichomonas mobilensis*	Sia	Bacteria
Vicia graminea agglutinin, VGA	*Vicia graminea*	GlcNAc	Plant
TRITC labeled lectin			
Con A	Jackbean (*Canavallaensiformis*)	Glc, Man	Plant

*Man=Mannose, Fuc=Fucose, Glc=Glucose, GlcA=Glucuronic acid, Gal=Galactose, GalNAc=*N*-acetylgalactosamine, GlcNAc=*N*-acetylglucosamine, ND=Not determined, Sia=Sialic acid, Lac=Lactose, Mal=Maltose

[#]For details of the lectin classification, see Doyle and Slifkin, 1994 and Van Damme *et al*., 1998.

References

Doyle, R.J., and Slifkin, M. (1994) *Lectin-microorganism interactions*. New York, USA: Marcel Dekker.

Mangold, S., Harneit, K., Rohwerder, T., Claus, G., and Sand, W. (2008) Novel combination of atomic force microscopy and epifluorescence microscopy for visualization of leaching bacteria on pyrite. *Appl Environ Microbiol* **74:** 410-415.

Van Damme, E.J., Peumans, W.J., Pusztai, A., and Bardocz, S. (1998) *Handbook of plant lectins: properties and biomedical applications*. Chichester; New York:John Wiley & Sons.

4.3 EPS analysis of the thermoacidophilic archaeon *S. metallicus*

Microbial sulfur metabolism plays an important role in the global sulfur cycle. It is closely related to many fields such as AMD/ARD, soil acidification and material corrosion. Protons produced during microbial S^0 oxidation are essential to enable a low pH environment in bioleaching systems. Meanwhile, S^0 and polysulfide deposited on mineral surfaces are hindering metal leaching rate in case of MS such as chalcopyrite. Previous work in our laboratory has been shown that EPS mediate the contact between cells and surfaces. S^0 has to be activated by cells (EPS compounds) before its intracellular oxidation happens (Rohwerder and Sand 2007).

In the present work, we focused on the EPS components of *S. metallicus*[T] forming biofilms on S^0. CLSM combined with FLBA were applied in order to visualize cell and EPS distribution. EPS was extracted and its composition was quantitatively analyzed. Capsular EPS from planktonic cells were mainly composed of carbohydrates and proteins. In contrast, colloidal EPS from planktonic cells were mainly composed of carbohydrates. Proteins were found to be among the major components of EPS from *S. metallicus*[T] biofilms on S^0. In addition, extracellular proteins and nucleic acids were present in the EPS matrix. The existence of these compounds suggest their potential roles in biofilm formation and stabilization. *S. metallicus*[T] cells were embedded in a flexible EPS matrix.

ENVIRONMENTAL BIOTECHNOLOGY

Visualization and analysis of EPS glycoconjugates of the thermoacidophilic archaeon *Sulfolobus metallicus*

Ruiyong Zhang[1] · Thomas R. Neu[2] · Yutong Zhang[1] · Sören Bellenberg[1] · Ute Kuhlicke[2] · Qian Li[1] · Wolfgang Sand[1] · Mario Vera[1]

Abstract Biofilms are surface-associated colonies of micro-organisms embedded in a matrix of extracellular polymeric substances (EPS). As EPS mediate the contact between cells and surfaces, an understanding of their composition and production is of particular interest. In this study, the EPS components of *Sulfolobus metallicus* DSM 6482[T] forming biofilms on elemental sulfur (S^0) were investigated by confocal laser scanning microscopy (CLSM). In order to visualize cell and EPS distributions, biofilm cells were stained with various dyes specific for glycoconjugates, proteins, nucleic acids and lipids. Biofilm cells on S^0 were heterogeneously distributed and characterized as individual cells, microcolonies, and large clusters up to a hundred micrometers in diameter. The glycoconjugates in biofilms were detected by fluorescence lectin-binding analysis (FLBA). Screening of 72 commercially available lectins resulted in the selection of 21 lectins useful for staining biofilms of *S. metallicus*[T]. Capsular EPS from planktonic cells were mainly composed of carbohydrates and proteins. In contrast, colloidal EPS from planktonic cells were dominated by carbohydrates. Proteins were found to be major components in EPS from biofilms on S^0. Using specific probes combined with CLSM, we showed that extracellular proteins and nucleic acids were present in the EPS matrix.

Finally, we showed that *S. metallicus*[T] cells were embedded in a flexible EPS matrix. This study provides new insights into archaeal biofilms and EPS composition and properties with respect to their interactions with S^0.

Keywords Biofilm · Glycoconjugates · Thermoacidophilic archaea · Lectin · Elemental sulfur

Introduction

Sulfur is important in central biochemistry as well as in industrial applications such as sulfur concretes, sulfur foams, sulfur asphalts, and sulfuric acid production. The biological sulfur cycle has important environmental and economic significance for many fields such as acid mine drainage (AMD), soil acidification, and material corrosion (Little et al. 2000). Sulfur-metabolizing acidophilic bacteria and archaea oxidize various reduced inorganic sulfur compounds (RISCs) that occur naturally (Dopson and Johnson 2012). Protons generated from microbial sulfur oxidation are an important agent to accelerate and cause dissolution of metal sulfides. In addition, the resulting acidic environments are essential for metal-oxidizing microorganisms to thrive. From another point of view, as one of the major intermediates in the course of metal sulfide oxidation (Sand et al. 1998), S^0 and polysulfides may form a passive layer during chalcopyrite ($CuFeS_2$, a refractory copper mineral) dissolution and, subsequently, metal leaching is hindered (Dutrizac 1990; Rodrıguez et al. 2003).

The microbial biofilm lifestyle brings various advantages such as mechanical stability, nutrient supply, and genetic exchange as well as protection from dehydration and environmental stress (Flemming and Wingender 2010). EPS include carbohydrates, proteins, lipids, and DNA among other macromolecules (Flemming et al. 2007). To date, studies on microbial

✉ Mario Vera
mario.vera@uni-due.de

[1] Aquatische Biotechnologie, Biofilm Centre, Universität Duisburg—Essen, Universitätsstraße 5, 45141 Essen, Germany

[2] Department of River Ecology, Helmholtz Centre for Environmental Research—UFZ, Brückstraße 3a, 39114 Magdeburg, Germany

🖄 Springer

biofilms and EPS have mainly been conducted on bacteria. In contrast, only very limited information is available for the archaeal domain, in which biofilms are as widespread and complex as the bacterial ones (Fröls 2013; Orell et al. 2013).

Attachment of microbes to sulfur is dependent on growth conditions, hydrophobic interactions, and other factors like osmotic pressure (Knickerbocker et al. 2000; Takeuchi and Suzuki 1997). Surfactants (e.g., Tween 80) were shown to be stimulatory for microbial growth and sulfur oxidation by *Acidithiobacillus albertensis* and *Acidithiobacillus ferrooxidans* (Sand 1985; Zhang et al. 2008a). Extracellular lipids (e.g., phospholipids), acting as a wetting agent, can also mediate microbial interactions with sulfur and are thought to play key roles during its oxidation (Arredondo et al. 1994). Also, microbial appendages (filamentous matrix) or extracellular compounds (glycocalyx) were found to play a role in sulfur colonization and oxidation by *Acidithiobacillus thiooxidans* and *A. albertis* (Blais et al. 1994; Bryant et al. 1984). These studies also indicate that microbial attachment may be a consequence of different mechanisms, e.g., attachment of *A. thiooxidans* and *A. albertis* to sulfur surface was favored by the presence of filamentous materials to a bacterial glycocalyx. However, sulfur colonization by *Thiobacillus thioparus* did not follow this attachment mechanism (Blais et al. 1994).

Sulfur oxidation by acidophilic microbes may involve the following steps: (1) cell attachment to and colonization of sulfur surfaces by chemotaxis and hydrophobic interactions among others; (2) a S^0 activation prior to oxidation (Rohwerder and Sand 2003), possibly conducted by thiol-rich proteins excreted after cell colonization (Peng et al. 2013; Zhang et al. 2008b); (3) a (yet unclear) process of transport of sulfur and/or polysulfides through the cell membrane; and (4) oxidation of sulfur in the periplasmic space (in case of Gram-negative bacteria) or cytoplasm, where sulfur oxidizing enzymes (e.g., the archaeal sulfur oxygenase-reductase, SOR) are located. Although RISC speciation during sulfur and mineral sulfide oxidation by *Sulfobacillus thermosulfidooxidans* and *Acidianus manzaensis* has been recently described (Liu et al. 2013; Nie et al. 2014), transformation of various sulfur allotropes makes the understanding of sulfur metabolism difficult. Current understanding of sulfur chemolithotrophic oxidation in Archaea is largely restricted to *Sulfolobales*, e.g., *Sulfolobus* and *Acidianus* (Kletzin 2008; Rohwerder and Sand 2007).

The archaeal cell envelope and surface structures are fundamentally different from the bacterial ones (Albers and Meyer 2011). Archaea and bacteria may use different surface compounds and mechanisms to interact with their surrounding environment. Most previous biofilm studies were mainly done using (preparative) destructive approaches, e.g., scanning electron microscopy (SEM) or transmission electron microscopy (TEM). In contrast, fluorescence lectin-binding analysis (FLBA) and attenuated total reflection-Fourier transform infrared (ATR-FTIR) spectroscopy are both non-destructive techniques for analyzing

biofilm formation and EPS components (Schmitt and Flemming 1998; Zippel and Neu 2011). FLBA usually involves screening of many lectins to establish a panel of probes which react with a particular biofilm sample and which may indicate the composition of EPS glycoconjugates in biofilms. The first FLBA of acidophilic archaeal biofilms revealed that various glycoconjugates, e.g., glucose, galactose, mannose, N-acetylglucosamine (GlcNAc), N-acetalgalactosamine (GalNAc), sialic acids, and fucose, were present in biofilms of *Ferroplasma acidiphilum*, *Sulfolobus metallicus*, and *Acidianus* sp. DSM 29099 grown on pyrite (Zhang et al. 2015). Fourier transform infrared (FTIR) is widely used to analyze functional groups in mixed biofilms and also to identify microbes at the strain level according to specific surface infrared spectra. In addition, key band ratios within a defined spectrum of a biological sample can correlate with the composition of biological materials and provide useful information about environmental biofilm samples (Nichols et al. 1985).

The Crenarchaeon *S. metallicus* is a thermoacidophilic obligate aerobe with an optimal growth temperature at 65 °C and an optimal growth pH of 2–3. It oxidizes ferrous iron, RISCs (e.g., S^0, tetrathionate), and metal sulfides. *S. metallicus* is the only species of this genus which can grow chemolithotrophically using metal sulfides or RISCs to sustain growth. In addition, compared to the mesophilic and moderate thermophilic archaeal and bacterial counterparts, *S. metallicus* grows at higher temperatures, leading to increased metal sulfide leaching rates.

In this report, biofilm formation and EPS matrix components were studied based on an in situ and non-destructive approaches using ATR-FTIR and FLBA. *S. metallicus* DSM 6482[T] was used as the model organism for screening 72 commercially available fluorescent-labeled lectins. These lectins which react with EPS glycoconjugates of *S. metallicus*[T] were obtained for in situ monitoring of biofilm development and potentially probing individual species in mixed biofilms. In addition, different EPS compounds including nucleic acids, proteins, and lipophilic compounds as well as various glycoconjugates were visualized by confocal laser scanning microscopy (CLSM). FTIR was used to identify functional groups (biopolymers) likely to be involved in microbial attachment to and biofilm formation on S^0. Conventional spectrophotometric methods were used to determine EPS components from planktonic and biofilm cells. This is the first report of biofilm and EPS analysis of *S. metallicus* grown on S^0.

Experimental procedures

Archaeal strains and growth conditions

S. metallicus DSM 6482[T] was purchased from Deutsche Sammlung von Mikroorganismen und Zellkulturen GmbH

(DSMZ). The new isolate *Acidianus* sp. DSM 29099 (=JCM 30227) was chosen to study the biofilm features and EPS production comparatively with *S. metallicus*[T]. Both strains were grown in Mackintosh (MAC) medium (Mackintosh 1978) at 65 °C and 120 rpm with an initial pH of 2.5. S^0 (10 g/L) and yeast extract (0.2 g/L) were added as energy source and growth factors, respectively.

Sulfur prills and cubes

To produce sulfur prills and cubes, sulfur powder (Carl Roth, Germany) was molten in a glass beaker at 130 °C and poured into ice-cold deionized water with agitation (250 rpm). Sulfur prills with a diameter of 1–3 mm were formed due to rapid cooling. Also, molten sulfur was poured on glass plates to obtain a sulfur layer after its solidification. Sulfur coupons with a size of approx. 0.5 cm × 0.5 cm × 2 mm were obtained by breaking the sulfur layer. Both, sulfur prills and coupons, were autoclaved at 110 °C for 90 min.

EPS extraction and analysis

After 7 days of incubation, planktonic cells and sulfur particles with biofilm cells were separated by filtration through sterile Whatman filter paper. Cells of *S. metallicus*[T] were collected afterwards by centrifugation at 8000 rpm (11,300 g) for 15 min. Cell pellets were washed by MAC medium and freeze-dried (ALPHA 2–4 LSC, −80 °C). The supernatant was further filtrated through polycarbonate filters (GTTB, Ø2.5 cm, 0.2 μm pore size, Millipore®) to remove whole cells. These cell-free supernatants (containing "colloidal EPS") were dialyzed using a cellulose membrane (cutoff 3.5 kDa) against deionized water at 4 °C for 48 h. Dialyzed colloidal EPS solutions were further freeze-dried. Capsular EPS were extracted from cell pellets using 20 mM EDTA as previously described (Castro et al. 2014). Sulfur particles were manually milled in a mortar and incubated with 20 mM EDTA at 4 °C and shaking at 180 rpm for 4 h to extract EPS from biofilm cells. The extraction was repeated three times and the resulting solutions were centrifuged, filtered, and dialyzed as described above.

Phenol–sulfuric acid method was used for carbohydrate determination with glucose as a standard (Dubois et al. 1956). Protein concentration was analyzed with bovine serum albumin (BSA) standard (Bradford 1976). DNA was determined using DNA from salmon sperm as a standard (Burton 1956). Cell lysis was estimated by measuring glucose-6-phosphate dehydrogenase activity (Ng and Dawes 1973).

Fourier transformed infrared spectroscopic assay

Powdered cell pellets, colloidal EPS, and EPS extracted from *S. metallicus*[T] biofilms on S^0 were spread on a diamond attenuated total reflectance (ATR) apparatus (Pike Technologies,

USA), separately attached to the FTIR. The spectra were recorded using a FTIR 430 spectrometer (JASCO, Japan). The baseline shift of blank spectra was corrected using Spectra Manager (JASCO, Japan). At least 64 scans, with a resolution of 4 cm^{-1}, were collected for all samples using the Happ-Genzel apodization function. Two measurements were done for each sample. As all cellular components possess characteristic absorbance frequencies and primary molecular vibrations between 4000 and 550 wave numbers (Naumann et al. 1991), the FTIR scan was carried out in this region.

Fluorescence staining of samples

Sulfur prills and cupons with attached cells were mounted in a Petri dish. The cell biomass and spatial distribution within the biofilms on S^0 were visualized after staining with the nucleic acid stains: DAPI (diamidino-2-phenylindole), Syto 9, Syto 61, Syto 64, SybrGreen (Invitrogen, Germany), and DDAO (7-hydroxy-9H^{-1},3-dichloro-9,9-dimethylacridin-2-one; Invitrogen, Germany). The cell-permeant Syto 64, a fluorescent nucleic acid stain, exhibits bright red fluorescence upon binding to nucleic acids. DDAO stains nucleic acids and normally does not penetrate cell membranes. Thus, it has been selected as the preferred fluorochrome for staining extracellular DNA (eDNA) (Koerdt et al. 2010). DDAO was incubated with samples for 20 min before CLSM observation. All other dyes were added to the samples and directly visualized. In addition, stains specific for proteins, lipophilic compounds, and β-polysaccharides were also tested to characterize biofilm components. The details of these stains are listed in Table 1.

Fluorescence lectin-binding assays

Based on a critical assessment of the lectin approach for EPS glycoconjugates (Neu et al. 2001), mainly FITC-labeled lectins but also some Alexa-labeled lectins were tested to select suitable ones for binding to *S. metallicus* biofilms. Staining was done in a Petri dish or a coverwell chamber of 20 mm in diameter with 0.5 mm spacer (Invitrogen, Germany) as described before (Zhang et al. 2015). In case of counter staining, lectin-stained samples were incubated with nucleic acid/protein/lipid stains and directly observed using CLSM without any further treatment. For staining cells from the planktonic phase, 1 mL of cultures grown for 4 days were filtered on polycarbonate filters as previously described (Bellenberg et al. 2012) and incubated with 16 selected lectins (Supplementary Table S1). Filters with stained cells were mounted using an anti-fading agent (Citifluor, Ltd. AF2) prior to CLSM observation.

Confocal laser scanning microscopy

Examination of stained samples was performed using a TCS SP5X AOBS (Leica, Heidelberg, Germany), controlled by the

Results and Discussion

Appl Microbiol Biotechnol (2015) 99:7343–7356

Table 1 Characteristics and binding targets of selected fluorochromes used in this study

Fluorochrome	Binding targets	Ex/Em wavelength (nm)	Concentration
SYTO 9	Nucleic acids (NA)	483/478–488, 500–560	6 μM
SYTO 64	NA	599/625–700	6 μM
SybrGreen	NA	483/475–489, 500–560	6 μM
DDAO	Extracellular NA	600/620–720	10 μg/mL
DAPI	NA	405/485–495, 515–600	100 μg/mL
SyproRed	Proteins	475, 500/470–480, 580–680	×1 work solution
SyproOrange	Proteins	475/470–480, 520–620	×1 work solution
FM1-43	Lipid-rich domain	475–485/580–650	10 μg/mL
FITC-conjugated lectins	EPS glycoconjugates	490/485–495, 510–600	50–100 μg/mL
Calcofluor white M2R	β-Polysaccharides	365/420–460	100 μg/mL
Nile red	Lipid-rich domain	550/650	10 μg/mL

All fluochromes were from Invitrogen, except Nile red (Sigma Aldrich).

LASAF 2.4.1 build 6384. The system was equipped with an upright microscope and a super continuum light source (470–670 nm) as well as a 405-nm pulsed laser diode. Images were collected with a ×63 water immersion lens with a numerical aperture (NA) of 1.2 and a ×63 water immersible lens with a NA of 0.9. Details of fluorescent dyes along with excitation and emission filters used are shown in Table 1. CLSM data sets were recorded in sequential mode to avoid cross talk of the fluorochromes between two different channels. Surface topography and texture of the pyrite as well as of the S^0 surface were recorded by using the CLSM in reflection mode.

Atomic force microscopy and epifluorescence microscopy

A NanoWizard II atomic force microscope (JPK Instruments, Germany) combined with the BioMaterial Workstation (JPK Instruments) was used. For atomic force microscopy (AFM) imaging, a silicon cantilever CSC37-A (Mikromasch, Estonia) with the following features was used: typical length, 250 μm; width, 35 μm; thickness, 2 μm; resonance frequency, 41 kHz; and nominal force/spring constant, 0.65 N/m. Each AFM image consists of 512 by 512 or 1024 by 1024 pixels. AFM imaging was performed in contact mode in air. Twenty microliters of cell suspension were spread on a glass slide and cells were fixed by evaporation. Cells and their EPS were stained by Syto 9 and TRITC-labeled Con A, respectively, as mentioned above. By using a shuttle stage, the same surface area of samples was both visualized by epifluorescence microscopy (EFM) (Zeiss, Germany) and AFM (BioMaterial™Workstation, JPK Instruments) with an error below 2 μm (Mangold et al. 2008). At least three different spots (around 100 by 100 μm) from each sample were checked and recorded by combined AFM and EFM.

Digital image analysis

Fluorescence images were analyzed using an extended version of the software ImageJ. Maximum intensity (MIP) and XYZ projections of 3-dimensional data sets were produced with the software IMARIS version 7.3.1 (Bitplane AG, Zurich, Switzerland) and Huygens-Adobe. In some cases, deconvolution of 3-dimensional data sets was processed to enhance the clarity of the images.

Results

EPS characterization

The presence of functional groups on archaeal cells and S^0 surfaces was examined using FTIR spectroscopy. ATR-FTIR spectra of cells and EPS from biofilms as well as from colloidal EPS from supernatant of *S. metallicus*[T] cultures are shown in Fig. 1. The spectra displayed different features which originate from various biopolymers. According to previous reports (Schmitt and Flemming 1998; Suci et al. 1997), the bands at approx. 1634 and 1536 cm^{−1} are due to proteins (amide I and amide II). Features with peaks at 1453 cm^{−1} are due to C-H bend from CH_2. The band at 1389 cm^{−1} represents the C-O bend from carboxylate groups. Features with peaks at 1211 primarily originate from phosphodiester linkages of RNA and DNA. Polysaccharides normally exhibit bands in the region from 1130 to 900 cm^{−1}. Obviously, cells of *S. metallicus*[T] have mainly proteins and carbohydrates on their surfaces, which is in agreement with the characteristics of *Sulfolobales*. By comparison of cells and EPS from biofilms, changes in the peak location and intensity of the amide groups were detected. This implies protein conformational variation (Parikh and Chorover 2006). In addition, EPS from biofilms showed small peaks in the polysaccharide region if compared
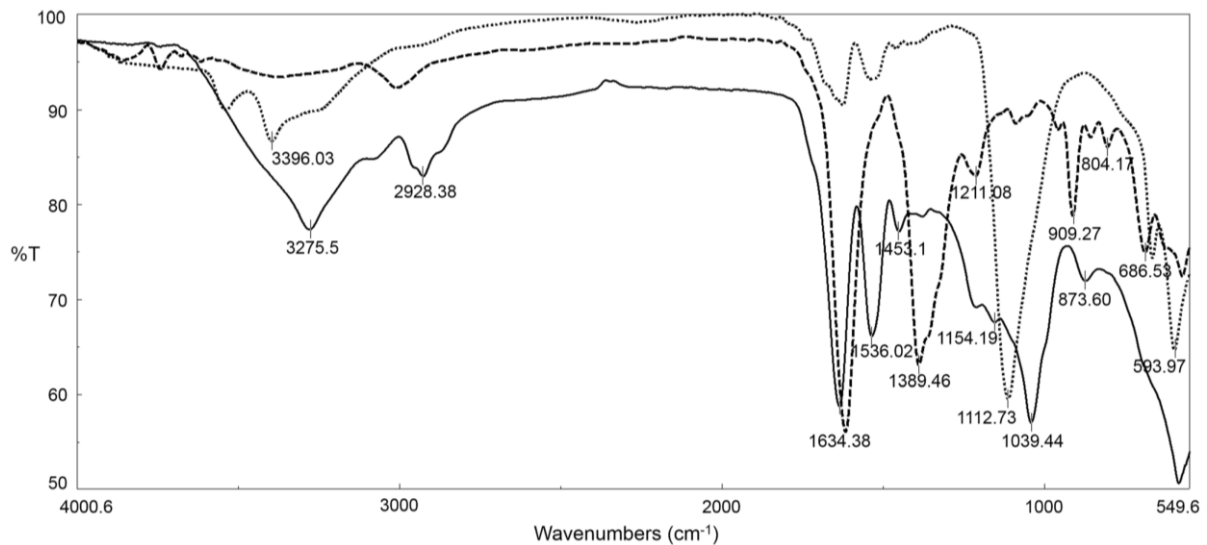
🖄 Springer

Fig. 1 ATR-FTIR spectra of cells and EPS of *S. metallicus*[T] grown on S[0]. Planktonic cells (*solid line*), colloidal EPS (*dotted line*), and EPS from biofilms on S[0] (*dashed line*) are shown

to cell signals. The band ratios of amide I/polysaccharide from cell surface (~1) and EPS from biofilms (~2) were observed to change. This finding suggests an increased protein proportion in cells attached to S[0]. Colloidal EPS showed only a strong polysaccharide peak at 1039 cm^{−1}. The variation of the peak position of cells and colloidal EPS in the polysaccharide region indicates a variation of sugar moieties. ATR-FTIR spectra of S[0] collected after cell growth showed characteristics of the presence of biopolymers (e.g., amide I and II adsorption; not shown). By conventional spectrophotometric methods, both colloidal EPS and capsular EPS from planktonic cells were found to be composed of carbohydrates and proteins (Supplementary Table S2). In colloidal EPS, the amount of carbohydrates (25.9 mg/L) was ~9 times higher than proteins (2.9 mg/L). In contrast, similar amount of carbohydrates (15.9 mg/g) and proteins (15.7 mg/g) were found in capsular EPS fractions. In the case of EPS from biofilms on S[0], proteins were the main components (8.8 mg/g). Also, carbohydrates (0.5 mg/g) and DNA (0.09 mg/g) were detected. In general, the spectrophotometric determination agreed with ATR-FTIR analysis. Taken together, EPS data indicated the following: (1) *S. metallicus*[T] cells attached to S[0] were capable of modifying their surface, (2) protein-like compounds dominated on the S[0] surface, and (3) the compounds excreted to the bulk solution were mostly carbohydrates.

Visualization of planktonic cells of *S. metallicus*[T] grown on S[0]

Planktonic cells on glass slides Cells of *S. metallicus*[T] appear as irregular shaped with a diameter of 1–1.5 μm when grown

on S[0] (Fig. 2b, c). In addition, by EFM, we observed that Syto 9 signals were mostly surrounded by Con A signals. This indicates that cells were covered with glycoconjugates rich in mannose and/or glucose. Obviously, the contact between cells and glass surfaces is mediated by these compounds. Few spots (footprints) were detected with only EPS signals devoid of nucleic acid signals (Fig. 2a, arrows). Additionally, these cell-free dots were only approx. one quarter as high as cells (not shown) as identified by a corresponding AFM scan (Fig. 2b, arrows). These findings indicate that these glycoconjugates were part of cell surfaces and remained on the glass after cell detachment (cell "footprints").

Glycoconjugates of planktonic cells on filters In order to assess surface compounds of planktonic cells of *S. metallicus*[T] grown on S[0], 16 lectins were selected to stain cells settled on polycarbonate filters under fully hydrated conditions. The lectins BPA, Con A, GS-II, PMA, PNA, and SBA were detected to bind planktonic cells, as shown in Supplementary Fig. S1 and Table S1. Surface compounds were characterized as sugar monomers like mannose, glucose, galactose, N-acetylgalactosamine (GalNAc), and N-acetylglucosamine (GlcNAc). These sugars are generally found in cell wall structures of *Sulfolobales* (Albers and Meyer 2011).

Visualization of *S. metallicus*[T] biofilm cells on S[0]

Nucleic acid staining For staining of nucleic acids, the dyes SybrGreen, Syto 64, Syto 9, Syto 61, DDAO, and DAPI were used. Biofilms of *S. metallicus*[T] on S[0] under fully hydrated conditions were visualized, as shown in Fig. 3. These were
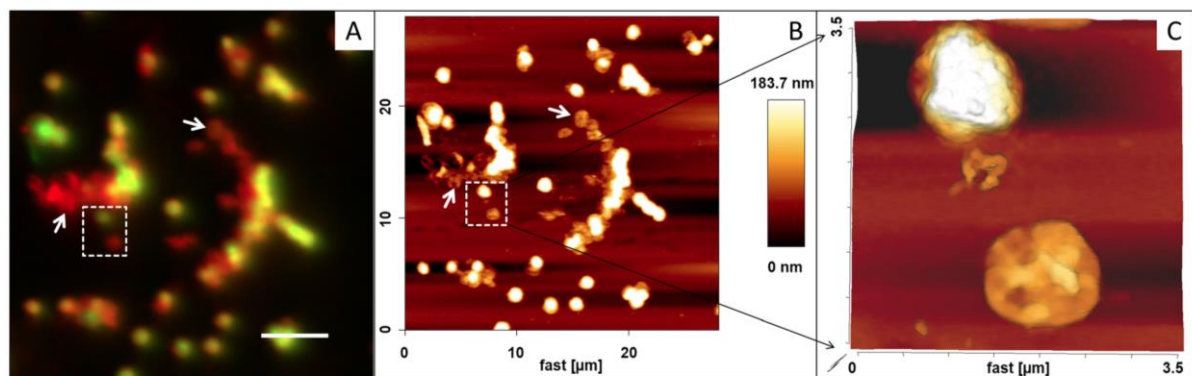
Fig. 2 Combined EFM with AFM Images of *S. metallicus*[T] cells on glass slides. **a** (EFM) Cells stained by Syto 9 (*green*) and Con A-TRITC (*red*). **b** An AFM scanning in contact mode in air from the corresponding area in **a**. **c** A 3-D image from an AFM scanning corresponding to the frame area in **a** and **b**. *Size bar* in **a** represents 5 μm

heterogeneous containing individual cells and large colonies after 5 days. Biofilm cells were often found in surface imperfections, while on flat areas, mostly, single cells were found. Apart from the cell distribution pattern, several extracellular DNA morphologies were visible. In Fig. 3b, cells were forming small colonies with approx. 10 μm. Diffuse DNA signals were covering individual cells. Thread-like and filamentous DNA was clearly visible (Fig. 3c, e, arrows). Some cells showed "cloud-like" signals and gave a blurred appearance, which was slightly bigger than normal cells (Fig. 3d). DAPI staining of biofilms showed also a cloud-like pattern, namely cells and materials (eDNA) connecting them (Fig. 3f). In case of *Acidianus* sp. DSMZ 29099, no such eDNA in biofilms was visible (Supplementary Fig. S2). Cell lysis caused by staining procedures was excluded because neutralization procedures did not result in cell disruption in our assays (not shown). However, an active excretion of DNA by cells due to a pH shock during staining cannot be ruled out.

Protein staining As shown in Fig. 4a–c, protein staining was revealed by several patterns: cell surfaces, areas near cell surfaces, and thread-like signals connecting cells. In comparison, these patterns of protein staining were not observed for biofilm cells of *Acidianus* sp. DSM 29099 (Fig. 4d). The presence of extracellular proteins in *S. metallicus*[T] biofilms was coincident with the ATR-FTIR and conventional spectrophotometric analysis (Fig. 1 and Supplementary Table S2). Although it has been suggested that (thiol-rich) proteins are involved in attachment and sulfur activation, this is the first time that the presence of extracellular proteins has been verified by direct observation.

Amphiphilic compounds The dyes Nile red, FM1-63, and FM4-64 for lipophilic compounds were tested with biofilm cells of *S. metallicus*[T]. FM1-43-stained cell surfaces and gave a "ring-like" (capsular) staining pattern (Fig. 4e). In contrast to protein or nucleic acid stains, no smear signals appeared. This seems to indicate that lipophilic compounds, apart from cell surfaces, are not present on S[0] surfaces, or their concentration is below the CLSM detection limit.

Visualization of glycoconjugates in biofilm cells

The screening of 72 commercially available lectins showed that 21 lectins bound to biofilm cells of *S. metallicus*[T] (Table 2). When compared with the lectins reacting with EPS and cells of *Acidianus* sp. DSM 29099, only 8 of them recognized cell glycoconjugates of both archaeal species (Supplementary Table S3). The lectin AAL has been reported to react with acidophiles such as *F. acidiphilum*, *Acidianus*, and *S. metallicus* biofilms grown on pyrite. Also, it reacts with biofilms of *Acidianus* sp. DSM 29099 on S[0] (Zhang et al. 2015). Interestingly, this lectin did not bind biofilm cells of *S. metallicus*[T] on S[0].

Binding patterns Among the positive lectins, two lectin-binding patterns became obvious. The first one represents lectin signals restricted to cell surfaces, named "capsular binding." As shown in Fig. 5 and Table 2, 15 lectins showed this pattern. The second one corresponds to lectins, whose signals covered cell surfaces as well as extended areas close to the cells, named "colloidal binding." In total, 6 lectins showed this pattern (Fig. 5 and Table 2). All positive lectins for both patterns are shown in Supplementary Figs. S3 and S4, respectively. These lectin-binding patterns were already reported for acidophilic archaeal biofilms on pyrite (Zhang et al. 2015).

Glycoconjugates on S[0] Apart from the two types of lectin-binding patterns, various glycoconjugates were detected in biofilm cells of *S. metallicus*[T]. These include glucose, galactose, mannose, fucose, sialic acids, GlcNAc, and GalNAc. Similar sugar moieties were reported to be present in biofilm cells of *Acidianus* sp. DSM 29099 grown on S[0] (Zhang et al. 2015). In addition, we compared 16 selected lectins to stain

Fig. 3 Visualization of
S. metallicus[T] biofilms on S[0] by
nucleic acid stains. Maximum
intensity projections of biofilms
stained by SybrGreen (**a**–**e**) and
DAPI (**f**). Diffuse (**a**, **b**, **d**) and
thread (**c**, **e**, **f**) signals were
visible. Cells were mostly
detected on edges (**b**), holes (**b**),
and cracks (**f**). *Arrows* indicate
thread-like eDNA. Inside the
circle in **c**, single cells were
highlighted. Color allocation:
green SybrGreen, *blue* DAPI. The
sulfur surface is shown in
reflection mode (*grey*)
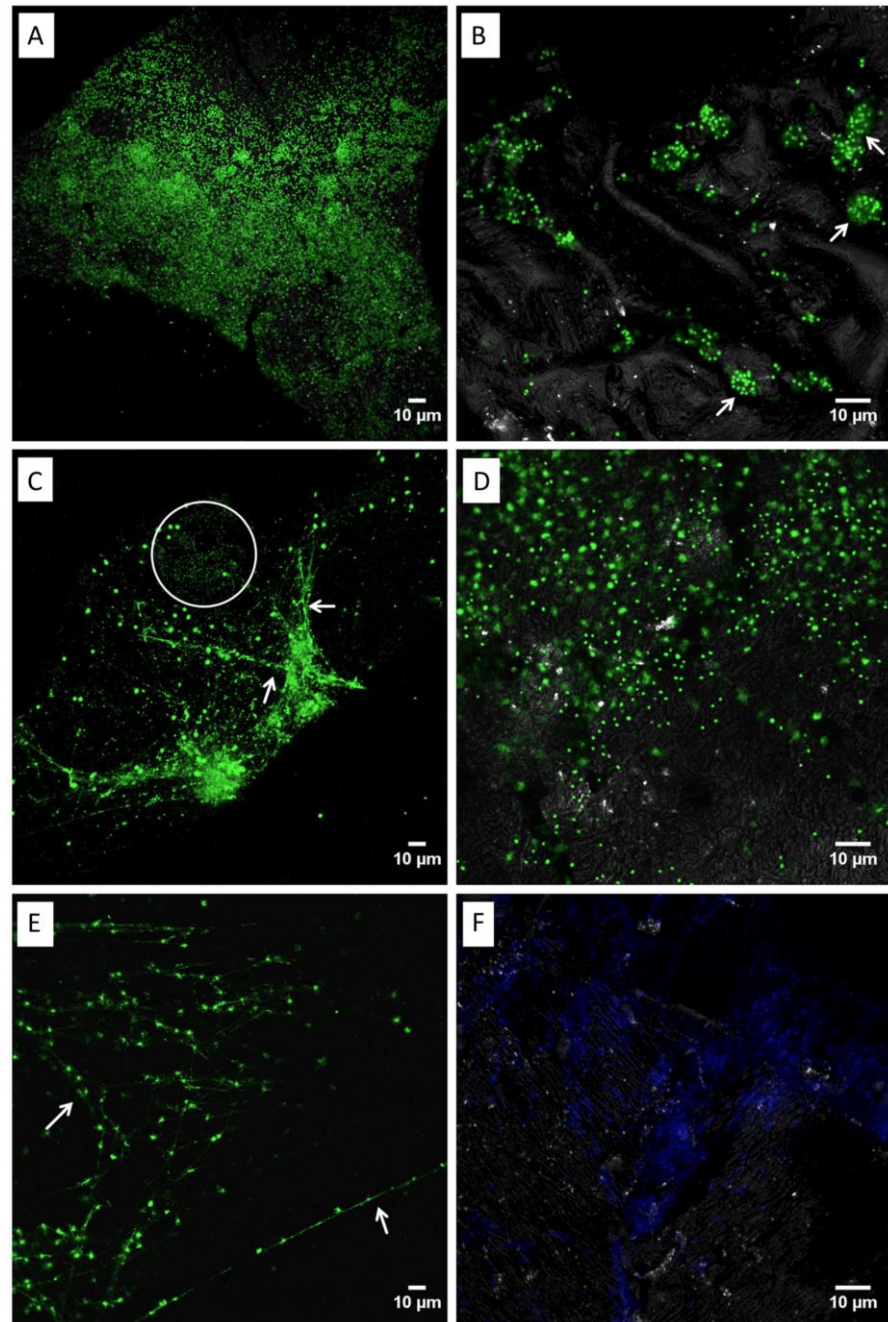
both, biofilm cells and planktonic cells of *S. metallicus*[T]
grown on S[0]. Among these, six lectins recognized biofilm
cells and five bound to planktonic cells, respectively
(Supplementary Table S1). Only Con A and PNA bound to
both biofilm and planktonic cells. The lectin-binding results
indicate that the cell surface polymers were quite similar, but
not identical. Glucose, galactose, mannose, GlcNAc, and

GalNAc were detected on planktonic cell and biofilm cell
surfaces. However, fucose was only present on biofilm cells.

AFM and EFM studies confirmed our CLSM observations
of cell and EPS distribution of *S. metallicus*[T] biofilms on S[0].
As shown in Fig. 6, biofilms in form of cell aggregates or
microcolonies up to hundred micrometers in diameter were
recorded by AFM scanning. Staining with Syto 9 and Con

Fig. 4 Visualization of thermophilic archaea biofilms on S^0 by protein and lipid stains. Maximum intensity projections of *S. metallicus*[T] biofilms stained by SyproOrange (**a**–**c**) and FM1-43 (**e**). **d** Biofilms of *Acidianus* sp. DSM 29099 stained by SyproOrange. Color allocation: *red* SyproOrange (**a, b, d**), *green* SyproOrange (**d**) or FM1-43. The sulfur surface is shown in reflection mode (*grey*).
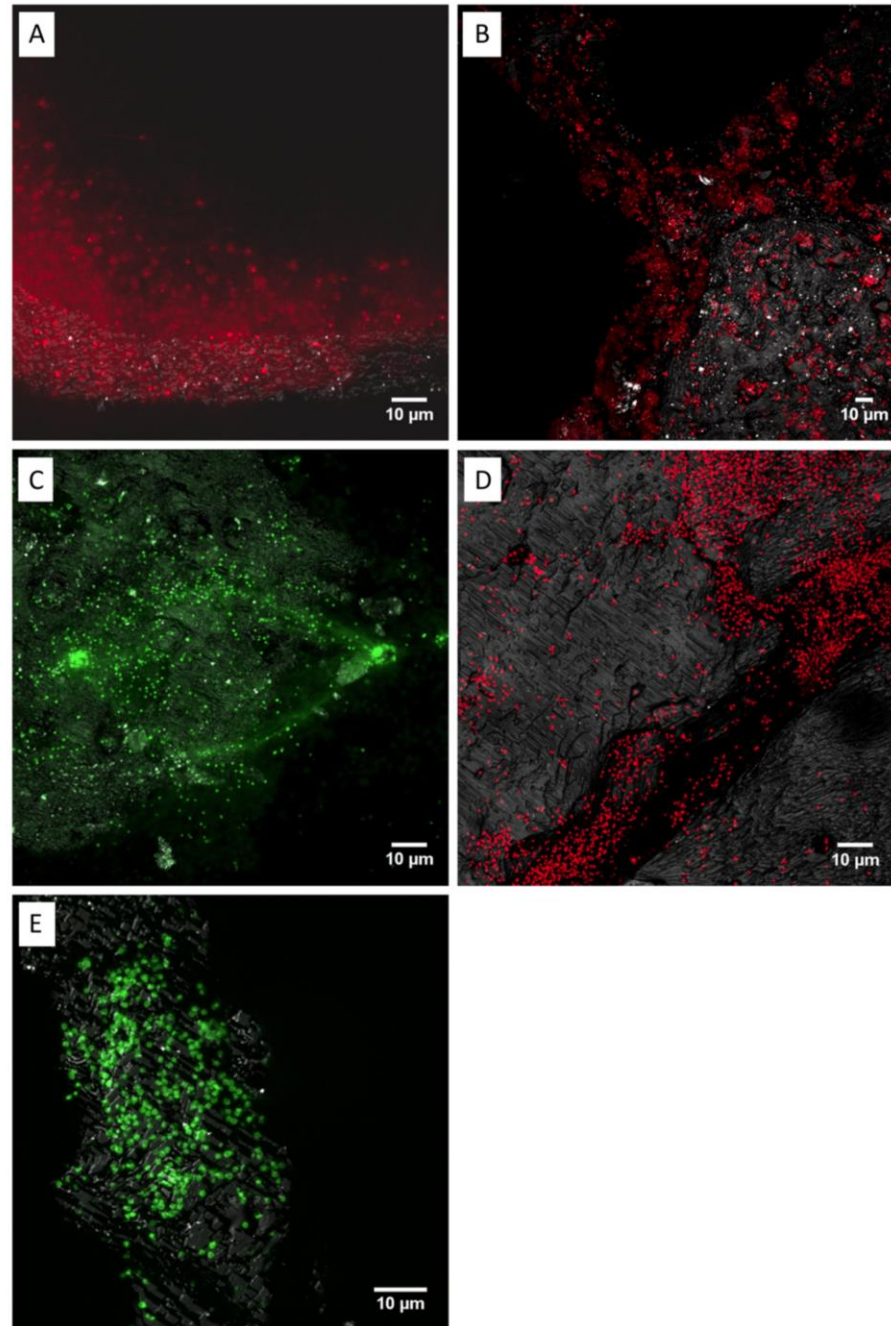
A-TRITC indicated the presence of EPS in biofilms. In addition, a heterogeneous distribution of biofilm cells and EPS was also observed.

Counter staining with a combination of nucleic acid-, protein-, lipophilic-, and glycoconjugate-specific fluorescent probes revealed localization and co-localization of these biomolecules. For instance, when SyproRed with the FITC-conjugated lectins HHA or PMA were used to stain *S. metallicus*[T] biofilms on sulfur, cells were shown to be embedded in an EPS matrix composed of extracellular proteins and glycoconjugates (Fig. 7 and Supplementary Fig. S5). When SyproOrange and DDAO were utilized, extracellular proteins and eDNA were simultaneously detected. A few cells were identified as

Table 2. Lectins binding to *S. metallicus*[T] biofilm cells on S[0]

Lectin[a]	Source	Binding target	Binding pattern	Binding affinity
AAA	Eel serum (*Anguilla anguilla*)	Fuc	Capsular	+
CAA	*Caragana arborescens*	GalNAc	Capsular	+
Con A	Jack bean (*Canavalla ensiformis*)	Glc, Man	Capsular	+•
DBA	*Dolichos biflorus*	GalNAc	Capsular	+
ECA	*Erythrina cristagalli*	GalNAc, Gal	Capsular	+•
GNA	Snowdrop (*Galanthus nivalis*)	Man	Colloidal	+
HAA	Snail (*Helix aspersa*)	GalNAc	Capsular	+
HHA	Amaryllis (*Hippeastrum hybrid*)	Man	Colloidal	++
LAL	*Laburnum anagyroides*	Fuc	Colloidal	+•
LEA	Tomato (*Lycopersicon esculentum*)	GlcNAc	Colloidal	+
MAA	*Maackia amurensis*	Sia	Capsular	+•
MNA-G	*Morus nigra*	Gal	Capsular	+
NPA	*Narcissus pseudonarcissus*	Man	Colloidal	+•
PMA	*Polygonatum multiflorum*	Man	Colloidal	++•
PNA	Peanut (*Arachis hypogea*)	Gal	Capsular	+•
PTA	*Psophocarpus tetragonolobus*	GalNAc	Capsular	+
RPA	Black locust (*Robinia pseudacacia*)	GalNAc	Capsular	+
TKA	*Trichosanthes kirilowii*	Gal	Capsular	+
UEA-I	Furze gorse (*Ulex europaeus*)	Fuc	Capsular	+
VGA	*Vicia graminea*	GlcNAc	Capsular	+
VVA	*Vicia villosa*	GalNAc	Capsular	+•

Examination of no less than three different sulfur prills for deciding positive or negative lectin staining. Only positive ones are listed in the table. Biological replicates were re-checked for the data reproducible. More than 100 images were recorded in our data library (UFZ, Magdeburg) to elucidate the interesting findings during microscopic observations. Visual observation of the binding affinity was recorded according to Staudt et al. 2003.

Glu glucose, *Man* mannose, *Fuc* fucose, *Gal* galactose, *Sia* sialic acid, *GalNAc* N-acetylgalactosamine, *GlcNAc* N-acetylglucosamine; + fair, +• good, ++ very good, ++• extremely good

[a] For details of the lectins, see Zhang et al. 2015.

"dead," as indicated by DDAO staining (Fig. 8). Nevertheless, in some cases, the combination of different dyes did not work properly. For example, when DAPI was combined with the lectin HHA-FITC, lectin signals were fuzzy rather than showing clear patterns (not shown). The reasons for the "fuzzy signals" are unclear. In addition, sulfur surfaces have a strong reflection of red light, which interfered with the use of TRITC-conjugated lectins. Unfortunately, under these conditions, the separation of the red signal from TRITC from the surface reflection was not possible.

The biofilm matrix of *S. metallicus*[T] on S[0] is flexible

During CLSM observations, biofilm cells were often observed to be loosely attached or immobile on sulfur surfaces. Major parts of the biofilms were slightly vibrating (Supplementary Movie S1). A few cells were either swimming away or moving back and forth. Interestingly, some cells seem to be either fixed on the surface by stalks or embedded in a gel matrix, in which

cells may be held by loose polymers (Figs. 7 and 8 and Supplementary Fig. S5), or connected by thread-like nucleic acid compounds (Fig. 3). A lateral movement of cells of *Sulfolobus* on sulfur surfaces has been observed, but attempts to directly visualize the "stalks" or connecting materials were unsuccessful (Weiss 1973). For *Sulfolobus* this is its first direct observation that biofilm cells are embedded in flexible EPS matrix. EPS networks or thread-like structures mediating cell-sulfur interaction are possibly in a nanoscale-range. Currently, no technique is available to visualize them routinely in situ. Summarizing, (1) biofilm cells are embedded in a gel-like matrix, (2) some cells are mobile either self-propelled by cellular appendages, e.g., archaella (Jarrell and Albers 2012) or by "Brownian motion," and (3) these biofilm matrixes are heterogeneous, complex mixtures, and only partly stainable by dyes.

The negative result of Calcoflour White M2R (not shown) staining indicates the absence of β-polysaccharides like cellulose in the biofilm matrix of *S. metallicus*[T] on S[0].

Fig. 5 Lectins showing "capsular" and "colloidal" binding patterns to *S. metallicus*[T] biofilms. Maximum intensity projections with deconvolution process of *S. metallicus*[T] biofilms on elemental sulfur stained by lectins Con A, VGA, NPA, and PMA are shown. Signals of Con A and VGA were mostly restricted to cell boundaries and showed a "capsular binding" pattern. Signals of NPA and PMA were found on cell surfaces and also on sulfur surfaces apart from cells. Color allocation: *green* FITC-conjugated lectins. For all positive lectin-binding results, see Supplementary Figs. S3 and S4
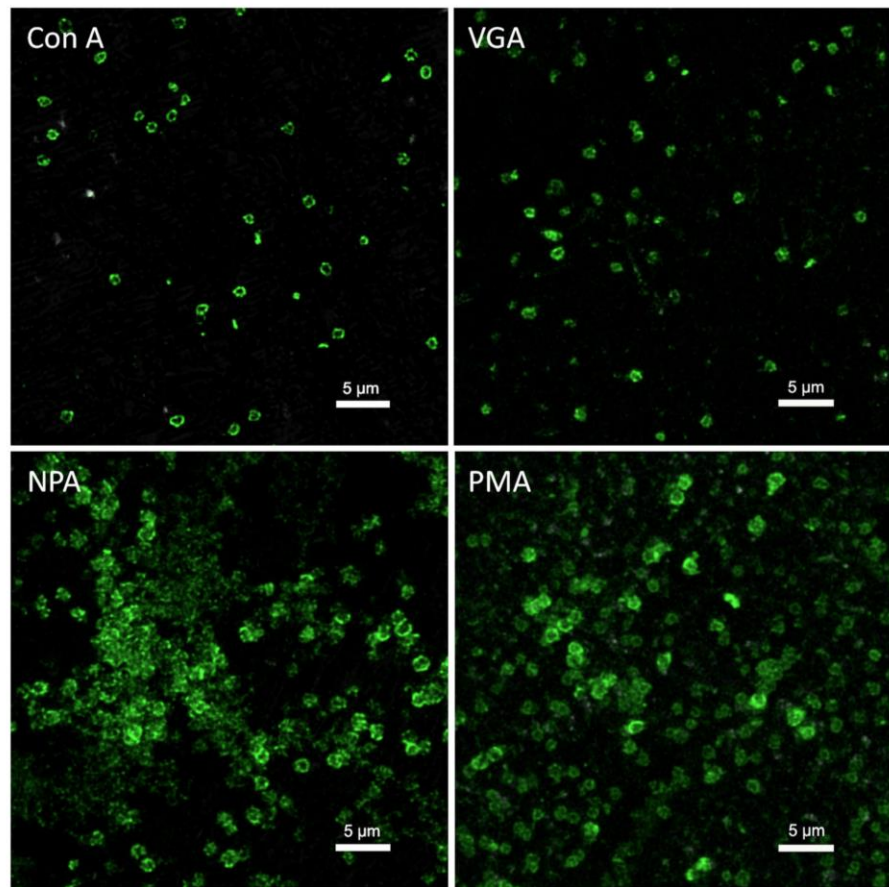
Discussion

Few studies have shown biofilms of thermophilic archaea. Biofilms with "carpet-like" structures by *Sulfolobus solfataricus* and *Sulfolobus tokodaii* and high density tower-like structures by *Sulfolobus acidocaldarius* were reported (Koerdt et al. 2010). Three type IV pili-like cell appendages of *S. acidocaldarius* were found to be involved in cell
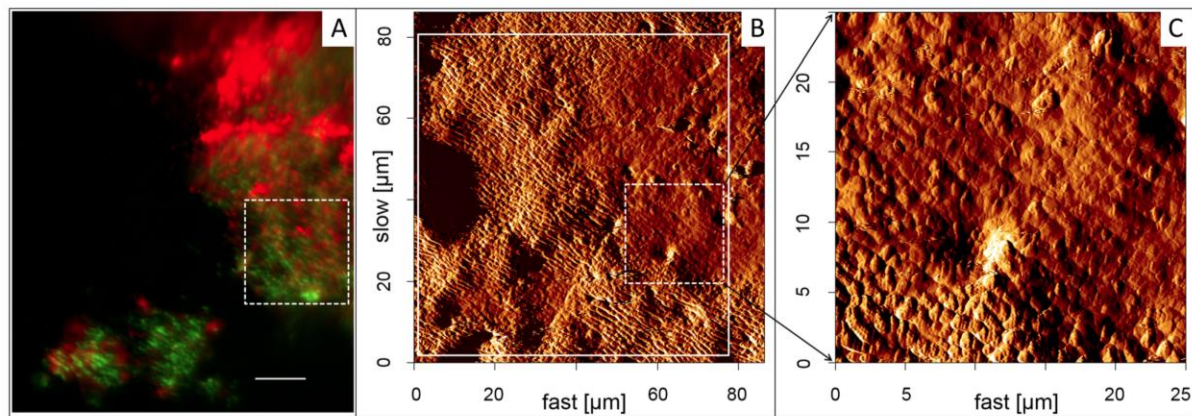

Fig. 6 Images of biofilm cells of *S. metallicus*[T] on S[0] by EFM (**a**) combined with AFM (**b**, **c**). **a** Cells stained by Syto 9 (*green*) and TRITC-Con A (*red*). **b** An AFM scanning (*solid frame*) in contact mode in air corresponding to the area in **a**. **c** Details from an AFM scanning corresponding to the frame (*dashed line*) area in **a** and **b**. *Arrows* in **c** indicates visible individual cells inside biofilms on elemental sulfur. *Bar* in **a** represents 10 μm
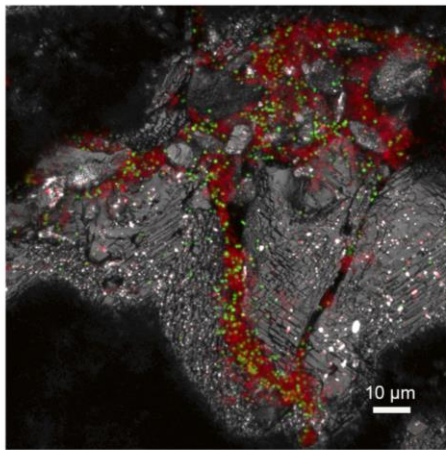
7353

Fig. 7 Maximum intensity projections of *S. metallicus*[T] biofilms on S[0] stained by SyproRed and subsequently by lectin HHA-FITC. Take notice of lectin signal at the cell surface and protein signal indicating extended EPS around the cell colonies. Cells are held together by means of EPS matrix. Color allocation: *green* HHA-FITC, *red* SyproRed, *grey* reflection

colonization and biofilm formation on glass surfaces (Henche et al. 2012). Cell appendages like pili or flagella were shown to be essential for initial attachment to various surfaces (e.g., glass, mica, pyrite, and carbon-coated gold grids) of *S. solfataricus* (Zolghadr et al. 2010). The enzymes mannosidase and galactosidase in *S. solfataricus* were first described as playing a role in archaeal EPS formation (Koerdt et al. 2012). However, these studies were carried out with cells grown in complex media and, almost always, biofilms were developed on non-natural substratum surfaces (e.g., glass slides). Consequently, there is a very limited knowledge of biofilm formation and EPS production by *Sulfolobus* species
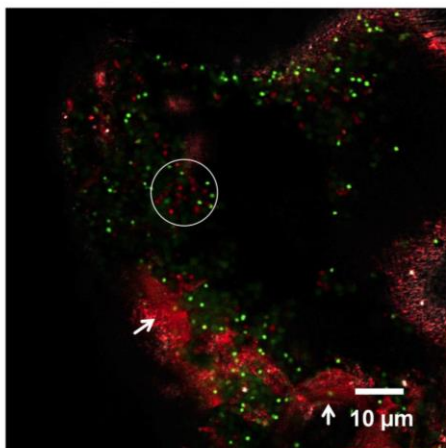

Fig. 8 Maximum intensity projections of *S. metallicus*[T] biofilms on S[0] stained by SyproOrange and subsequently by DDAO. Inside the *circle*, several red cells with DDAO signals are *highlighted*. *Arrows* indicate polymers stained both by SyproOrgange and DDAO. Color allocation: *green* SyproOrgane, *red* DDAO, *grey* reflection

grown on solid inorganic substrates (S[0] or pyrite). In the present study, we applied FTIR, various stains, and CLSM to examine biofilms of *S. metallicus* 6482[T] grown on S[0] (one of their natural substrates) in order to get more details of archaeal EPS characteristics and their involvement in interactions with S[0].

The combination of AFM and EFM allows to understand both biological origins and their detailed structures at a high resolution (Harneit et al. 2006; Mangold et al. 2008; Zhang et al. 2014). Such a combination enabled us to detect the footprints of *S. metallicus*[T] after detachment (Fig. 2). These microbial footprints have been reported to occur in *A. ferrooxidans* or *S. thermosulfidooxidans* grown on pyrite (Mangold et al. 2008; Becker et al. 2011) and in a mixed culture of mesophilic acidophilic chemolitotrophs grown on sphalerite, where *Leptospirillum ferriphilum* was predominant (Ghorbani et al. 2012). For thermoacidophilic archaea, this is the first observation of such phenomenon on rigid surfaces. Clearly, sugar residues like mannose and glucose were involved in cellular attachment to surfaces. Further analysis showed that these two sugars accounted for 90 % of total carbohydrates in *S. metallicus*[T] EPS, both from capsular and colloidal fractions (R. Zhang and V. Blanchard, unpublished). Nevertheless, to understand the initial interaction of *S. metallicus*[T] with surfaces, the nature of these footprints needs to be further analyzed.

Extracellular DNA was first described for *Pseudomonas aeruginosa* biofilms (Whitchurch et al. 2002) and is thought to be a critical component of the biofilm matrix (Dominiak et al. 2011; Okshevsky and Meyer 2013). Biofilm eDNA originates either from cell lysis or from an (unknown) excretion process (Flemming and Wingender 2010). In the present study, the nucleic acid staining indicates the existence of eDNA with different morphologies on the S[0] surfaces after biofilm formation (Fig. 3). The presence of eDNA in EPS from biofilms was also confirmed by ATR-FTIR (Fig. 2) and colorimetric determination (Supplementary Table S2). However, no eDNA in capsular EPS or colloidal EPS was found. In addition, our previous study showed that no eDNA was detected in *S. metallicus*[T] biofilms on pyrite (Zhang et al. 2015). Thus, it is reasonable to assume that eDNA excretion by *S. metallicus*[T] is substrate-mediated. The presence of eDNA in *S. metallicus*[T] biofilms on S[0] may be essential to convey certain advantages for biofilm integrity, stability, and cell survival.

Protein secretion has been proved in *S. solfataricus*, *S. acidocaldarius*, and *S. tokodaii* grown on medium supplemented with glucose, casamino acids, starch, and/or NZ-amine as a limited process. Only a few proteins were detected in the bulk solution (Ellen et al. 2010). Our present study showed similar results. Mainly carbohydrates and few proteins were present in the colloidal EPS fraction of *S. metallicus*[T] grown on S[0] (Supplementary Table S2). However, proteins were dominating the EPS from biofilms on S[0].

The production of proteins in biofilms on sulfur surfaces suggests that these proteins may have a structural role in stabilizing biofilm structures as well as a functional role in the activation of S^0 and transportation of linear polysulfides for their subsequent oxidation. A high-throughput proteomic study of *A. ferrooxidans* revealed that several proteins were related to biofilm formation on pyrite (Vera et al., 2013a). Future omics projects of *S. metallicus*[T] would facilitate analysis and understanding of the role of extracellular proteins in sulfur colonization and metabolism.

Previous reports claimed that lipids/phospholipids play important roles in microbial attachment and the dissolution of S^0 (Beebe and Umbreit 1971; Umbreit et al. 1942). In the present study, lipids were visualized by CLSM combined with specific stains. However, these were cell surface-associated. Probably in case of *S. metallicus*[T], lipophilic compounds play a role in initial attachment by interacting with the hydrophobic S^0 surface. However, in the later stages of cell-S^0 interaction and dissolution, proteins rather than lipids seem to be the major functional components of EPS.

Generally, initial attachment, irreversible attachment, mature biofilm, and detachment are the four major steps/periods of a biofilm cycle (Stoodley et al. 2002). After initial attachment, EPS are excreted by cells in order to enlarge spaces for metabolic activities. We detected two lectin-binding patterns of *S. metallicus*[T] biofilms on S^0: "capsular" and "colloidal." The former represents glycoconjugates tightly associated with cell surface. The later indicates EPS glycoconjugates which were not only present on cell surface but also spread on S^0 surface at which it was cell free. These colloidal EPS actively excreted by cells might be also involved in modification of S^0 surfaces (from hydrophobic to hydrophilic) and S^0 activation. Our results also support the theory that cells excrete EPS in order to extend reacting spaces, which has been postulated in the case of microbial dissolution of metal sulfides, e.g., pyrite (Sand et al. 1998; Vera et al. 2013b).

It is well known that biofilm cells are phenotypically distinct from their planktonic counterparts (Vera et al. 2013a). Among three *Sulfolobus* spp., planktonic and biofilm lifestyles have distinctive influence on the physiology of cells (Koerdt et al. 2011). In this context, biofilm and planktonic cells of *S. metallicus*[T] can be distinguished by using certain lectins. Lectins have also revealed differences in the EPS composition of *T. thioparus* biofilms developed under alternative growth modes (Boretska et al. 2013).

Due to the huge structural diversity of EPS matrix, especially polysaccharides, there is neither a general stain for EPS compounds nor a fluorescent stain for all types of polysaccharides. FLBA involves the tests of a specific biofilm against a range of lectins (Neu et al. 2001). The selected 21 positive lectins (Table 2) enabled us to simultaneously visualize and characterize some glycoconjugates and additional EPS compounds when combined with other stains. In addition, these selected lectins may be useful to distinguish *S. metallicus*[T] in mixed biofilm populations.

It has been shown that extracellular proteins of cells of *Sulfolobus* are highly glycosylated. The high glycosylation density in the S-layer represents an adaptation to the high temperature of their acidic environment (Jarrell et al. 2014; Meyer and Albers 2013). The overlapping of protein and lectin signals suggests that some lectins may also bind to some glycoproteins present in S-layers of biofilms of *S. metallicus*[T] (Fig. 7) (Zhang et al. 2015).

Four acid-stable fluorescent dyes were reported for visualizing acidophilic microorganisms in acid mine drainage communities (Brockmann et al. 2010). However, these stains are in general for cell staining and some binding properties are not fully clear. Acid-stable lectins/stains reacting with compounds of acidophilic leaching microorganisms will be necessary for an improved analysis of microbial biofilms in bioleaching process. In this context, isolation of lectins from acidophiles seems to be meaningful.

In summary, CLSM combined with various fluorophores was used to map the distribution of macromolecules of EPS and differentiate several compounds like polysaccharides, proteins, lipids, and nucleic acids of *S. metallicus*[T] biofilm cells and the developing EPS matrix. Polysaccharides, proteins, and eDNA were found in biofilm matrix. Twenty-one lectins were found to be useful for visualization and monitoring *S. metallicus* biofilms. Different lectin reacting patterns including capsular and colloidal binding patterns were detected. Lectin-specific EPS glycoconjuates indicated that fucose, mannose, glucose, galactose, GlcNAc, and GalNAc were present on S^0-grown cells. The detection of eDNA and extracellular proteins in biofilm EPS of *S. metallicus* suggests their potential roles in biofilm formation and stabilization of biofilm structures. Our data improve the understanding of acidophilic archaeal biofilm organization and interactions with S^0.

Conflict of interest The authors declare that they have no competing interests.

References

Albers S-V, Meyer BH (2011) The archaeal cell envelope. Nat Rev Microbiol 9:414–426

Arredondo R, García A, Jerez CA (1994) Partial removal of lipopolysaccharide from *Thiobacillus ferrooxidans* affects its adhesion to solids. Appl Environ Microbiol 60:2846–2851

Becker T, Gorham N, Shiers D, Watling H (2011) In situ imaging of *Sulfobacillus thermosulfidooxidans* on pyrite under conditions of variable pH using tapping mode atomic force microscopy. Process Biochem 46:966–976

Beebe JL, Umbreit W (1971) Extracellular lipid of *Thiobacillus thiooxidans*. J Bacteriol 108:612–614

Bellenberg S, Leon-Morales C-F, Sand W, Vera M (2012) Visualization of capsular polysaccharide induction in *Acidithiobacillus ferrooxidans*. Hydrometallurgy 129:82–89

Blais J-F, Tyagi R, Meunier N, Auclair J (1994) The production of extracellular appendages during bacterial colonization of elemental sulphur. Process Biochem 29:475–482

Boretska M, Bellenberg S, Moshynets O, Pokholenko I, Sand W (2013) Change of extracellular polymeric substances composition of *Thiobacillus thioparus* in presence of sulfur and steel. J Microb Biochem Technol 5:68–73

Bradford MM (1976) A rapid and sensitive method for the quantitation of microgram quantities of protein utilizing the principle of protein-dye binding. Anal Biochem 72:248–254

Brockmann S, Arnold T, Schweder B, Bernhard G (2010) Visualizing acidophilic microorganisms in biofilm communities using acid stable fluorescence dyes. J Fluoresc 20:943–951

Bryant R, Costerton J, Laishley E (1984) The role of *Thiobacillus albertis* glycocalyx in the adhesion of cells to elemental sulfur. Can J Microbiol 30:81–90

Burton K (1956) A study of the conditions and mechanism of the diphenylamine reaction for the colorimetric estimation of deoxyribonucleic acid. Biochem J 62:315–323

Castro L, Zhang R, Muñoz JA, González F, Blázquez ML, Sand W, Ballester A (2014) Characterization of exopolymeric substances (EPS) produced by *Aeromonas hydrophila* under reducing conditions. Biofouling 30:501–511

Dominiak DM, Nielsen JL, Nielsen PH (2011) Extracellular DNA is abundant and important for microcolony strength in mixed microbial biofilms. Environ Microbiol 13:710–721

Dopson M, Johnson DB (2012) Biodiversity, metabolism and applications of acidophilic sulfur-metabolizing microorganisms. Environ Microbiol 14:2620–2631

Dubois M, Gilles KA, Hamilton JK, Rebers P, Smith F (1956) Colorimetric method for determination of sugars and related substances. Anal Chem 28:350–356

Dutrizac J (1990) Elemental sulphur formation during the ferric chloride leaching of chalcopyrite. Hydrometallurgy 23:153–176

Ellen AF, Albers S-V, Driessen AJ (2010) Comparative study of the extracellular proteome of *Sulfolobus* species reveals limited secretion. Extremophiles 14:87–98

Flemming H-C, Wingender J (2010) The biofilm matrix. Nat Rev Microbiol 8:623–633

Flemming H-C, Neu TR, Wozniak DJ (2007) The EPS matrix: the "house of biofilm cells". J Bacteriol 189:7945–7947

Fröls S (2013) Archaeal biofilms: widespread and complex. Biochem Soc Trans 41:393–398

Ghorbani Y, Petersen J, Harrison ST, Tupikina OV, Becker M, Mainza AN, Franzidis J-P (2012) An experimental study of the long-term bioleaching of large sphalerite ore particles in a circulating fluid fixed-bed reactor. Hydrometallurgy 129:161–171

Harneit K, Göksel A, Kock D, Klock J-H, Gehrke T, Sand W (2006) Adhesion to metal sulfide surfaces by cells of *Acidithiobacillus ferrooxidans*, *Acidithiobacillus thiooxidans* and *Leptospirillum ferrooxidans*. Hydrometallurgy 83:245–254

Henche AL, Koerdt A, Ghosh A, Albers SV (2012) Influence of cell surface structures on crenarchaeal biofilm formation using a thermostable green fluorescent protein. Environ Microbiol 14:779–793

Jarrell KF, Albers S-V (2012) The archaellum: an old motility structure with a new name. Trends Microbiol 20:307–312

Jarrell KF, Ding Y, Meyer BH, Albers S-V, Kaminski L, Eichler J (2014) N-linked glycosylation in Archaea: a structural, functional, and genetic analysis. Microbiol Mol Biol Rev 78:304–341

Kletzin A (2008) Oxidation of sulfur and inorganic sulfur compounds in *Acidianus ambivalens*. In: Dahl C, Friedrich CG (Eds) Microbial sulfur metabolism. Springer, Heidelberg, pp 184-201

Knickerbocker C, Nordstrom D, Southam G (2000) The role of "blebbing" in overcoming the hydrophobic barrier during biooxidation of elemental sulfur by *Thiobacillus thiooxidans*. Chem Geol 169:425–433

Koerdt A, Gödeke J, Berger J, Thormann KM, Albers S-V (2010) Crenarchaeal biofilm formation under extreme conditions. PLoS One 5:e14104

Koerdt A, Orell A, Pham TK, Mukherjee J, Wlodkowski A, Karunakaran E, Biggs CA, Wright PC, Albers S-V (2011) Macromolecular fingerprinting of *Sulfolobus* species in biofilm: a transcriptomic and proteomic approach combined with spectroscopic analysis. J Proteome Res 10:4105–4119

Koerdt A, Jachlewski S, Ghosh A, Wingender J, Siebers B, Albers S-V (2012) Complementation of *Sulfolobus solfataricus* PBL2025 with an α-mannosidase: effects on surface attachment and biofilm formation. Extremophiles 16:115–125

Little B, Ray R, Pope R (2000) Relationship between corrosion and the biological sulfur cycle: a review. Corrosion 56:433–443

Liu H-C, Xia J-L, Nie Z-Y, Peng A-A, Ma C-Y, Zheng L, Zhao Y-D (2013) Comparative study of sulfur utilization and speciation transformation of two elemental sulfur species by thermoacidophilic Archaea *Acidianus manzaensis* YN-25. Process Biochem 48: 1855–1860

Mackintosh ME (1978) Nitrogen fixation by *Thiobacillus ferrooxidans*. J Gen Microbiol 105:215–218

Mangold S, Harneit K, Rohwerder T, Claus G, Sand W (2008) Novel combination of atomic force microscopy and epifluorescence microscopy for visualization of leaching bacteria on pyrite. Appl Environ Microbiol 74:410–415

Meyer BH, Albers S-V (2013) Hot and sweet: protein glycosylation in Crenarchaeota. Biochem Soc Trans 41:384–392

Naumann D, Helm D, Labischinski H (1991) Microbiological characterizations by FT-IR spectroscopy. Nature 351:81–82

Neu TR, Swerhone GD, Lawrence JR (2001) Assessment of lectinbinding analysis for in situ detection of glycoconjugates in biofilm systems. Microbiology 147:299–313

Ng F-W, Dawes E (1973) Chemostat studies on the regulation of glucose metabolism in *Pseudomonas aeruginosa* by citrate. Biochem J 132: 129–140

Nichols PD, Michael Henson J, Guckert JB, Nivens DE, White DC (1985) Fourier transform-infrared spectroscopic methods for microbial ecology: analysis of bacteria, bacteri-polymer mixtures and biofilms. J Microbiol Methods 4:79–94

Nie Z-Y, Liu H-C, Xia J-L, Zhu H-R, Ma C-Y, Zheng L, Zhao Y-D, Qiu G-Z (2014) Differential utilization and transformation of sulfur allotropes, μ-S and α-S_8, by moderate thermoacidophile *Sulfobacillus thermosulfidooxidans*. Res Microbiol 165:639–646

Okshevsky M, Meyer RL (2013) The role of extracellular DNA in the establishment, maintenance and perpetuation of bacterial biofilms. Crit Rev Microbiol 1-11

Orell A, Fröls S, Albers S-V (2013) Archaeal biofilms: the great unexplored. Annu Rev Microbiol 67:337–354

Parikh SJ, Chorover J (2006) ATR-FTIR spectroscopy reveals bond formation during bacterial adhesion to iron oxide. Langmuir 22:8492–8500

Peng AA, Xia JL, Liu HC, Zhu W, Zhang RY, Zhang CG, Nie ZY (2013) Thiol-rich proteins play important role in adhesion and sulfur oxidation process of *Acidithiobacillus ferroxidans*. Adv Mater Res 825: 137–140

Rodrıguez Y, Ballester A, Blazquez M, Gonzalez F, Munoz J (2003) New information on the chalcopyrite bioleaching mechanism at low and high temperature. Hydrometallurgy 71:47–56

Rohwerder T, Sand W (2003) The sulfane sulfur of persulfides is the actual substrate of the sulfur-oxidizing enzymes from *Acidithiobacillus* and *Acidiphilium* spp. Microbiology 149:1699–1710

Rohwerder T, Sand W (2007) Oxidation of inorganic sulfur compounds in acidophilic prokaryotes. Eng Life Sci 7:301–309

Sand W (1985) The influence of four detergents on the substrate oxidation by *Thiobacillus ferrooxidans*. Environ Technol 6:439–444

Sand W, Gehrke T, Hallmann R, Schippers A (1998) Towards a novel bioleaching mechanism. Miner Process Extr Metall Rev 19:97–106

Schmitt J, Flemming H-C (1998) FTIR-spectroscopy in microbial and material analysis. Int Biodeterior Biodegrad 41:1–11

Staudt C, Horn H, Hempel D, Neu T (2003) Screening of lectins for staining lectin-specific glycoconjugates in the EPS of biofilms. In: Lens P, O'Flaherty V, Moran AP, Stoodley P, Mahony T (eds) Biofilms in medicine, industry and environmental technology. IWA Publishing, London, pp 308–327

Stoodley P, Sauer K, Davies D, Costerton JW (2002) Biofilms as complex differentiated communities. Annu Rev Microbiol 56: 187–209

Suci P, Siedlecki K, Palmer R, White D, Geesey G (1997) Combined light microscopy and attenuated total reflection fourier transform infrared spectroscopy for integration of biofilm structure, distribution, and chemistry at solid-liquid interfaces. Appl Environ Microbiol 63: 4600–4603

Takeuchi TL, Suzuki I (1997) Cell hydrophobicity and sulfur adhesion of *Thiobacillus thiooxidans*. Appl Environ Microbiol 63:2058–2061

Umbreit W, Vogel H, Vogler K (1942) The significance of fat in sulfur oxidation by *Thiobacillus thiooxidans*. J Bacteriol 43:141–148

Vera M, Krok B, Bellenberg S, Sand W, Poetsch A (2013a) Shotgun proteomics study of early biofilm formation process of *Acidithiobacillus ferrooxidans* ATCC 23270 on pyrite. Proteomics 13:1133–1144

Vera M, Schippers A, Sand W (2013b) Progress in bioleaching: fundamentals and mechanisms of bacterial metal sulfide oxidation—part A. Appl Microbiol Biotechnol 97:7529–7541

Weiss R (1973) Attachment of bacteria to sulphur in extreme environments. J Gen Microbiol 77:501–507

Whitchurch CB, Tolker-Nielsen T, Ragas PC, Mattick JS (2002) Extracellular DNA required for bacterial biofilm formation. Science 295:1487–1487

Zhang C-G, Xia J-L, Zhang R-Y, Peng A-A, Nie Z-Y, Qiu G-Z (2008a) Comparative study on effects of Tween-80 and sodium isobutyl-xanthate on growth and sulfur-oxidizing activities of *Acidithiobacillus albertensis* BY-05. T Nonferr Metal Soc 18: 1003–1007

Zhang C-G, Zhang R-Y, Xia J-L, Zhang Q, Z-Y NIE (2008b) Sulfur activation-related extracellular proteins of *Acidithiobacillus ferrooxidans*. T Nonferr Metal Soc 18:1398–1402

Zhang R, Bellenberg S, Castro L, Neu TR, Sand W, Vera M (2014) Colonization and biofilm formation of the extremely acidophilic archaeon *Ferroplasma acidiphilum*. Hydrometallurgy 150:245–252

Zhang RY, Neu TR, Bellenberg S, Kuhlicke U, Sand W, Vera M (2015) Use of lectins to in situ visualize glycoconjugates of extracellular polymeric substances in acidophilic archaeal biofilms. Microb Biotechnol 8:448–461

Zippel B, Neu T (2011) Characterization of glycoconjugates of extracellular polymeric substances in tufa-associated biofilms by using fluorescence lectin-binding analysis. Appl Environ Microbiol 77:505–516

Zolghadr B, Klingl A, Koerdt A, Driessen AJ, Rachel R, Albers S-V (2010) Appendage-mediated surface adherence of *Sulfolobus solfataricus*. J Bacteriol 192:104–110

Supplementary Material

Applied Microbiology and Biotechnology

Visualization and analysis of EPS glycoconjugates of the thermo-acidophilic archaeon *Sulfolobus metallicus*

Ruiyong Zhang[1], Thomas R. Neu[2], Yutong Zhang[1], Sören Bellenberg[1]

Ute Kuhlicke[2], Qian Li[1], Wolfgang Sand[1] and Mario Vera[1]*

[1]Aquatische Biotechnologie, Biofilm Centre, Universität Duisburg – Essen, Universitätsstraße 5, 45141 Essen, Germany

[2]Department of River Ecology, Helmholtz Centre for Environmental Research – UFZ, Brueckstrasse 3A, 39114 Magdeburg, Germany

Corresponding Author

E-mail: mario.vera@uni-due.de

Tel: + 49 0201/183 7083

Fax: + 49 0201/183 7090

Supplementary Table S1. Comparison of lectin binding assays of planktonic and biofilm cells of *S. metallicus*[T]

Lectin	Binding target	Biofilm cells	Planktonic cells
BPA	GalNAc	-	+
ConA	Glc, Man	+	+
DBA	GalNAc	+	-
ECA	GalNAc, Gal	+	-
GS-I	GalNAc, Gal	-	-
GS-II	GlcNAc	ND	+
LcH	GlcNAc	-	-
LPA	Sia	-	-
MPA	GalNAc	-	-
PHA-E	Man	-	-
PMA	Man	+	-
PNA	Gal	+	+
PWA	GlcNAc	-	-
SBA	GalNAc, Gal	-	+
UEA-I	Fuc	+	-
WGA	GlcNAc	-	-

Note: +, lectin binding to cells, - lectin not binding to cells, ND, not determined

Supplementary Table S2. EPS composition of *S. metallicus*[T] grown on $S^{0\Delta}$

EPS type	Carbohydrates	Proteins	DNA	G6PDH[*]
Colloidal[a]	25.9	2.9	BL	<5 %
Capsular[b]	15.9	15.7	BL	<2 %
EPS from biofilms[c]	0.5	8.8	0.09	ND

[a]: mg/L, the unit of content and it indicates the weight (mg) of EPS per liter of culture medium. [b]: mg/g, the weight (mg) of EPS per gram of cell biomass. [c]: mg/g, the weight (mg) of EPS from biofilms per gram of elemental sulfur.

[*]: percentage of G6PDH activity from EPS samples accounts for the G6PDH activity from whole cell biomass.

BL: Below detection limit

ND: Not determined

[Δ]: Experiments were carried out in duplicates. Results are given as mean values. Standard deviations (± SD) generally amounted to ≤15 %.

Supplementary Table S3. Comparison of lectin-binding assays of *S. metallicus*[T] and *Acidianus* sp. DSM 29099 biofilms* grown on S[0]

Lectin	*Acidianus* sp. DSM 29099	*S. metallicus*[T]
AAA	+ Capsular	+ Capsular
AAL	+ Capsular/cell-associated structures	-
CAA	-	+ Capsular
Con A	+ Capsular/cell-associated structures	+ Capsular
DBA	+ Capsular	+ Capsular
ECA	+ Colloidal	-
EEA	+ Capsular	-
GHA	+ Capsular	-
GNA	-	+ Colloidal
GS-I	+ Colloidal/cell-associated structures	-
HAA	-	+ Capsular
HHA	+ Colloidal	+ Colloidal
HMA	+ Colloidal	-
IAA	+ Colloidal	-
IRA	+ Capsular	-
LAL	+ Capsular	+ Colloidal
LBA	+ Capsular	-
LcH	+ Capsular	-
LEA	-	+ Colloidal
MAA	-	+ Capsular
MNA-G	-	+ Capsular
MOA	+ Colloidal	-
NPA	-	+ Colloidal
PMA	-	+ Colloidal
PNA	+ Capsular	+ Capsular
PSA	+ Capsular	-
PTA	-	+ Capsular
RPA	-	+

		Capsular	
SJA	+	-	
	Capsular		
TKA	-	+	
	Capsular	Capsular	
TL	+	-	
	Capsular		
UDA	-	+	
	Capsular	Capsular	
VGA	+	+	
	Capsular	Capsular	
VVA	-	+	
		Capsular	

* Lectin binding pattern of *Acidianus* sp. DSM 29099 in Zhang. et al 2014b
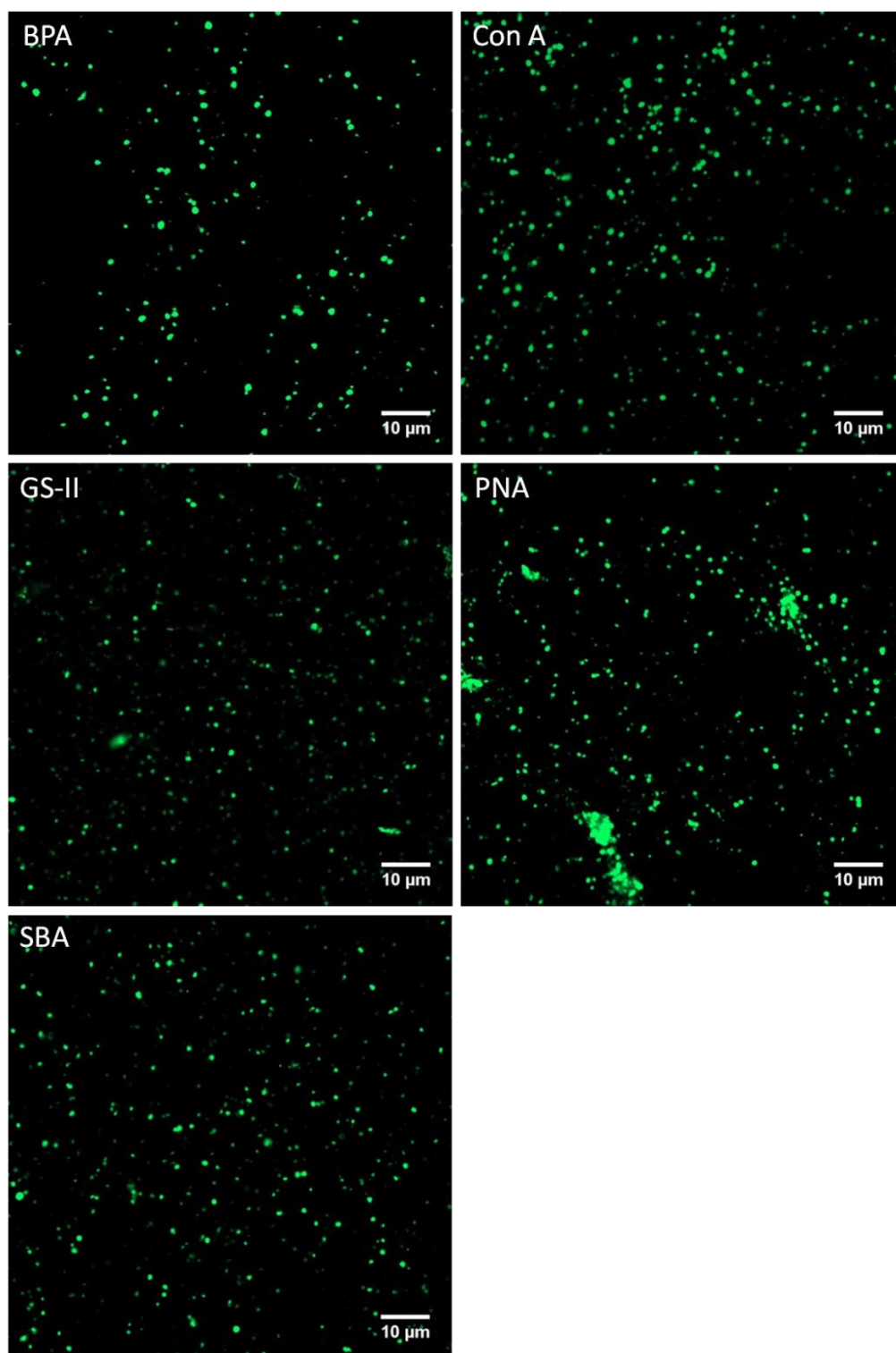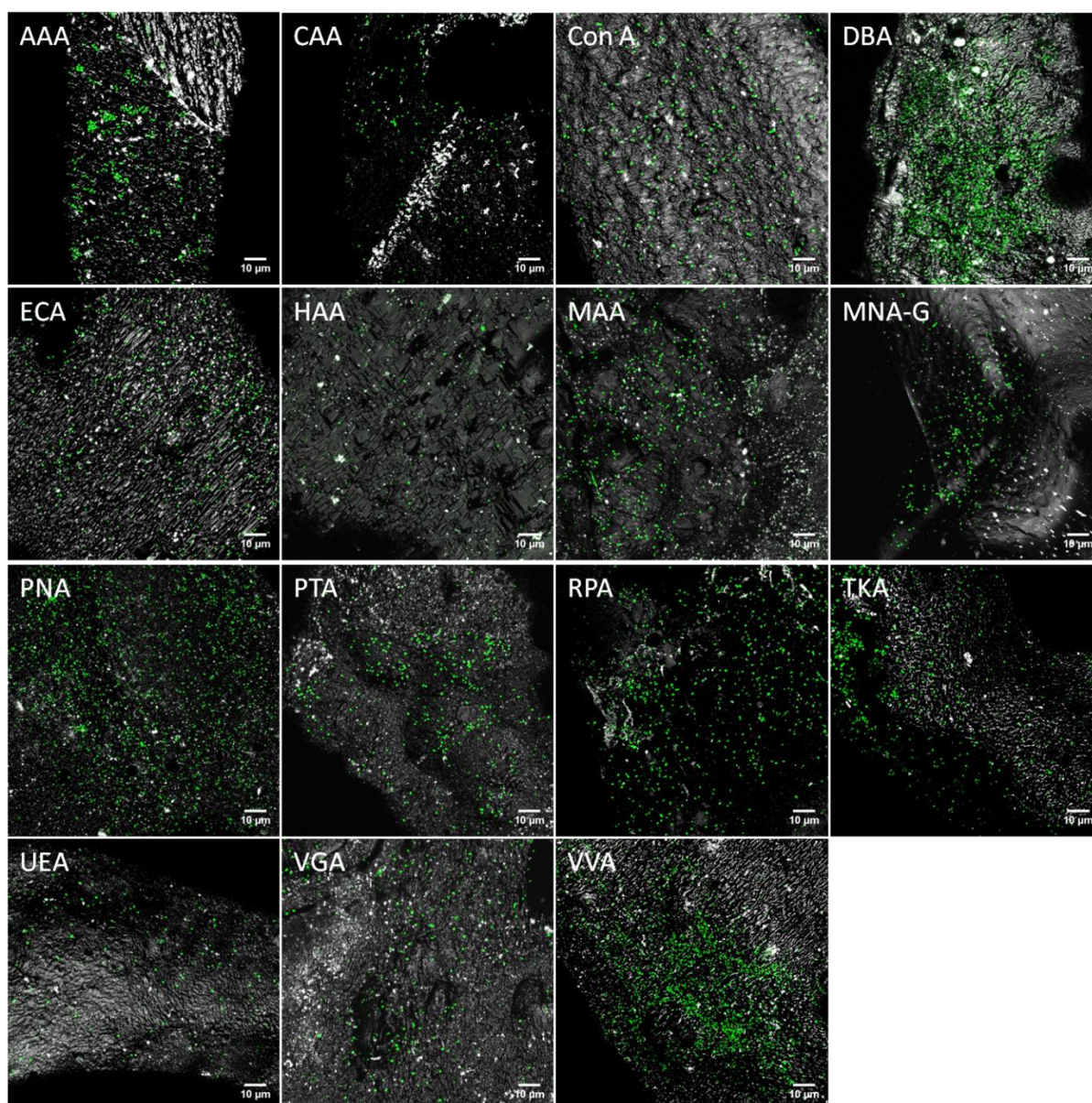
Supplementary Fig. S1.

Lectin staining of planktonic cells of *S. metallicus*^{T} grown on S^0. CLSM images of planktonic cells on polycarbonate filters stained by the FITC-conjugated lectins BPA, Con A, GS-II, PNA and SBA are shown.
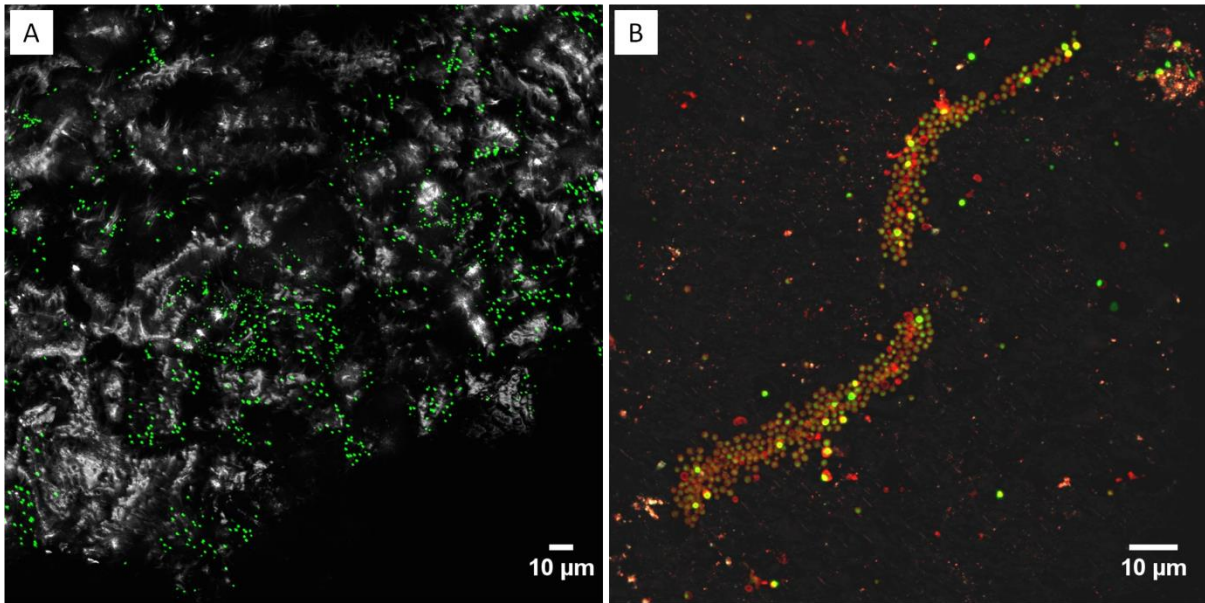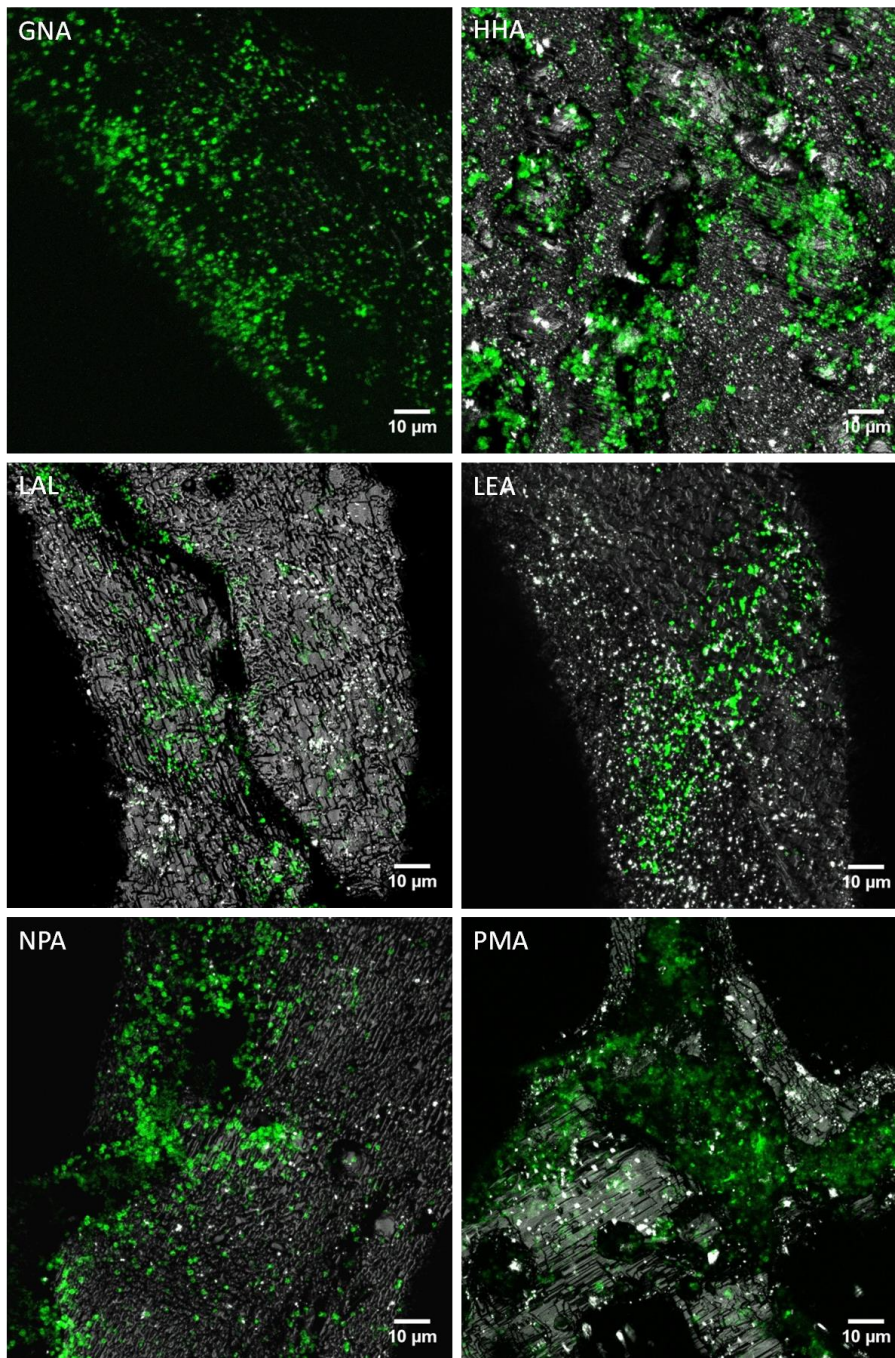
Supplementary Fig. S2. Maximum intensity projections of *Acidianus* sp. DSM 29099 biofilms on S^0 stained by SybrGreen (A), and Con A-TRITC plus SybrGreen (B). Cells are either individually distributed or clustered in defective sites. Color allocation: green = SybrGreen, red = Con A-TRITC, grey = reflection.

Supplementary Fig. S3.

Lectins showing capsular binding pattern to *S. metallicus*[T] biofilms. Maximum intensity projections of *S. metallicus*[T] biofilms on S^0 stained by FITC-conjugated lectins AAA, CAA, Con A, DBA, ECA, HAA, MAA, MNA-G, PNA, PTA, RPA, TKA, UEA, VGA and VVA are shown. Lectin signals were mostly restricted to cell boundaries. Color allocation: green = FITC-conjugated lectins, grey= reflection.
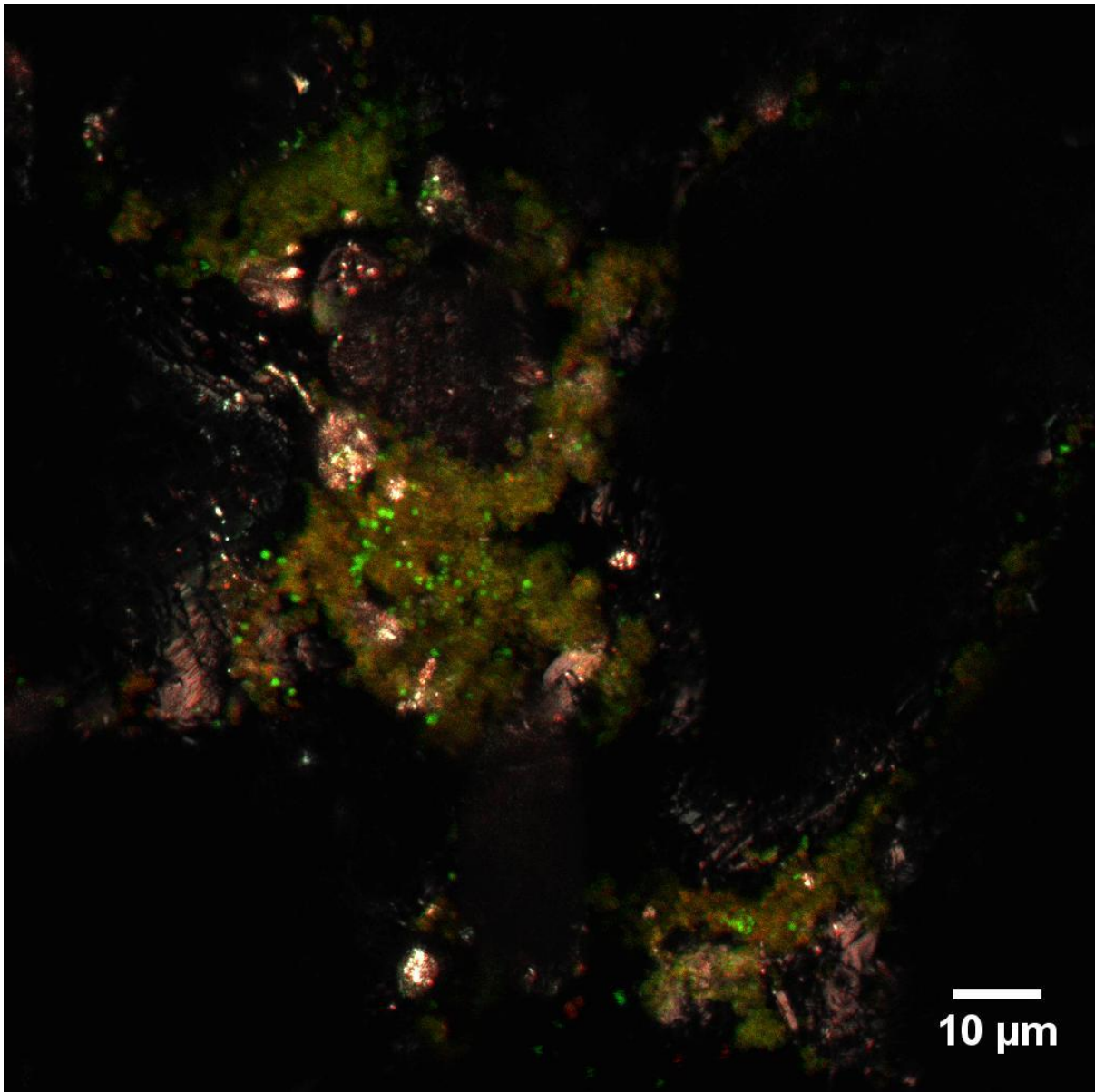
Supplementary Fig. S4.

Lectins showing colloidal binding pattern to *S. metallicus*[T] biofilms. Maximum intensity projections of *S. metallicus*[T] biofilms on S^0 stained by the FITC-conjugated lectins GNA, HHA, LAL, LEA, NPA and PMA are shown. Lectin signals covered both cell surface and partially S^0 surfaces. Color allocation: green = FITC-conjugated lectins, grey= reflection.

Supplementary Fig. S5. Maximum intensity projection of *S. metallicus*[T] biofilms on S[0] stained by SyproRed and subsequently by the lectin PMA-FITC. Lectin signals and protein signals were almost overlapped indicating extended EPS around the colonies. Cells are held together by means of the EPS matrix. Color allocation: green = PMA-FITC, red = SyproRed, grey = reflection.

Supplementary Movie Caption

Movie S1. Biofilms of *S. metallicus*[T] in a crack/groove on S^0 surface stained by Syto 61 (red). Images were collected with a z-model. Major parts of biofilm matrix are non-motile. Few cells within the gel matrix are vibrating and moving.

Please visit the following website for details.

http://link.springer.com/article/10.1007/s00253-015-6775-y

5. Summary and Conclusions

Bioleaching, as a widely used technique, has attracted great attention both in fundamental and applied industrial fields such as biomining and AMD. Iron and/or sulfur-oxidizers like *Ferroplasma*, *Acidianus* and *Sulfolobus* enhance pyrite leaching by replenishing the iron(III) ions and/or protons which allow leaching of MS. EPS, mediating contact between cells and surfaces, play an essential role in biofilm formation and consequently affecting bioleaching efficiencies. In order to better control bioleaching process it is essential to understand the mechanisms regarding microbial attachment and subsequent biofilm formation on minerals.

In this study the first detailed investigation of acidophilic archaeal biofilms and EPS on MS and S^0 has been performed. Several advanced microscopy techniques such as CLSM, AFM & EFM and SEM were used for visualization and analysis of the characteristics of these biofilms. Biofilm morphology was shown to be substrate dependent. It was shown that three archaeal strains formed monolayered biofilms on pyrite surfaces. As previously shown for acidophilic bacteria, the archaeal strains attached to pyrite surfaces along the cracks or preferentially attached to defect/imperfect sites of the minerals. With regards to S^0, the two thermophilic species used, *Acidianus* sp. DSM 29099 and *S. metallicus*^{T}, formed large colonies and multilayer biofilms were visible in some cases. Furthermore, FLBA together with conventional spectroscopic techniques provided the first analysis of the diversity of glycoconjugates and EPS composition during bioleaching. The first comprehensive lectin study using a full lectin library for acidophilic archaea resulted in a panel of lectins, which may be useful for the subsequent monitoring of acidophilic archaeal biofilms. These lectins will be used in studies for assessment of interactions between various members of microbial bioleaching communities, especially in order to elucidate the role of archaea in detail. In addition, lectins which are species or

strain-specific (e.g. lectin LPA staining *F. acidiphilum*) may be used as probes to differentiate a target archaeon from others in multi-species biofilms.

Furthermore, the visualization of abundant extracellular proteins in biofilms of *S. metallicus* on S^0 surfaces indicates the potential role of these extracellular proteins in S^0 solublization. Another interesting finding was that threads like eDNA were part of *S. metallicus* biofilms. The existence of eDNA was also confirmed by conventional spectroscopic determination. In contrast, no such eDNA was found in the pyrite grown biofilms. Summarizing, we have shown that acidophilic archaea adjust their biofilm lifestyle (structure and EPS composition) according to their substrate and environmental changes.

6. Outlook

Current knowledge on the chemical compositions and microbial dynamics of acidophilic archaeal biofilms is still restricted. The presence and functional roles of macromolecules and metabolites within EPS from these biofilms remains to be clarified. This work shows the first detailed study of meso and thermoacidophilic archaeal species relevant for biomining. Several points remain open regarding to the initial archaeal attachment and subsequent biofilm formation on MS and S^0:

1) We did not investigate in depth archaeal detachment mechanisms. It has been only observed that a mature biofilm of *Acidianus* sp. DSM 29099 on pyrite was developed after 2-4 days of incubation. Before that cellular detachment often was detected from remaining footprints containing lipids, fucose, mannose and glucose. These compounds may be responsible for interactions with these surfaces after mediating initial cellular adhesion. More data are needed to elucidate the dynamics and molecular mechanisms of archaeal detachment from MS and S^0 surfaces.

2) The existence of extracellular proteins and eDNA in leaching archaea was demonstrated for the first time in this work. Their existence raises question for their functions in biofilm formation and S^0 metabolism. Thus, further work should focus on the molecular mechanisms how these compounds are interacting with mineral surfaces.

3) Sialic acids were shown to be part of *F. acidiphilum* EPS and biofilm components on pyrite. Their presence in biofilm population but not planktonic cells suggests a specific role for these compounds during biofilm lifestyle in interaction with MS. The mechanism of sialic acid interaction with MS remains

to be elucidated. Also, due to the structural and functional roles of polysaccharides in biofilms, carbohydrate chemistry of acidophilic biofilms should be developed in order to determine the composition and structure of polysaccharides and their roles in interactions of acidophiles with MS.

Future molecular studies shall include polymer chemistry, metabolomics as well as protein chemistry of proteins remaining as "unknown". These may have important roles in controlling the dynamics of acidophilic biofilm phenotypes and interactions with other microbial populations. Acid-stable fluorescent stains, e.g. isolation of lectins from metal/sulfur-oxidizing acidophiles shall be developed. A combination of novel physical and chemical microscopic techniques, e.g. Raman microscopy and nanoscopy techniques such as blink microscopy may allow a detailed investigation of biofilm composition and function.

7. References

Abramoff MD, Magalhaes PJ, Ram SJ (2004) Image processing with ImageJ. Biophotonics Int 11:36-42

Acharya C, Kar R, Sukla L (2002) Bioleaching of low grade manganese ore with *Penicillium citrinum*. Eur J Miner Process Environ Prot 2:197-204

Acuna J, Rojas J, Amaro A, Toledo H, Jerez C (1992) Chemotaxis of *Leptospirillum ferrooxidans* and other acidophilic chemolithotrophs: comparison with the *Escherichia coli* chemosensory system. FEMS Microbiol Lett 96:37-42

Africa C-J, van Hille RP, Sand W, Harrison STL (2013) Investigation and *in situ* visualisation of interfacial interactions of thermophilic microorganisms with metal-sulphides in a simulated heap environment. Miner Eng 48:100-107

Akcil A, Vegliò F, Ferella F, Okudan MD, Tuncuk A (2015) A review of metal recovery from spent petroleum catalysts and ash. Waste Manage 45:420-433

Alvarez-Ordonez A, Mouwen D, Lopez M, Prieto M (2011) Fourier transform infrared spectroscopy as a tool to characterize molecular composition and stress response in foodborne pathogenic bacteria. J Microbiol Methods 84:369-378

Auernik KS, Cooper CR, Kelly RM (2008) Life in hot acid: pathway analyses in extremely thermoacidophilic archaea. Curr Opin Biotechnol 19:445-453

Baker-Austin C, Dopson M, Wexler M, Sawers RG, Bond PL (2005) Molecular insight into extreme copper resistance in the extremophilic archaeon 'Ferroplasma acidarmanus' Fer1. Microbiology 151:2637-2646

Baker-Austin C, Potrykus J, Wexler M, Bond P, Dopson M (2010) Biofilm development in the extremely acidophilic archaeon '*Ferroplasma acidarmanus*' Fer1. Extremophiles 14:485-491

Baldensperger J, Guarraia L, Humphreys W (1974) Scanning electron microscopy of thiobacilli grown on colloidal sulfur. Arch Microbiol 99:323-329

Becker T, Gorham N, Shiers D, Watling H (2011) *In situ* imaging of *Sulfobacillus thermosulfidooxidans* on pyrite under conditions of variable pH using tapping mode atomic force microscopy. Process Biochem 46:966-976

Bellenberg S, Barthen R, Boretska M, Zhang R, Sand W, Vera M (2015) Manipulation of pyrite colonization and leaching by iron-oxidizing *Acidithiobacillus* species. Appl Microbiol Biotechnol 99:1435-1449

Bellenberg S, Diaz M, Noel N, Sand W, Poetsch A, Guiliani N, Vera M (2014) Biofilm formation, communication and interactions of leaching bacteria during colonization of pyrite and sulfur surfaces. Res Microbiol 165:773-781

Bellenberg S, Leon-Morales C-F, Sand W, Vera M (2012) Visualization of capsular polysaccharide induction in *Acidithiobacillus ferrooxidans*. Hydrometallurgy 129-130:82-89

Bennke CM, Neu TR, Fuchs BM, Amann R (2013) Mapping glycoconjugate-mediated interactions of marine *Bacteroidetes* with diatoms. Syst Appl Microbiol 36:417-425

Bharadwaj A, Ting Y-P (2013) Bioleaching of spent hydrotreating catalyst by acidophilic thermophile *Acidianus brierleyi*: Leaching mechanism and effect of decoking. Bioresour Technol 130:673-680

Binnig G, Quate CF, Gerber C (1986) Atomic force microscope. Phys Rev Lett 56:930-933

Binnig G, Rohrer H, Gerber C, Weibel E (1982) Surface studies by scanning tunneling microscopy. Phys Rev Lett 49:57-61

Blake RC, Howard GT, McGinness S (1994) Enhanced yields of iron-oxidizing bacteria by in situ electrochemical reduction of soluble iron in the growth medium. Appl Environ Microbiol 60:2704-2710

Bosecker K (1997) Bioleaching: metal solubilization by microorganisms. FEMS Microbiol Rev 20:591-604

Bradford MM (1976) A rapid and sensitive method for the quantitation of microgram quantities of protein utilizing the principle of protein-dye binding. Anal Biochem 72:248-254

Brock T, Brock K, Belly R, Weiss R (1972) *Sulfolobus*: A new genus of sulfur-oxidizing bacteria living at low pH and high temperature. Archiv Mikrobiol 84:54-68

Bryan CG, Joulian C, Spolaore P, Challan-Belval S, El Achbouni H, Morin DHR, d'Hugues P (2009) Adaptation and evolution of microbial consortia in a stirred tank reactor bioleaching system: indigenous population versus a defined consortium. Adv Mat Res 71:79-82

Bryant R, Costerton J, Laishley E (1984) The role of *Thiobacillus albertis* glycocalyx in the adhesion of cells to elemental sulfur. Can J Microbiol 30:81-90

Bryant R, McGroarty K, Costerton J, Laishley E (1983) Isolation and characterization of a new acidophilic *Thiobacillus* species (*T. albertis*). Can J Microbiol 29:1159-1170

Burton K (1956) A study of the conditions and mechanism of the diphenylamine reaction for the colorimetric estimation of deoxyribonucleic acid. Biochem J 62:315-323

Castelle CJ, Roger M, Bauzan M, Brugna M, Lignon S, Nimtz M, Golyshina OV, Giudici-Orticoni M-T, Guiral M (2015) The aerobic respiratory chain of the acidophilic archaeon *Ferroplasma acidiphilum*: A

membrane-bound complex oxidizing ferrous iron. Biochim Biophys Acta 1847:717-728

Castro L, Zhang R, Muñoz JA, González F, Blázquez ML, Sand W, Ballester A (2014) Characterization of exopolymeric substances (EPS) produced by *Aeromonas hydrophila* under reducing conditions. Biofouling 30:501-511

Crescenzi F, Crisari A, D'Angel E, Nardella A (2006) Control of acidity development on solid sulfur due to bacterial action. Environ Sci Technol 40:6782-6786

Crundwell F (2003) How do bacteria interact with minerals? Hydrometallurgy 71:75-81

d'Hugues P, Joulian C, Spolaore P, Michel C, Garrido F, Morin D (2008) Continuous bioleaching of a pyrite concentrate in stirred reactors: Population dynamics and exopolysaccharide production vs. bioleaching performance. Hydrometallurgy 94:34-41

Darland G, Brock TD, Samsonoff W, Conti S (1970) A thermophilic, acidophilic mycoplasma isolated from a coal refuse pile. Science 170:1416-1418

Deng X, Chai L, Yang Z, Tang C, Wang Y, Shi Y (2013) Bioleaching mechanism of heavy metals in the mixture of contaminated soil and slag by using indigenous *Penicillium chrysogenum* strain F1. J Hazard Mater 248-249:107-114

Diao M, Taran E, Mahler S, Nguyen AV (2014a) A concise review of nanoscopic aspects of bioleaching bacteria–mineral interactions. Adv Colloid Interface Sci 212:45-63

Diao M, Taran E, Mahler SM, Nguyen AV (2014b) Comparison and evaluation of immobilization methods for preparing bacterial probes using acidophilic bioleaching bacteria *Acidithiobacillus thiooxidans* for AFM studies. J Microbiol Methods 102:12-14

Dinkla IJ, Gericke M, Geurkink B, Hallberg KB (2009) *Acidianus brierleyi* is the dominant thermoacidophile in a bioleaching community processing chalcopyrite containing concentrates at 70 °C. Adv Mat Res 71:67-70

Dopson M, Baker-Austin C, Bond P (2007) Towards determining details of anaerobic growth coupled to ferric iron reduction by the acidophilic archaeon '*Ferroplasma acidarmanus*' Fer1. Extremophiles 11:159-168

Dopson M, Baker-Austin C, Hind A, Bowman JP, Bond PL (2004) Characterization of *Ferroplasma* isolates and *Ferroplasma acidarmanus* sp. nov., extreme acidophiles from acid mine drainage and industrial bioleaching environments. Appl Environ Microbiol 70:2079-2088

Dorobantu LS, Goss GG, Burrell RE (2012) Atomic force microscopy: A nanoscopic view of microbial cell surfaces. Micron 43:1312-1322

du Plessis CA, Slabbert W, Hallberg KB, Johnson DB (2011) Ferredox: a biohydrometallurgical processing concept for limonitic nickel laterites. Hydrometallurgy 109:221-229

Dubois M, Gilles KA, Hamilton JK, Rebers P, Smith F (1956) Colorimetric method for determination of sugars and related substances. Anal Chem 28:350-356

Dufrêne YF (2004) Using nanotechniques to explore microbial surfaces. Nat Rev Microbiol 2:451-460

Dziurla MA, Achouak W, Lam BT, Heulin T, Berthelin J (1998) Enzyme-linked immunofiltration assay to estimate attachment of thiobacilli to pyrite. Appl Environ Microbiol 64:2937-2942

Edwards KJ, Bond PL, Banfield JF (2000a) Characteristics of attachment and growth of *Thiobacillus caldus* on sulphide minerals: a chemotactic response to sulphur minerals? Environ Microbiol 2:324-332

Edwards KJ, Bond PL, Gihring TM, Banfield JF (2000b) An archaeal iron-oxidizing extreme acidophile important in acid mine drainage. Science 287:1796-1799

Edwards KJ, Goebel BM, Rodgers TM, Schrenk MO, Gihring TM, Cardona MM, Mcguire MM, Hamers RJ, Pace NR, Banfield JF (1999) Geomicrobiology of pyrite (FeS$_2$) dissolution: Case study at Iron Mountain, California. Geomicrobiol J 16:155-179

Edwards KJ, Hu B, Hamers RJ, Banfield JF (2001) A new look at microbial leaching patterns on sulfide minerals. FEMS Microbiol Ecol 34:197-206

Edwards KJ, Schrenk MO, Hamers R, Banfield JF (1998) Microbial oxidation of pyrite: experiments using microorganisms from an extreme acidic environment. Am Mineral 83:1444-1453

Espejo RT, Romero P (1987) Growth of *Thiobacillus ferrooxidans* on elemental sulfur. Appl Environ Microbiol 53:1907-1912

Etzel K, Klingl A, Huber H, Rachel R, Schmalz G, Thomm M, Depmeier W (2008) Etching of {111} and {210} synthetic pyrite surfaces by two archaeal strains, *Metallosphaera sedula* and *Sulfolobus metallicus*. Hydrometallurgy 94:116-120

Evangelou VPB, Zhang YL (1995) A review: pyrite oxidation mechanisms and acid mine drainage prevention. Crit Rev Environ Sci Technol 25:141-199

Ferrer M, Golyshina OV, Beloqui A, Golyshin PN, Timmis KN (2007) The cellular machinery of *Ferroplasma acidiphilum* is iron-protein-dominated. Nature 445:91-94

Flemming H-C, Wingender J (2010) The biofilm matrix. Nat Rev Microbiol 8:623-633

Florian B, Noël N, Sand W (2010) Visualization of initial attachment of bioleaching bacteria using combined atomic force and epifluorescence microscopy. Miner Eng 23:532-535

Florian B, Noël N, Thyssen C, Felschau I, Sand W (2011) Some quantitative data on bacterial attachment to pyrite. Miner Eng 24:1132-1138

Fuchs T, Huber H, Burggraf S, Stetter KO (1996) 16S rDNA-based phylogeny of the archaeal order *Sulfolobales* and reclassification of *Desulfurolobus*

ambivalens as *Acidianus ambivalens* comb. nov. Syst Appl Microbiol 19:56-60

Fuchs T, Huber H, Teiner K, Burggraf S, Stetter KO (1995) *Metallosphaera prunae*, sp. nov., a novel metal-mobilizing, thermoacidophilic archaeum, isolated from a uranium mine in Germany. Syst Appl Microbiol 18:560-566

Gautier V, Escobar B, Vargas T (2008) Cooperative action of attached and planktonic cells during bioleaching of chalcopyrite with *Sulfolobus metallicus* at 70 °C. Hydrometallurgy 94:121-126

Gehrke T, Hallmann R, Kinzler K, Sand W (2001) The EPS of *Acidithiobacillus ferrooxidans* - a model for structure-function relationships of attached bacteria and their physiology. Water Sci Technol 43:159-167

Gehrke T, Telegdi J, Thierry D, Sand W (1998) Importance of extracellular polymeric substances from *Thiobacillus ferrooxidans* for bioleaching. Appl Environ Microbiol 64:2743-2747

Ghorbani Y, Petersen J, Harrison ST, Tupikina OV, Becker M, Mainza AN, Franzidis J-P (2012) An experimental study of the long-term bioleaching of large sphalerite ore particles in a circulating fluid fixed-bed reactor. Hydrometallurgy 129:161-171

Giaveno MA, Urbieta MS, Ulloa JR, Toril EG, Donati ER (2013) Physiologic versatility and growth flexibility as the main characteristics of a novel thermoacidophilic *Acidianus* strain isolated from Copahue geothermal area in Argentina. Microb Ecol 65:336-346

Gleisner M, Herbert RB, Kockum PCF (2006) Pyrite oxidation by *Acidithiobacillus ferrooxidans* at various concentrations of dissolved oxygen. Chem Geol 225:16-29

Golovacheva R, Valekhoroman K, Troitskii A (1987) *Sulfurococcus mirabilis* gen. nov., sp. nov., a new thermophilic archaebacterium with the ability to oxidize sulfur. Microbiology 56:84-91

Goltsman DSA, Comolli LR, Thomas BC, Banfield JF (2015) Community transcriptomics reveals unexpected high microbial diversity in acidophilic biofilm communities. ISME J 9:1014-1023

Golyshina OV (2011) Environmental, biogeographic, and biochemical patterns of archaea of the Family *Ferroplasmaceae*. Appl Environ Microbiol 77:5071-5078

Golyshina OV, Golyshin PN, Timmis KN, Ferrer M (2006) The 'pH optimum anomaly' of intracellular enzymes of *Ferroplasma acidiphilum*. Environ Microbiol 8:416-425

Golyshina OV, Pivovarova TA, Karavaiko GI, Kondrateva TF, Moore ER, Abraham WR, Lunsdorf H, Timmis KN, Yakimov MM, Golyshin PN (2000) *Ferroplasma acidiphilum* gen. nov., sp. nov., an acidophilic, autotrophic, ferrous-iron-oxidizing, cell-wall-lacking, mesophilic member of the *Ferroplasmaceae* fam. nov., comprising a distinct lineage of the Archaea. Int J Syst Evol Microbiol 50:997-1006

Golyshina OV, Timmis KN (2005) *Ferroplasma* and relatives, recently discovered cell wall-lacking archaea making a living in extremely acid, heavy metal-rich environments. Environ Microbiol 7:1277-1288

Golyshina OV, Yakimov MM, Lünsdorf H, Ferrer M, Nimtz M, Timmis KN, Wray V, Tindall BJ, Golyshin PN (2009) *Acidiplasma aeolicum* gen. nov., sp. nov., a euryarchaeon of the family *Ferroplasmaceae* isolated from a hydrothermal pool, and transfer of *Ferroplasma cupricumulans* to *Acidiplasma cupricumulans* comb. nov. Int J Syst Evol Microbiol 59:2815-2823

Gómez E, Ballester A, González F, Blázquez ML (1999) Leaching capacity of a new extremely thermophilic microorganism, *Sulfolobus rivotincti*. Hydrometallurgy 52:349-366

Gonzalez A, Bellenberg S, Mamani S, Ruiz L, Echeverria A, Soulere L, Doutheau A, Demergasso C, Sand W, Queneau Y, Vera M, Guiliani N

(2013) AHL signaling molecules with a large acyl chain enhance biofilm formation on sulfur and metal sulfides by the bioleaching bacterium *Acidithiobacillus ferrooxidans*. Appl Microbiol Biotechnol 97:3729-3737

Govender Y, Gericke M (2011) Extracellular polymeric substances (EPS) from bioleaching systems and its application in bioflotation. Miner Eng 24:1122-1127

Grogan D, Palm P, Zillig W (1990) Isolate B12, which harbours a virus-like element, represents a new species of the archaebacterial genus *Sulfolobus*, *Sulfolobus shibatae*, sp. nov. Arch Microbiol 154:594-599

Hallberg K (2010) New perspectives in acid mine drainage microbiology. Hydrometallurgy 104:448-453

Harneit K, Göksel A, Kock D, Klock J-H, Gehrke T, Sand W (2006) Adhesion to metal sulfide surfaces by cells of *Acidithiobacillus ferrooxidans*, *Acidithiobacillus thiooxidans* and *Leptospirillum ferrooxidans*. Hydrometallurgy 83:245-254

Hawkes RB, Franzmann PD, O'hara G, Plumb JJ (2006) *Ferroplasma cupricumulans* sp. nov., a novel moderately thermophilic, acidophilic archaeon isolated from an industrial-scale chalcocite bioleach heap. Extremophiles 10:525-530

He H, Yang Y, Xia J-L, Ding J-N, Zhao X-J, Nie Z-Y (2008) Growth and surface properties of new thermoacidophilic Archaea strain *Acidianus manzaensis* YN-25 grown on different substrates. T Nonferr Metal Soc 18:1374-1378

He ZG, Zhong H, Li Y (2004) *Acidianus tengchongensis* sp. nov., a new species of acidothermophilic archaeon isolated from an acidothermal spring. Curr Microbiol 48:159-163

Henche AL, Koerdt A, Ghosh A, Albers SV (2012) Influence of cell surface structures on crenarchaeal biofilm formation using a thermostable green fluorescent protein. Environ Microbiol 14:779-793

Hong Y, Valix M (2014) Bioleaching of electronic waste using acidophilic sulfur oxidising bacteria. J Clean Prod 65:465-472

Huber G, Spinnler C, Gambacorta A, Stetter KO (1989) *Metallosphaera sedula* gen, and sp. nov. represents a new genus of aerobic, metal-mobilizing, thermoacidophilic archaebacteria. Syst Appl Microbiol 12:38-47

Huber G, Stetter KO (1991) *Sulfolobus metallicus*, sp. nov., a novel strictly chemolithoautotrophic thermophilic archaeal species of metal-mobilizers. Syst Appl Microbiol 14:372-378

Huber H, Prangishvili D (2006) *Sulfolobales*. In: Dworkin M, Falkow S, Rosenberg E, Schleifer K-H, Stackebrandt E (eds) The prokaryotes: A Handbook on the Biology of Bacteria. Springer, pp 23-51

Itoh T, Yoshikawa N, Takashina T (2007) *Thermogymnomonas acidicola* gen. nov., sp. nov., a novel thermoacidophilic, cell wall-less archaeon in the order *Thermoplasmatales*, isolated from a solfataric soil in Hakone, Japan. Int J Syst Evol Microbiol 57:2557-2561

Jan R-L, Wu J, Chaw S-M, Tsai C-W, Tsen S-D (1999) A novel species of thermoacidophilic archaeon, *Sulfolobus yangmingensis* sp. nov. Int J Syst Evol Microbiol 49:1809-1816

Janosch C, Remonsellez F, Sand W, Vera M (2015) Sulfur oxygenase reductase (Sor) in the moderately thermoacidophilic leaching bacteria: studies in *Sulfobacillus thermosulfidooxidans* and *Acidithiobacillus caldus*. Microorganisms 3:707-724

Jiao Y, Cody GD, Harding AK, Wilmes P, Schrenk M, Wheeler KE, Banfield JF, Thelen MP (2010) Characterization of extracellular polymeric substances from acidophilic microbial biofilms. Appl Environ Microbiol 76:2916-2922

Johnson DB (1998) Biodiversity and ecology of acidophilic microorganisms. FEMS Microbiol Ecol 27:307-317

Johnson DB (2013) Development and application of biotechnologies in the metal mining industry. Environ Sci Pollut Res 20:7768-7776

Johnson DB (2014) Biomining—biotechnologies for extracting and recovering metals from ores and waste materials. Curr Opin Biotechnol 30:24-31

Johnson DB (2015) Biomining goes underground. Nature Geoscience 8:165-166

Johnson DB, Grail BM, Hallberg KB (2013) A new direction for biomining: Extraction of metals by reductive dissolution of oxidized ores. Minerals 3:49-58

Jones DS, Schaperdoth I, Macalady JL (2014) Metagenomic evidence for sulfide oxidation in extremely acidic cave biofilms. Geomicrobiol J 31:194-204

Jordan H, Sanhueza A, Gautier V, Escobar B, Vargas T (2006) Electrochemical study of the catalytic influence of *Sulfolobus metallicus* in the bioleaching of chalcopyrite at 70 °C. Hydrometallurgy 83:55-62

Karavaiko G, Lobyreva L (1994) An overview of the bacteria and archaea involved in removal of inorganic and organic sulfur compounds from coal. Fuel Process Technol 40:167-182

Karavaiko GI, Golyshina OV, Troitskiĭ AV, Val'ekho-Roman KM, Golovacheva RS, Pivovarova TA (1994) *Sulfurococcus yellowstonensis* sp. nov., a new species of iron- and sulfur-oxidizing thermoacidophilic archaebacterium. Mikrobiologiia 63:668-682

Kletzin A, Urich T, Müller F, Bandeiras TM, Gomes CM (2004) Dissimilatory oxidation and reduction of elemental sulfur in thermophilic archaea. J Bioenerg Biomembr 36:77-91

Knickerbocker C, Nordstrom D, Southam G (2000) The role of "blebbing" in overcoming the hydrophobic barrier during biooxidation of elemental sulfur by *Thiobacillus thiooxidans*. Chem Geol 169:425-433

Koerdt A, Gödeke J, Berger J, Thormann KM, Albers S-V (2010) Crenarchaeal biofilm formation under extreme conditions. PloS one 5:e14104

Koerdt A, Jachlewski S, Ghosh A, Wingender J, Siebers B, Albers S-V (2012) Complementation of *Sulfolobus solfataricus* PBL2025 with an α-mannosidase: effects on surface attachment and biofilm formation. Extremophiles 16:115-125

Konishi Y, Asai S, Tokushige M, Suzuki T (1999) Kinetics of the bioleaching of chalcopyrite concentrate by acidophilic thermophile *Acidianus brierleyi*. Biotechnol Prog 15:681-688

Konishi Y, Tokushige M, Asai S, Suzuki T (2001) Copper recovery from chalcopyrite concentrate by acidophilic thermophile *Acidianus brierleyi* in batch and continuous-flow stirred tank reactors. Hydrometallurgy 59:271-282

Konishi Y, Yoshida S, Asai S (1995) Bioleaching of pyrite by acidophilic thermophile *Acidianus brierleyi*. Biotechnol Bioeng 48:592-600

Konishi Y, Yoshida S, Asai S (1998) Effect of yeast extract supplementation in leach solution on bioleaching rate of pyrite by acidophilic thermophile *Acidianus brierleyi*. Biotechnol Bioeng 58:663-667

Kozubal M, Macur R, Korf S, Taylor W, Ackerman G, Nagy A, Inskeep W (2008) Isolation and distribution of a novel iron-oxidizing crenarchaeon from acidic geothermal springs in Yellowstone National Park. Appl Environ Microbiol 74:942-949

Kurosawa N, Itoh YH, Itoh T (2003) Reclassification of *Sulfolobus hakonensis* Takayanagi et al. 1996 as *Metallosphaera hakonensis* comb. nov. based on phylogenetic evidence and DNA G+C content. Int J Syst Evol Microbiol 53:1607-1608

Kurosawa N, Itoh YH, Iwai T, Sugai A, Uda I, Kimura N, Horiuchi T, Itoh T (1998) *Sulfurisphaera ohwakuensis* gen. nov., sp. nov., a novel extremely

thermophilic acidophile of the order *Sulfolobales*. Int J Syst Bacteriol 48 Pt 2:451-456

Laishley E, Bryant R, Kobryn B, Hyne J (1986) Microcrystalline structure and surface area of elemental sulphur as factors influencing its oxidation by *Thiobacillus albertis*. Can J Microbiol 32:237-242

Larsson L, Olsson G, Holst O, Karlsson HT (1990) Pyrite oxidation by thermophilic archaebacteria. Appl Environ Microbiol 56:697-701

Lawrence J, Korber D, Hoyle B, Costerton J, Caldwell D (1991) Optical sectioning of microbial biofilms. J Bacteriol 173:6558-6567

Lawrence J, Swerhone G, Leppard G, Araki T, Zhang X, West M, Hitchcock A (2003) Scanning transmission X-ray, laser scanning, and transmission electron microscopy mapping of the exopolymeric matrix of microbial biofilms. Appl Environ Microbiol 69:5543-5554

Lawrence JR, Korber DR, Neu TR (2007) Analytical imaging and microscopy techniques. In: Hurst CJ, Crawford RL, Garland JL, Lipson DA, Mills AL, Stetzenbach LD (eds) Manual of environmental microbiology. ASM Press, Washington D.C., pp 40-68

Lee E, Han Y, Park J, Hong J, Silva RA, Kim S, Kim H (2015) Bioleaching of arsenic from highly contaminated mine tailings using *Acidithiobacillus thiooxidans*. J Environ Manage 147:124-131

Lei J, Huaiyang Z, Xiaotong P, Zhonghao D (2009) The use of microscopy techniques to analyze microbial biofilm of the bio-oxidized chalcopyrite surface. Miner Eng 22:37-42

Liang C-L, Xia J-L, Nie Z-Y, Yang Y, Ma C-Y (2012) Effect of sodium chloride on sulfur speciation of chalcopyrite bioleached by the extreme thermophile *Acidianus manzaensis*. Bioresour Technol 110:462-467

Liang C-L, Xia J-L, Zhao X-J, Yang Y, Gong S-Q, Nie Z-Y, Ma C-Y, Zheng L, Zhao Y-D, Qiu G-Z (2010) Effect of activated carbon on chalcopyrite

bioleaching with extreme thermophile *Acidianus manzaensis*. Hydrometallurgy 105:179-185

Lim M, Han G-C, Ahn J-W, You K-S, Kim H-S (2009) Leachability of arsenic and heavy metals from mine tailings of abandoned metal mines. Int J Env Res Public Health 6:2865-2879

Lis H, Sharon N (1973) The biochemistry of plant lectins (phytohemagglutinins). Annu Rev Biochem 42:541-574

Little B, Ray B, Pope R, Franklin M, White DC (2000) Spatial and temporal relationships between localised corrosion and bacterial activity on iron-containing substrata. In: Sequeira CAC (ed) Microbial corrosion. European Federation of Corrosion Publications; Institute of Materials, London, pp 21-35

Liu L-J, You X-Y, Guo X, Liu S-J, Jiang C-Y (2011) *Metallosphaera cuprina* sp. nov., an acidothermophilic, metal-mobilizing archaeon. Int J Syst Evol Microbiol 61:2395-2400

Liu Y-G, Zhou M, Zeng G-M, Li X, Xu W-H, Fan T (2007) Effect of solids concentration on removal of heavy metals from mine tailings via bioleaching. J Hazard Mater 141:202-208

Liu Y, Berná A, Climent V, Feliu JM (2015) Real-time monitoring of electrochemically active biofilm developing behavior on bioanode by using EQCM and ATR/FTIR. Sensors Actuators B: Chem 209:781-789

Macalady JL, Vestling MM, Baumler D, Boekelheide N, Kaspar CW, Banfield JF (2004) Tetraether-linked membrane monolayers in *Ferroplasma* spp: a key to survival in acid. Extremophiles 8:411-419

Mackintosh M (1978) Nitrogen fixation by *Thiobacillus ferrooxidans*. J Gen Microbiol 105:215-218

Mangold S, Harneit K, Rohwerder T, Claus G, Sand W (2008) Novel combination of atomic force microscopy and epifluorescence microscopy

for visualization of leaching bacteria on pyrite. Appl Environ Microbiol 74:410-415

Martinez P, Vera M, Bobadilla-Fazzini RA (2015) Omics on bioleaching: current and future impacts. Appl Microbiol Biotechnol 99:8337-8350

Méndez-García C, Peláez AI, Mesa V, Sánchez J, Golyshina OV, Ferrer M (2015) Microbial diversity and metabolic networks in acid mine drainage habitats. Front Microbiol 6:475

Meng C, Lin H, Chen J, Guo Y (2007) UV induced mutations in *Acidianus brierleyi* growing in a continuous stirred tank reactor generated a strain with improved bioleaching capabilities. Enzyme Microb Technol 40:1136-1140

Merino M, Andrews B, Asenjo J (2014) Stoichiometric model and flux balance analysis for a mixed culture of *Leptospirillum ferriphilum* and *Ferroplasma acidiphilum*. Biotechnol Prog 34:307-315

Meyer G, Schneider-Merck, T., Böhme, S., Sand, W. (2002) A simple method for investigations on the chemotaxis of *A. ferrooxidans* and *D. vulgaris*. Acta Biotechnol 22:391-399

Mikkelsen D, Kappler U, Webb R, Rasch R, McEwan A, Sly L (2007) Visualisation of pyrite leaching by selected thermophilic archaea: nature of microorganism–ore interactions during bioleaching. Hydrometallurgy 88:143-153

Mitsunobu S, Zhu M, Takeichi Y, Ohigashi T, Suga H, Makita H, Sakata M, Ono K, Mase K, Takahashi Y (2015) Nanoscale identification of extracellular organic substances at the microbe–mineral interface by Scanning Transmission X-ray microscopy. Chem Lett 44:91-93

Monroe D (2007) Looking for chinks in the armor of bacterial biofilms. PLoS Biol 5:e307

Murr L, Berry V (1976) Direct observations of selective attachment of bacteria on low-grade sulfide ores and other mineral surfaces. Hydrometallurgy 2:11-24

Nancucheo I, Grail BM, Hilario F, du Plessis C, Johnson DB (2014) Extraction of copper from an oxidized (lateritic) ore using bacterially catalysed reductive dissolution. Appl Microbiol Biotechnol 98:6297-305

Naumann D, Helm D, Labischinski H (1991) Microbiological characterizations by FT-IR spectroscopy. Nature 351:81-82

Nemati M, Harrison STL (2000a) A comparative study on thermophilic and mesophilic biooxidation of ferrous iron. Miner Eng 13:19-24

Nemati M, Harrison STL (2000b) Effect of solid loading on thermophilic bioleaching of sulfide minerals. J Chem Technol Biotechnol 75:526-532

Nemati M, Lowenadler J, Harrison S (2000) Particle size effects in bioleaching of pyrite by acidophilic thermophile *Sulfolobus metallicus* (BC). Appl Microbiol Biotechnol 53:173-179

Neu T, Lawrence J (2009) Extracellular polymeric substances in microbial biofilms. In: Moran AP, Holst O, Brennan PJ, von Itzstein M (eds) Microbial Glycobiology: Structures, Relevance and Applications. Elsevier, San Diego, pp 735-758

Neu TR, Lawrence JR (2014a) Advanced techniques for in situ analysis of the biofilm matrix (structure, composition, dynamics) by means of laser scanning microscopy. In: Donelli G (ed) Microbial Biofilms: Methods and Protocols, Methods in Molecular Biology. Springer, New York, pp 43-64

Neu TR, Lawrence JR (2014b) Investigation of microbial biofilm structure by laser scanning microscopy. Adv Biochem Eng Biotechnol 146:1-51

Neu TR, Lawrence JR (2015) Innovative techniques, sensors, and approaches for imaging biofilms at different scales. Trends Microbiol 23:233-242

Neu TR, Marshall KC (1990) Bacterial polymers: physicochemical aspects of their interactions at interfaces. J Biomater Appl 5:107-133

Neu TR, Marshall KC (1991) Microbial "footprints"—a new approach to adhesive polymers. Biofouling 3:101-112

Neu TR, Swerhone GD, Lawrence JR (2001) Assessment of lectin-binding analysis for in situ detection of glycoconjugates in biofilm systems. Microbiology 147:299-313

Ng FM, Dawes EA (1973) Chemostat studies on the regulation of glucose metabolism in Pseudomonas aeruginosa by citrate. Biochem J 132:129-40

Nichols PD, Michael Henson J, Guckert JB, Nivens DE, White DC (1985) Fourier transform-infrared spectroscopic methods for microbial ecology: analysis of bacteria, bacteri-polymer mixtures and biofilms. J Microbiol Methods 4:79-94

Noël N, Florian B, Sand W (2010) AFM & EFM study on attachment of acidophilic leaching organisms. Hydrometallurgy 104:370-375

Nordstrom DK, Blowes DW, Ptacek CJ (2015) Hydrogeochemistry and microbiology of mine drainage: An update. Appl Geochem 57:3-16

Norris PR (2007) Acidophile diversity in mineral sulfide oxidation. In: Rawlings DE, Johnson DB (eds) Biomining. Springer-Verlag, Berlin Heidelberg, pp 199-216

Ofori-Sarpong G, Osseo-Asare K, Tien M (2013) Mycohydrometallurgy: Biotransformation of double refractory gold ores by the fungus, *Phanerochaete chrysosporium*. Hydrometallurgy 137:38-44

Ohmura N, Kitamura K, Saiki H (1993) Selective adhesion of *Thiobacillus ferrooxidans* to pyrite. Appl Environ Microbiol 59:4044-4050

Okibe N, Gericke M, Hallberg KB, Johnson DB (2003) Enumeration and characterization of acidophilic microorganisms isolated from a pilot plant stirred-tank bioleaching operation. Appl Environ Microbiol 69:1936-1943

Okibe N, Johnson DB (2004) Biooxidation of pyrite by defined mixed cultures of moderately thermophilic acidophiles in pH-controlled bioreactors: Significance of microbial interactions. Biotechnol Bioeng 87:574-583

Orell A, Navarro CA, Arancibia R, Mobarec JC, Jerez CA (2010) Life in blue: Copper resistance mechanisms of bacteria and Archaea used in industrial biomining of minerals. Biotechnol Adv 28:839-848

Pant D, Joshi D, Upreti MK, Kotnala RK (2012) Chemical and biological extraction of metals present in E waste: A hybrid technology. Waste Manage 32:979-990

Parikh SJ, Chorover J (2006) ATR-FTIR spectroscopy reveals bond formation during bacterial adhesion to iron oxide. Langmuir 22:8492-8500

Pathak A, Dastidar M, Sreekrishnan T (2009) Bioleaching of heavy metals from sewage sludge: a review. J Environ Manage 90:2343-2353

Peltola M, Neu TR, Raulio M, Kolari M, Salkinoja‐Salonen MS (2008) Architecture of *Deinococcus geothermalis* biofilms on glass and steel: a lectin study. Environ Microbiol 10:1752-1759

Plumb JJ, Haddad CM, Gibson JA, Franzmann PD (2007) *Acidianus sulfidivorans* sp. nov., an extremely acidophilic, thermophilic archaeon isolated from a solfatara on Lihir Island, Papua New Guinea, and emendation of the genus description. Int J Syst Evol Microbiol 57:1418-1423

Pradhan N, Nathsarma KC, Srinivasa Rao K, Sukla LB, Mishra BK (2008) Heap bioleaching of chalcopyrite: A review. Miner Eng 21:355-365

Quilès F, Humbert F, Delille A (2010) Analysis of changes in attenuated total reflection FTIR fingerprints of *Pseudomonas fluorescens* from planktonic state to nascent biofilm state. Spectrochimi Acta A 75:610-616

Rawlings DE (2002) Heavy metal mining using microbes. Annu Rev Microbiol 56:65-91

Rimstidt JD, and Vaughan, D.J. (2003) Pyrite oxidation: A state-of-the-art assessment of the reaction mechanism. Geochim Cosmochim Acta 67:873-880

Rodriguez-Leiva M, Tributsch H (1988) Morphology of bacterial leaching patterns by *Thiobacillus ferrooxidans* on synthetic pyrite. Arch Microbiol 149:401-405

Rodriguez Y, Ballester A, Blazquez ML, Gonzalez F, Munoz JA (2003) New information on the pyrite bioleaching mechanism at low and high temperature. Hydrometallurgy 71:37-46

Rohwerder T, Sand W (2007) Oxidation of inorganic sulfur compounds in acidophilic prokaryotes. Eng Life Sci 7:301-309

Rojas-Chapana JA, Giersig M, Tributsch H (1996) The path of sulfur during the bio-oxidation of pyrite by *Thiobacillus ferrooxidans*. Fuel 75:923-930

Rossi G (1990) Biohydrometallurgy. McGraw-Hill, New York

Sampson M, Phillips C, Ball A (2000) Investigation of the attachment of *Thiobacillus ferrooxidans* to mineral sulfides using scanning electron microscopy analysis. Miner Eng 13:643-656

Sand W, Gehrke T, Hallmann R, Schippers A (1998) Towards a novel bioleaching mechanism. Miner Process Extract Metall Rev 19:97-106

Sand W, Gehrke T, Jozsa PG, Schippers A (2001) (Bio) chemistry of bacterial leaching—direct vs. indirect bioleaching. Hydrometallurgy 59:159-175

Sand W, Jozsa P-G, Kovacs Z-M, Sasaran N, Schippers A (2007) Long-term evaluation of acid rock drainage mitigation measures in large lysimeters. J Geochem Explor 92:205-211

Sanhueza A, Ferrer I, Vargas T, Amils R, Sánchez C (1999) Attachment of *Thiobacillus ferrooxidans* on synthetic pyrite of varying structural and electronic properties. Hydrometallurgy 51:115-129

Santos C, Fraga ME, Kozakiewicz Z, Lima N (2010) Fourier transform infrared as a powerful technique for the identification and characterization of filamentous fungi and yeasts. Res Microbiol 161:168-175

Schaeffer W, Holbert P, Umbreit W (1963) Attachment of *Thiobacillus thiooxidans* to sulfur crystals. J Bacteriol 85:137-140

Schippers A (2007) Microorganisms involved in bioleaching and nucleic acid-based molecular methods for their identification and quantification. In: Donati E, Sand W (eds) Microbial Processing of Metal Sulfides. Springer Netherlands, pp 3-33

Schippers A, Breuker A, Blazejak A, Bosecker K, Kock D, Wright T (2010) The biogeochemistry and microbiology of sulfidic mine waste and bioleaching dumps and heaps, and novel Fe (II)-oxidizing bacteria. Hydrometallurgy 104:342-350

Schippers A, Hedrich S, Vasters J, Drobe M, Sand W, Willscher S (2014) Biomining: metal recovery from ores with microorganisms. In: Schippers A, Glombitza F, Sand W (eds) Geobiotechnology I. Springer, Berlin, pp 1-47

Schippers A, Jozsa P, Sand W (1996) Sulfur chemistry in bacterial leaching of pyrite. Appl Environ Microbiol 62:3424-3431

Schippers A, Sand W (1999) Bacterial leaching of metal sulfides proceeds by two indirect mechanisms via thiosulfate or via polysulfides and sulfur. Appl Environ Microbiol 65:319-321

Schleper C, Puehler G, Holz I, Gambacorta A, Janekovic D, Santarius U, Klenk H-P, Zillig W (1995) *Picrophilus* gen. nov., fam. nov.: a novel aerobic, heterotrophic, thermoacidophilic genus and family comprising archaea capable of growth around pH 0. J Bacteriol 177:7050-7059

Schmitt J, Flemming H-C (1998) FTIR-spectroscopy in microbial and material analysis. Int Biodeterior Biodegrad 41:1-11

Segerer A, Langworthy TA, Stetter KO (1988) *Thermoplasma acidophilum* and *Thermoplasma volcanium* sp. nov. from Solfatara Fields. Syst Appl Microbiol 10:161-171

Segerer A, Neuner A, Kristjansson JK, Stetter KO (1986) *Acidianus infernus* gen. nov., sp. nov., and *Acidianus brierleyi* comb. nov.: facultatively aerobic, extremely acidophilic thermophilic sulfur-metabolizing archaebacteria. Int J Syst Bacteriol 36:559-564

Segerer AH, Trincone A, Gahrtz M, Stetter KO (1991) *Stygiolobus azoricus* gen. nov., sp. nov. represents a novel genus of anaerobic, extremely thermoacidophilic archaebacteria of the order *Sulfolobales*. Int J Syst Bacteriol 41:495-501

Sharma P, Das A, Rao KH, Forssberg K (2003) Surface characterization of *Acidithiobacillus ferrooxidans* cells grown under different conditions. Hydrometallurgy 71:285-292

Sharon N, Lis H (1972) Lectins: cell-agglutinating and sugar-specific proteins. Science 177:949-959

Sheng G-P, Yu H-Q, Wang C-M (2006) FTIR-spectral analysis of two photosynthetic H_2-producing strains and their extracellular polymeric substances. Appl Microbiol Biotechnol 73:204-210

Shrihari RK, Modak, J.M., Kumar, R., Gandhi, K.S. (1995) Dissolution of particles of pyrite mineral by direct attachment of *Thiobacillus ferrooxidans*. Hydrometallurgy 38:175-187

Solari JA, Huerta G, Escobar B, Vargas T, Badilla-Ohlbaum R, Rubio J (1992) Interfacial phenomena affecting the adhesion of *Thiobacillus ferrooxidans* to sulphide mineral surfaces. Colloid Surf 69:159-166

Staudt C, Horn H, Hempel D, Neu T (2003) Screening of lectins for staining lectin-specific glycoconjugates in the EPS of biofilms. In: Lens P, O'Flaherty V, Moran AP, Stoodley P, Mahony T (eds) Biofilms in

medicine, industry and environmental technology. IWA Publishing, London, pp 308-327

Sumner JB, Howell SF (1936) Identification of hemagglutinin of jack bean with concanavalin A. J Bacteriol 32:227-237

Suzuki T, Iwasaki T, Uzawa T, Hara K, Nemoto N, Kon T, Ueki T, Yamagishi A, Oshima T (2002) *Sulfolobus tokodaii* sp. nov.(f. *Sulfolobus* sp. strain 7), a new member of the genus *Sulfolobus* isolated from Beppu Hot Springs, Japan. Extremophiles 6:39-44

Syed S (2012) Recovery of gold from secondary sources—A review. Hydrometallurgy 115-116:30-51

Takayanagi S, Kawasaki H, Sugimori K, Yamada T, Sugai A, Ito T, Yamasato K, Shioda M (1996) *Sulfolobus hakonensis* sp. nov., a novel species of acidothermophilic archaeon. Int J Syst Bacteriol 46:377-382

Tamura H, Goto K, Yotsuyanagi T, Nagayama M (1974) Spectrophotometric determination of iron (II) with 1, 10-phenanthroline in the presence of large amounts of iron (III). Talanta 21:314-318

Tamura K, Stecher G, Peterson D, Filipski A, Kumar S (2013) MEGA6: molecular evolutionary genetics analysis version 6.0. Mol Biol Evol 30:2725-2729

Tapia J, Munoz J, Gonzalez F, Blazquez M, Malki M, Ballester A (2009) Extraction of extracellular polymeric substances from the acidophilic bacterium *Acidiphilium* 3.2Sup(5). Water Sci Technol 59:1959-1967

Taylor ES, Lower SK (2008) Thickness and surface density of extracellular polymers on *Acidithiobacillus ferrooxidans*. Appl Environ Microbiol 74:309-311

Telegdi J, Keresztes Z, Pálinkás G, Kálmán E, Sand W (1998) Microbially influenced corrosion visualized by atomic force microscopy. Appl Phys A: Mater Sci Process 66:S639-S642

Tributsch H (2001) Direct versus indirect bioleaching. Hydrometallurgy 59:177-185

Tributsch H, Rojas-Chapana JA (2000) Metal sulfide semiconductor electrochemical mechanisms induced by bacterial activity. Electrochim Acta 45:4705-4716

Urbieta MS, Rascovan N, Castro C, Revale S, Giaveno MA, Vazquez M, Donati ER (2014) Draft genome sequence of the novel thermoacidophilic archaeon *Acidianus copahuensis* strain ALE1, isolated from the Copahue volcanic area in Neuquén, Argentina. Genome Announc 2:e00259-14

Valdes J, Ossandon F, Quatrini R, Dopson M, Holmes DS (2011) Draft genome sequence of the extremely acidophilic biomining bacterium *Acidithiobacillus thiooxidans* ATCC 19377 provides insights into the evolution of the *Acidithiobacillus* genus. J Bacteriol 193:7003-7004

Vera M, Krok B, Bellenberg S, Sand W, Poetsch A (2013a) Shotgun proteomics study of early biofilm formation process of *Acidithiobacillus ferrooxidans* ATCC 23270 on pyrite. Proteomics 13:1133-1144

Vera M, Schippers A, Sand W (2013b) Progress in bioleaching: fundamentals and mechanisms of bacterial metal sulfide oxidation-part A. Appl Microbiol Biotechnol 97:7529-7541

Wakao N, Mishina M, Sakurai Y, Shiota H (1984) Bacterial pyrite oxidation III. Adsorption of *Thiobacillus ferrooxidans* cells on solid surfaces and its effect on iron release from pyrite. J Gen Appl Microbiol 30:63-77

Watkinson A, Hadgraft J, Walters K, Brain K (1994) Measurement of diffusional parameters in membranes using ATR‐FTIR spectroscopy. Int J Cosmetic Sci 16:199-210

Weiss R (1973) Attachment of bacteria to sulphur in extreme environments. J Gen Microbiol 77:501-507

Wheaton G, Counts J, Mukherjee A, Kruh J, Kelly R (2015) The confluence of heavy metal biooxidation and heavy metal resistance: Implications for bioleaching by extreme thermoacidophiles. Minerals 5:397-451

Whitaker RJ, Grogan DW, Taylor JW (2003) Geographic barriers isolate endemic populations of hyperthermophilic Archaea. Science 301:976-978

Wilmes P, Remis JP, Hwang M, Auer M, Thelen MP, Banfield JF (2009) Natural acidophilic biofilm communities reflect distinct organismal and functional organization. ISME J 3:266-270

Xia JL, Liu HC, Nie ZY, Peng AA, Zhen XJ, Yang Y, Zhang XL (2013) Synchrotron radiation based STXM analysis and micro-XRF mapping of differential expression of extracellular thiol groups by *Acidithiobacillus ferrooxidans* grown on Fe^{2+} and S^0. J Microbiol Methods 94:257-261

Xiang X, Dong X, Huang L (2003) *Sulfolobus tengchongensis* sp. nov., a novel thermoacidophilic archaeon isolated from a hot spring in Tengchong, China. Extremophiles 7:493-498

Yang H-Y, Liu Q, Song X-L, Dong J-K (2013) Research status of carbonaceous matter in carbonaceous gold ores and bio-oxidation pretreatment. T Nonferr Metal Soc 23:3405-3411

Yoshida N, Nakasato M, Ohmura N, Ando A, Saiki H, Ishii M, Igarashi Y (2006) *Acidianus manzaensis* sp. nov., a novel thermoacidophilic archaeon growing autotrophically by the oxidation of H_2 with the reduction of Fe^{3+}. Curr Microbiol 53:406-411

Zhang L-M, Peng J-H, Wei M-M, Ding J-N, Zhou H-B (2010) Bioleaching of chalcopyrite with *Acidianus manzaensis* YN25 under contact and non-contact conditions. T Nonferr Metal Soc 20:1981-1986

Zhang L, Zhou W, Li K, Mao F, Wan L, Chen X, Zhou H, Qiu G (2015) Synergetic effects of *Ferroplasma thermophilum* in enhancement of copper concentrate bioleaching by *Acidithiobacillus caldus* and *Leptospirillum ferriphilum*. Biochem Eng J 93:142-150

Zhang X, Bishop PL, Kupferle MJ (1998) Measurement of polysaccharides and proteins in biofilm extracellular polymers. Water Sci Technol 37:345-348

Zhou H, Zhang R, Hu P, Zeng W, Xie Y, Wu C, Qiu G (2008) Isolation and characterization of *Ferroplasma thermophilum* sp. nov., a novel extremely acidophilic, moderately thermophilic archaeon and its role in bioleaching of chalcopyrite. J Appl Microbiol 105:591-601

Zhu J, Li Q, Jiao W, Jiang H, Sand W, Xia J, Liu X, Qin W, Qiu G, Hu Y (2012) Adhesion forces between cells of *Acidithiobacillus ferrooxidans*, *Acidithiobacillus thiooxidans* or *Leptospirillum ferrooxidans* and chalcopyrite. Colloids Surf, B 94:95-100

Zhu J, Wang Q, Zhou S, Li Q, Gan M, Jiang H, Qin W, Liu X, Hu Y, Qiu G (2015) Insights into the relation between adhesion force and chalcopyrite-bioleaching by *Acidithiobacillus ferrooxidans*. Colloids Surf, B 126:351-357

Zhu W, Xia J-L, Yang Y, Nie Z-Y, Zheng L, Ma C-Y, Zhang R-Y, Peng A-A, Tang L, Qiu G-Z (2011) Sulfur oxidation activities of pure and mixed thermophiles and sulfur speciation in bioleaching of chalcopyrite. Bioresour Technol 102:3877-3882

Zillig W, Stetter KO, Wunderl S, Schulz W, Priess H, Scholz I (1980) The *Sulfolobus*-"*Caldariella*" group: taxonomy on the basis of the structure of DNA-dependent RNA polymerases. Arch Microbiol 125:259-269

Zillig W, Yeats S, Holz I, Böck A, Rettenberger M, Gropp F, Simon G (1986) *Desulfurolobus ambivalens*, gen. nov., sp. nov., an autotrophic archaebacterium facultatively oxidizing or reducing sulfur. Syst Appl Microbiol 8:197-203

Zippel B, Neu T (2011) Characterization of glycoconjugates of extracellular polymeric substances in tufa-associated biofilms by using fluorescence lectin-binding analysis. Appl Environ Microbiol 77:505-516

Zolghadr B, Klingl A, Koerdt A, Driessen AJ, Rachel R, Albers S-V (2010) Appendage-mediated surface adherence of *Sulfolobus solfataricus*. J Bacteriol 192:104-110

Acknowledgements

I am very grateful to my supervisor **Prof. Dr. Wolfgang Sand** who offered me the opportunity to join the group and to conduct my PhD thesis. My thanks are not only for his great guidance and support during the entire study, but also for his encouragement, help, and suggestions for my general life. His positive attitude and philosophy of life always inspire me.

Special thanks to **Dr. Mario Vera** for his great support during the PhD thesis. I am grateful to him for the helpful discussions and valuable suggestions during preparations of manuscripts. Great thanks for his inspiration and excellent guidance.

Prof. Dr. Thomas R. Neu at Department of River Ecology, Helmholtz Centre for Environmental Research-UFZ, Magdeburg, is acknowledged for offering me the chances to get access to the excellent CLSM and the lectin library. I am deeply motivated by his critical attitude and devotion to science. Special thanks to him for accepting as my co-adviser.

Ute Kuhlicke at Department of River Ecology, Helmholtz Centre for Environmental Research-UFZ, Magdeburg, is appreciated for her excellent technical assistance in CLSM examination and data processing.

Dr. Véronique Blanchard at Charité Medical University, Berlin, is gratefully acknowledged for her kind assistance with sugar and sialic acid analysis.

Sören is appreciated for his support, helpful discussion and the friendship.

Dr. Laura Castro at Department of Material Science and Metallurgical Engineering, Complutense University of Madrid, Madrid, is acknowledged for her motivation and support.

Dajana Valenta at Department of Material Engineering and **Mark Schumann** at Department of Geology are acknowledged for their kind assistance in mineral processing.

I am thankful to **Felipe** and **Claudia** for their help in my first days in Germany.

Dr. Arevik Vardanyan, **Dr. Narine Vardanyan** and **Prof. Dr. Levon Markosyan** at National Academy of Science, Armenia, are appreciated for their kind assistance during my stay in Yerevan for the nice cooperation via BMBF (Bundesministrium für Bildung und Forschung, Germany).

I would like to acknowledge **all colleagues** from Prof. Sand's working group who helped and supported me during the last years (Qian, Christian, Jing, Yutong, Nova, Beate, Andrzej, Nanni, Bianca, Friederike, Natascha, Tilman, Petra, Camila, Agata, Mauricio, Yeryna and Maria).

Colleagues at Biofilm Centre from **Prof. Dr. Meckenstock**, **Prof. Dr. Siebers** and **Prof. Dr. Flemming**'s groups are acknowledged for their kind assistance and support.

Prof. Dr. Jinlan Xia at Central South University, Changsha, **Prof. Dr. Hongying Yang** at Northeastern University of China, Shenyang, and **Prof. Dr. Xiaorong Liu** at Shanghai Institute of Technology, Shanghai, are acknowledged for their helpful discussions, great support and guidance in studies and general life.

My PhD study was financially supported by **China Scholarship Council** (CSC) and **Fraunhofer-Umsicht (**Fraunhofer Institute for Environmental, Safety and Energy Technology), Oberhausen, Germany.

Finally, I'd like to express my deepest thanks to **my parents**, **my brother** and **sister**, for their love, selfless support and encouragement to finish my thesis.

Curriculum Vitae

Name: Ruiyong Zhang

Gender: Male

Birthday: 12.12.1984

Place of Birth: Kaifeng,   Henan,
                         China

Nationality: Chinese

Marital status: Single

Education:

From January 2011 to 2015: PhD study at Universität Duisburg-Essen (Essen, Germany)

From September 2006 to June 2009: Master study at Central South University (Changsha, China)

From September 2002 to June 2006: Bachelor study at Central South University (Changsha, China)

From September 1999 to June 2002: High school at Qi county (Kaifeng, China)

Conference Presentations:

i. Bioleaching: Metal recovery from ores with microorganisms. GCCCD 25th Annual Conference, 7-8. September 2013, Duisburg, Germany.

ii. Attachment to minerals and biofilm development of an extremely acidophilic archaeon *Ferroplasma acidiphilum*. 20th International Biohydrometallurgy Symposium, 8-11. October 2013, Antofagasta, Chile.

iii. Visualization and analysis of archaeal biofilms / extracellular polymeric substances (EPS) during bioleaching. SPC «Armbiotechnology» of NAS

of Armenia, 9. September 2014, Yerevan, Armenia.

iv. Use of lectins to *in situ* visualize glycoconjugates of EPS in acidophilic archaeal biofilms. 2nd Transnational Workshop Genomics and Transcriptomics in Geobiotechnology and White Biotechnology, 26-29. October 2014, Freiberg, Germany.

v. Initial attachment and biofilm formation of a novel crenarchaeote on mineral sulfides. 21th International Biohydrometallurgy Symposium, 5-9. October 2015, Bali, Indonesia.

Conference Posters:

i. **R. Y. Zhang**, J. L. Xia, A. A. Peng, C. G. Zhang, Z. Y. Nie, G. Z. Qiu and W. Sand. Screening and characterization of sulfur activation proteins of *Acidithiobacillus ferrooxidans* ATCC 23270. 19th International Biohydrometallurgy Symposium, 18-22. September 2011, Changsha, China.

ii. **R. Zhang**, S. Bellenberg, M. Vera, T. R. Neu and W. Sand. Visualization and analysis of extracellular polymeric substances of bioleaching-relevant archaea by using fluorescent-labelled lectin-binding analysis. Swiss International Conference on Industrial Microbiology, 16-17. October 2012, Olten, Switzerland.

iii. **R. Zhang**, S. Bellenberg, M. Vera, T. R. Neu and W. Sand. Biofilm development and extracellular polymeric substances distribution of extreme acidophilic archaeon *Ferroplasma acidiphilum*. GeoHannover, 1-3. October 2012, Hannover, Germany.

iv. S. Bellenberg, **R. Zhang**, M. Vera and W. Sand. Is Quorum sensing involved in regulation of polysaccharide export in *Acidithiobacillus ferrooxidans*? GeoHannover, 1-3. October 2012, Hannover, Germany.

v. S. Barahona, **R. Zhang**, C. Dorador, W. Sand, M. Vera and F.

Remonsellez. Effect of low temperature in oxidation and attachment of pyrite by an *Acidithiobacillus ferrivorans* isolate from Chilean Altiplano. 20th International Biohydrometallurgy Symposium, 8-11. October 2013, Antofagasta, Chile.

vi. **R. Zhang**, Y. Zhang, V. Blanchard, T. R. Neu, S. Bellenberg, W. Sand and M. Vera. Surface characterization and extracellular polymeric substances analysis of *Ferroplasma acidiphilum*: an extremely acidophilic and cell wall-lacking archaeon. The Perfect Slime - Nature, Properties, Regulation and Dynamics of EPS, 10-12. September 2014, Essen, Germany.

vii. A. Vardanyan, N. Vardanyan, L. Markosyan, W. Sand, M. Vera and **R. Zhang**. Biofilm formation and extracellular polymeric substances (EPS) analysis by new isolates of *Leptospirillum*, *Acidithiobacillus* and *Sulfobacillus* from Armenia. 21th International Biohydrometallurgy Symposium, 5-9. October 2015, Bali, Indonesia.

List of Publications

Zhang R, Bellenberg S, Neu TR, Sand W, Vera M (2016) The biofilm lifestyle of acidophilic metal/sulfur-oxidizing microorganisms. In: Rampelotto PH (ed) Biotechnology of Extremophiles: Advances and Challenges. Springer, Switzerland

Zhang R, Neu TR, Zhang Y, Bellenberg S, Kuhlicke U, Li Q, Sand W, Vera M (2015) Visualization and analysis of EPS glycoconjugates of the thermoacidophilic archaeon *Sulfolobus metallicus*. Appl Microbiol Biotechnol 99:7343-7356

Zhang RY, Neu TR, Bellenberg S, Kuhlicke U, Sand W, Vera M (2015) Use of lectins to in situ visualize glycoconjugates of extracellular polymeric substances in acidophilic archaeal biofilms. Microb Biotechnol 8:448-461

Zhang R, Zhang Y, Neu TR, Li Q, Bellenberg S, Sand W, Vera M (2015) Initial attachment and biofilm formation of a novel crenarchaeote on mineral sulfides. Adv Mat Res 1130:127-130

Zhang R, Liu J, Neu TR, Li Q, Bellenberg S, Sand W, Vera M (2015). Interspecies interactions of metal-oxidizing thermo-acidophilic archaea *Acidianus* and *Sulfolobus*. Adv Mat Res 1130:105-108

Bellenberg S, Barthen R, Boretska M, **Zhang R**, Sand W, Vera M (2015) Manipulation of pyrite colonization and leaching by iron-oxidizing *Acidithiobacillus* species. Appl Microbiol Biotechnol 99:1435-1449

Vardanyan A, Stepanyan S, Vardanyan N, Markosyan L, Sand W, Vera M, **Zhang R** (2015) Study and assessment of microbial communities in natural and commercial bioleaching systems. Miner Eng 81:167-172

Zhang R, Bellenberg S, Castro L, Neu TR, Sand W, Vera M (2014) Colonization and biofilm formation of the extremely acidophilic archaeon *Ferroplasma acidiphilum*. Hydrometallurgy 150:245-252

Barahona S, Dorador C, **Zhang R**, Aguilar P, Sand W, Vera M, Remonsellez F (2014) Isolation and characterization of a novel *Acidithiobacillus ferrivorans* strain from the Chilean Altiplano: attachment and biofilm formation on pyrite at low temperature. Res Microbiol 165:782-793

Castro L, **Zhang R**, Muñoz JA, González F, Blázquez ML, Sand W, Ballester A (2014) Characterization of exopolymeric substances (EPS) produced by *Aeromonas hydrophila* under reducing conditions. Biofouling 30:501-511

Xu A-L, Xia J-L, Song Z-W, Jiang P, Xia Y, Wan M-X, **Zhang R-Y**, Yang Y, Liu K-K (2013) The effect of energy substrates on PHB accumulation of *Acidiphilium cryptum* DX1-1. Curr Microbiol 67:379-387

Peng AA, Xia JL, Liu HC, Zhu W, **Zhang RY**, Zhang CG, Nie ZY (2013) Thiol-rich proteins play important role in adhesion and sulfur oxidation process of *Acidithiobacillus ferroxidans*. Adv Mater Res 825:137-140

Zhang RY, Vera M, Bellenberg S, Sand W (2013) Attachment to minerals and biofilm development of extremely acidophilic archaea. Adv Mater Res 825:103-106

Ding J, **Zhang R**, Yu Y, Jin D, Liang C, Yi Y, Zhu W, Xia J (2011) A novel acidophilic, thermophilic iron and sulfur-oxidizing archaeon isolated from a hot spring of Tengchong, Yunnan, China. Braz J Microbiol 42:514-525

Xia J-L, Xiong J, **Zhang R-Y**, Liu K-K, Huang B, Nie Z-Y (2011) Production of chitinase and its optimization from a novel isolate *Serratia marcescens* XJ-01. Indian J Microbiol 51:301-306

Xia JL, Wu S, **Zhang RY**, Zhang CG, He H, Jiang HC, Nie ZY, Qiu GZ (2011) Effects of copper exposure on expression of glutathione-related genes in *Acidithiobacillus ferrooxidans*. Curr Microbiol 62:1460-1466

Zhu W, Xia J-L, Yang Y, Nie Z-Y, Zheng L, Ma C-Y, **Zhang R-Y**, Peng A-A, Tang L, Qiu G-Z (2011) Sulfur oxidation activities of pure and mixed

thermophiles and sulfur speciation in bioleaching of chalcopyrite. Bioresour Technol 102:3877-3882

Deklaration

Hiermit versichere ich, dass ich die vorliegende Arbeit mit dem Titel

„**Biofilm formation and extracellular polymeric substances of acidophilic metal/sulfur-oxidizing archaea**"

selbst verfasst und keine außer den angegebenen Hilfsmitteln und Quellen benutzt habe, und dass die Arbeit in dieser oder ähnlicher Form noch bei keiner anderen Universität eingereicht wurde.

Essen, im Oktober 2015

RUIYONG ZHANG